NTNU

Norwegian University of
Science and Technology

Design of the measurment setup for the friction torque and axial load on the Francis turbine test rig

Magomed Selmurzaev

Mechanical Engineering
Submission date: June 2016
Supervisor: Ole Gunnar Dahlhaug, EPT

Norwegian University of Science and Technology
Department of Energy and Process Engineering

NTNU

Norwegian University
of Science and Technology

Department of Energy
and Process Engineering

EPT-M-2016-116

MASTER THESIS

for

Magomed Selmurzaev

Spring 2016

Design of the measurement setup for the friction torque and axial load on the Francis turbine test rig

Design av målearrangement for friksjonsmoment og aksial last på en Francis turbin test rigg

Background

The Waterpower laboratory at NTNU was built in 1917, and has been in use for nearly a century for developments and improvements of hydraulic machinery used in both Norwegian and international hydro power plants. In 2001, the laboratory was thoroughly rehabilitated to further meet the increasing demand in turbine performance improvement research.

The laboratory is built up around a main pipe system, with the two main booster pumps located in the basement. Various running configurations are possible by utilizing different pipe loops, enabling both open and closed loop conditions. The laboratory consists of several test rigs equipped with high-precision measuring instruments in accordance with the IEC 60193 standard, enabling performance guarantee tests of Pelton and Francis turbines, along with pump turbines.

The Francis turbine test rig is being used for research and development tests, along with model acceptance tests. The tests comprise determination of performances, such as efficiency, discharge, head and power. The operating behaviors are investigated, such as cavitation behavior and operation at runaway. The dynamic phenomena such as pressure fluctuations, torques and forces are also investigated. The test rig will have an improved bearing block installed during the spring of 2016. The remaining work before the installation starts is the development of a measurement setup for the friction torque and axial load, which is the aim for the work in this thesis .

Objectives

Design a system for the measurement and calibration for friction torque and axial load on the Francis turbine test rig for both the Waterpower Laboratory at NTNU and the Turbine Testing Laboratory at Kathmandu University

The following tasks are to be considered:

1. Literature study
    a. Get familiar with IEC60193
    b. Friction torque in bearings
2. Software knowledge
    a. CAD-drawing by CREO
3. Waterpower laboratory at NTNU
    a. Design a system for the measurement of the axial load and friction torque.
    b. Make a complete 3D-drawing of the thrust block including the friction torque measurement system and axial load calibration system
    c. Install and calibrate the arm and load cell for the friction torque
    d. Install and calibrate the pressure sensors for the axial load
4. Turbine Testing Laboratory, Kathmandu University
    a. Design a bearing block for the Francis turbine test rig
    b. Design a measurement system for the axial load

Within 14 days of receiving the written text on the master thesis, the candidate shall submit a research plan for his project to the department.

When the thesis is evaluated, emphasis is put on processing of the results, and that they are presented in tabular and/or graphic form in a clear manner, and that they are analyzed carefully.

The thesis should be formulated as a research report with summary both in English and Norwegian, conclusion, literature references, table of contents etc. During the preparation of the text, the candidate should make an effort to produce a well-structured and easily readable report. In order to ease the evaluation of the thesis, it is important that the cross-references are correct. In the making of the report, strong emphasis should be placed on both a thorough discussion of the results and an orderly presentation.

The candidate is requested to initiate and keep close contact with his/her academic supervisor(s) throughout the working period. The candidate must follow the rules and regulations of NTNU as well as passive directions given by the Department of Energy and Process Engineering.

Risk assessment of the candidate's work shall be carried out according to the department's procedures. The risk assessment must be documented and included as part of the final report. Events related to the candidate's work adversely affecting the health, safety or security, must be documented and included as part of the final report. If the documentation on risk assessment represents a large number of pages, the full version is to be submitted electronically to the supervisor and an excerpt is included in the report.

Pursuant to "Regulations concerning the supplementary provisions to the technology study program/Master of Science" at NTNU §20, the Department reserves the permission to utilize all the results and data for teaching and research purposes as well as in future publications.

The final report is to be submitted digitally in DAIM. An executive summary of the thesis including title, student's name, supervisor's name, year, department name, and NTNU's logo and name, shall be submitted to the department as a separate pdf file. Based on an agreement with the supervisor, the final report and other material and documents may be given to the supervisor in digital format.

☒ Work to be done in lab (Waterpower lab, Fluids engineering lab, Thermal engineering lab)
☐ Field work

Department of Energy and Process Engineering, 11th January 2016

Olav Bolland
Department Head

Ole Gunnar Dahlhaug
Academic Supervisor

Co-Supervisors:

- Torbjørn K. Nielsen
- Pål-Tore S. Storli
- Biraj Singh Thapa

Preface

This master thesis has been written at the Waterpower Laboratory at the Norwegian University of Science and Technology. The thesis deal with the design of friction torque and axial force measurement and calibrations systems.

A special thanks goes to my supervisor Professor Ole Gunnar Dahlhaug for his advice and guidance throughout the thesis. He has assisted me in every step of the task, and the help has been highly appreciated.

PhD students Peter Joachim Gogstad, Carl Werdelin Bergan and Bjørn Winther Solemslie deserve a special thanks as well for their immense help, being always available for questions and discussions.

I would also like to express my gratitude towards the staff responsible in the lab, Bård Brandåstrø, Joar Grillstad and Trygve Opland. Their guidance on the technical aspect of the thesis has been of crucial importance. As someone that started this thesis with very limited knowledge on the subject, the assistance of Joar Grillstad and the rest of the staff has meant a great deal to me.

The contribution of Biraj Singh and Sailesh Chitrakar, providing me with every necessary information on the Turbine Testing Laboratory, has played an important role in shaping the outcome of results.

Lastly, every student at the Waterpower Laboratory deserve a thanks. The social experience with these people, including everything from lunch breaks to the trip to Nepal, has been an experience for lifetime. I am grateful for getting the opportunity of taking part in this extraordinary environment.

Abstract

Hydropower laboratories are used to determine the hydraulic performance of model turbines, which can then be used as an indication of expected prototype operation. The rules and guidelines for performance of complete model tests are provided by the international IEC 60193 [2] standard. An important part of model testing is the determination of turbine shaft torque and axial forces.

The objective of this thesis is to design a system for measurement and calibration of friction torque and axial load on the Francis turbine test rig for both the Waterpower Laboratory at NTNU and the Turbine Testing Laboratory at Kathmandu. The systems must comply with the requirements of IEC 60193 [2].

The friction torque measuring system at the Waterpower Laboratory is based on the existing setup, with a load cell attached to an arm, sensing the torsional movement of the bearing cover. A linear stepper has been introduced to the design, to counteract the frictional forces of the membrane. The system has been evaluated for total systematic uncertainty.

Pressure taps inside the hydrostatic bearing are used to measure axial forces acting on the Francis turbine at the Waterpower Laboratory. A design has been developed for calibration of the pressure transducers, able to perform calibration of forces in both axial directions. Stress analysis are performed on the consisting parts, and total systematic uncertainty of the setup is determined.

For the Turbine Testing Laboratory, the friction torque and axial loads are measured with silicon strain gauges. The existing shaft and bearing design has been modified to fit the space requirements of the measurement setups. A telemetry system is utilized for wireless transmission of the signal.

3D model of the Francis turbine test rigs at both Waterpower Laboratory and Turbine Testing Laboratory are developed. Detailed machine drawings of the measurement setups are presented in this thesis.

Sammendrag

Vannkraftslaboratoriet benyttes til å bestemme hydraulisk ytelse av turbin modeller, for så å bruke dette til å anslå driftstilstanden til prototypen. Retningslinjer for gjennomføring av laboratorietester på modellturbiner er gitt av den internasjonale IEC 60193 [2] standarden. En viktig del av testene er å finne momentet levert til akslingen, samt fastsette aksielle krefter som virker på turbinen.

Målet med denne oppgaven er å designe et oppsett for måling og kalibrering av friksjonsmomentet og aksielle krefter på en Francis turbin for både Vannkraftlaboratoriet på NTNU og Turbine Testing Laboratory Kathmandu University (KU). Oppsettet skal tilfredstille kravene til IEC 60193 [2].

Målesystemet for friksjonsmomentet på Vannkraftslaboratoriet er basert på et eksisterende design, med en kraftcelle som måler momentet ut ifra bevegelsen til en arm montert på thrust blokken. En linjær aktuator er introdusert i det nye konseptet; noe som gjør det mulig å kontrollere momentet påført av membranen. Måleoppsettet har blitt analysert for systematisk usikkerhet.

Aksielle krefter på Francis turbinen på Vannkraftlaboratoriet er målt ved hjelp av trykkinntak på det hydrauliske lageret. Et konsept for å kalibrere disse trykksensorene for krefter i begge retninger er blitt utviklet i dette prosjektet. Spenningsanalyse av komponentene er utført, og den total systematiske usikkerheten er fastsatt i rapporten.

For Turbine Testing Laboratory på KU er friksjonsmomentet og aksielle kreftene målt ved bruk av strekklapper. Det eksisterende designet av thrustblokk og aksling er blitt modifisert for å passe med plassbehovet til strekklapp målingene. Telemetri er benyttet for trådløs overføring av måledata.

3D modeller av Francis turbin test riggene på både Vannkraftlaboratoriet og Turbine Testing Laboratory er utviklet. Detaljerte maskintegninger av måleoppsettene er også presentert i denne rapporten.

Table of content

Contents

List of Figures

List of Tables

Nomenclature

Symbol	Description	Units
n	Rotational speed	rpm
D	Diameter	m
r	Radius	m
B	Inlet height	m
h	Head	m
Q	Volumetric flow rate	m^3/s
z	Height	m
P_t	Total power	W
P_h	Hydraulic power	W
P_m	Mechanical power	W
T	Torque	Nm
T_m	Mechanical torque	Nm
T_{Lm}	Friction torque	Nm
η	Efficiency	$-$
η_h	Hydraulic efficiency	$-$
μ	Coefficient of friction	$-$
g	Gravitational constant	m/s^2
F	Force	N
ρ	Mass density	kg/m^3
p	pressure	Pa
E_s	Specific energy	W
M	Moment	Nm
H_n	Net head	m
ω	Angular velocity	rad/s
f_x	Relative uncertainty in measurement x	$-$
e_x	Absolute uncertainty in measurement x	$-$
s_c	Standard deviation	$-$
E	Young's modulus	N/m^2
σ	Stress	N/m^2
ε	Strain	$-$
τ	Torsion	N/m^2
L	Cycles	$-$
σ_y	Yield strength	N/m^2

Abbreviations

NTNU	Norwegian University of Science and Technology
KU	Kathmandu University
TTL	Turbine Testing Laboratory
CAD	Computer Aided Design
API	Application Programming Interface
mwc	meters water column
BEP	Best Efficiency Point
rpm	revolutions per minute
UTS	Ultimate tensile strength
SF	Safety factor

Chapter 1
Introduction

The Waterpower laboratory at NTNU is one of the main research facilities on hydropower in Scandinavia. The Laboratory consists of two main test rigs, Francis turbine test rig and Pelton turbine test rig. Different methods are available for controlling the water reservoir conditions, with an upper and lower reservoirs giving a maximum natural head of approximately 15 meters. The system can also be operated in closed loop, where a head of 100 meters can be obtained. Both test rigs are well equipped with every necessary accessory in order to satisfy the requirements of international standards for model acceptance tests [2]. This also includes measurement and calibration of friction torque and axial forces on the turbine units. The current arrangement for calibration of these measures on the Francis test rig are considered inadequate, and require an upgrade.

The individual challenges of the arrangements are discussed in Chapter 3. This work covers the new design for friction torque and axial load measurement systems with a goal of improving the related uncertainties.

For several years there has been a close research collaboration between NTNU and the University of Kathmandu in Nepal. Even though it is located between two of the world's fastest growing economies, India and China, Nepal is considered to be among the poorest countries in the world. One of the main challenges of Nepal is to meet the increasing energy demand in the region. With an estimated potential hydropower resources of 42 000 MW, the country is exploiting only 750 MW, equivalent to 5% of the total potential [12]. This has been a major objective for the government officials in recent years, with an intention of increasing the energy production from hydropower to 38000 MW within year 2035 [16]. In order to aid and support the research on hydropower, a Turbine Testing Laboratory (TTL) has been developed at the University of Kathmandu. The staff at NTNU has aided in this development, with several related projects

conducted on the subject in recent years. The goal is to make TTL a research facility that meets the requirements of IEC 60193 [2], with the possibility of conducting complete model acceptance tests in the laboratory.

TTL has been operating since 2011, yet there is still a lot of work remaining. As of today, the Francis test rig in the facility only contains parts of pipe arrangement along with the steel frame to support the turbine units. As a cooperation between the Waterpower Laboratory and Turbine Testing Laboratory, this work suggests a bearing design for calibration and measurement of friction torque and axial forces on the Francis test rig at TTL. The purpose is to propose an initial design, from which improvements and adjustments can be implemented towards developing a final solution.

1.1 Objective and Scope

The objective of the thesis is divided in two categories:

- Waterpower Laboratory, NTNU, Norway
- Turbine Testing Laboratory, Kathmandu University, Nepal

The first part is to complete the remaining work on the new, recently received thrust block at the NTNU Waterpower Laboratory. This includes the design of a system for measurement and calibration of friction torque and axial load on the shaft. The scope of the thesis is to design the setups, develop 3D models along with corresponding machine drawings and estimate the related uncertainty.

For the Turbine Testing Laboratory in Kathmandu, the task is similar, with the main objective on the design of friction torque and axial load measuring systems for the Francis turbine test rig. As the rig lacks most of the initial components, the dimensional values of the Francis turbine at the Waterpower Laboratory are used in the process of designing the setups. A critical constraint for the task is the economical aspect of the design. The objective is to suggest a solution that is simple and cost efficient, and meets the requirements of the international standard for model acceptance tests, IEC 60193 [2].

Chapter 2
Theory

The first part of this chapter covers the fundamental theory of bearing design in hydraulic turbines. Evaluating friction in rotating parts is essential when determining the total efficiency. Bearings, often being the only connection between the rotating and stationary parts in rotating machinery, are one of the main sources of mechanical friction losses in Francis turbines.

Friction losses in bearings is a topic too extensive to be covered in detail in this report. This chapter provides the fundamental theory of friction forces in bearings, as well as simplified calculation methods for approximate estimation of performance parameters, such as moment and power loss. The theory is mainly concentrated around ball bearings and hydrostatic bearings, as these components are most relevant for further design. For full coverage on the subject, Ref. [17], [18] and [19] are listed as the main sources.

Section 2.4 gives an introduction to IEC 60193 [2], and its importance in model testing of hydraulic machines. The guidelines of this standard have been crucial in solving of the tasks.

The chapter is concluded with a short description of PTC Creo Parametric 3.0 and Ansys Workbench, as the software's have been frequently used throughout the project.

2.1 Vertical Francis Turbine

Francis turbines can be mounted vertically or horizontally. Vertical mounting of the turbine is more space efficient, as it reduces the horizontal plan area and permits a deeper setting of the turbine with respect to tailwater elevation [34]. A disadvantage is the generator cost, increasing with larger units due to the higher axial loads. However, this increase in equipment cost becomes insignificant compared to the reduced construction costs with use of vertically aligned units in case of large

hydropower plants. In general, horizontal turbines are economically advantageous only for small high speed applications where standard generators are available.

In order to understand the requirements on the bearings of a vertical shaft, it is important to define several aspects around vertically installed turbines. The first thing is the shaft alignment. Accurate shaft alignment is necessary in order to obtain trouble free operation of the turbine. A misaligned unit will cause excessive vibrations, and wear down not only bearings, but also other parts of the machinery [9].

Vertical shaft turbines are also exposed to a larger load distribution in vertical direction than horizontal turbines. The axial loads are higher for vertical shafts, as the rotating weight of the turbine, shaft and bearing assessment are contributing to the increased weighting load. Additionally, the axial hydraulic forces present during operation of the unit, can become significantly large for high head operational conditions. This puts high requirements on the bearing connection between the generator and the turbine.

2.2 Bearings in rotating machinery

Bearings in hydropower turbines are used to support the rotating shaft. The main purpose is to shift the dynamic loads apparent on rotating parts of the turbine over to the bearing. An important aspect of bearing design is to extend the bearing life in the machinery, while minimizing friction between the moving parts. The bearings are also used to prevent a motion in axial/radial direction by controlling the vectors of normal forces that bear on the moving parts.

Bearings are divided in two main categories; *contact bearings* and *non-contact bearings* [8].

2.2.1 Contact bearings

In contact-type bearings, the consisting components are in mechanical contact to each other. Wear and fatigue due to frictional forces is critical for this unit. There are numerous types of contact bearings, with small deviations in design depending on the application requirements. The most common types of contact bearings used in turbomachinery are listed below.

Ball bearings

The basic design, consisting of balls rolling between inner and outer surface tracks, is frequently used in turbomachinery. With the raceway closely conforming to the rolling ball-elements, the unit can handle loads in both axial and radial directions. With relatively small contact points between the rolling elements and races, the bearings are vulnerable when exposed to larger loads. The simple design and low friction between the contact surfaces make ball bearings ideal for smaller, low cost applications.

Roller bearings

Often referred to as cylindrical, or needle, these bearings are perfectly suited for areas exposed to high loads. The roller function is provided by a number of cylindrical elements mounted between to circular surfaces. The bearings are low friction, and the elongated contact area can withstand high radial forces. As a result of the longer contact surface, the ability to withstand loads in axial direction is reduced, making the units unsuitable for thrust load applications. There are, however, other types of roller bearings specially designed to handle high axial loads, such as *Tapered Roller Bearings* and *Roller Thrust Bearings.* Roller bearings are space efficient, cost efficient, and are often utilized in areas of turbomachinery where high radial loads are present.

Sliding contact bearings

Sliding contact bearings are mostly used when the contact elements are of different material. The shaft is in sliding contact with the inner bearing ring, while the outer ring is held stationary. Due to the large contact area, the bearing has high requirements for lubrication in order to reduce the wear and friction. A common type of sliding bearing used in vertical hydro power units is the thrust bearing. The bearing supporting pressure is parallel to the vertical shaft alignment, and the unit is

designed to withstand high axial forces. The high friction uncertainty makes sliding bearings less accurate in comparison to other types of contact bearings.

As mentioned in the introduction to this section, there are numerous types of contact bearings used in hydropower turbines, and only the most common types are reviewed. The theory in this chapter is from "*Bearing Design in Machinery",* [8].

2.2.2 Non-contact bearings

Non-contact bearings are friction-free connections, consisting of two surface elements separated by either a fluid, or a magnetic field. The bearings are characterized by high load handling capability and low maintenance requirements. There are two types of non-contact bearing; *fluid bearings* and *magnetic bearings*.

Hydraulic bearings

Hydraulic bearings are frequently used in hydropower units in Norway. The concept consist of a thin layer of fluid between the bearing surfaces supporting the load in both axial and radial directions. These bearings are classified into two main types: *hydrodynamic* and *hydrostatic*. In case of hydrodynamic bearings, the load is supported by a lubricant film located in between the bearing surfaces. The bearing is robust, with simple design, high load capacity and easy manufacturing, but suffers from fluid whirl when it comes to high rotational speeds. Hydrostatic bearings use external high pressure fluid for load support. The fluid, usually pressurized oil, is kept in place with a surrounding bearing block, which is in turn connected to a hydraulic supply. Correct design of the bearing block is essential in order to achieve the desired output. It is a complex unit, described in detail in Chapter 3. High load capacity, noise and vibration reduction and extended lifetime make hydraulic bearings ideal for large, high speed application. They are also cost efficient due to the low maintenance requirements, as the only wearing to this unit comes from start-up and shutdown operations. A disadvantage of hydraulic bearings is that they are highly sensitive to grit or dust containments, which might lead to quick failure of the unit.

Magnetic bearings

These bearings rely on magnetic fields to separate the surface faces. The load is supported using magnetic levitation, and similar to hydraulic units, they can handle high loads in both directions. With practically no speed limit and low maintenance time, these bearings are suited for almost any application. The main disadvantage of these units is the operational cost. Use of magnetic bearings is expensive compared to other bearing types. In order to keep the load stable, these units require a constant supply of power input along with an active control system. Reliability is also a questionable aspect of the bearing. Units operating on magnetic bearings often require additional bearing, in case of system failure.

2.3 Friction in Bearings

Reduced friction in bearings is important for higher efficiency output of hydraulic machines. The evolution of bearings is shaped around this demand, which involves improved shape, material selection and lubrication fluids. Naturally, fluid based components, such as journal and hydrostatic bearings, have a significantly lower frictional coefficient than contact bearings. In case of hydro turbines, the rotating components are often supported by a combination of contact and non-contact bearings.

The theory in this section is from "*Rolling-Element Bearings"* [17], *"The ball bearing: In the making, under test and on service"* [18] and "*Applied Tribology: Bearing Design and Lubrication"* [19].

2.3.1 Rolling bearings

Friction in rolling, contact bearings is defined as roller friction. There are several contributing factors to roller friction. One of the main causes is the slip effect. Heathcote [18] explained this phenomenon as the required energy to overcome the interfacial slip occurring due to the curved shape of the bearing design. In Figure 2.1, four points on the inner surface are marked: a, b, c and d. Points a and b indicate contact spots of the ball and inner bearing race, whilst c and d represent

the location of the rolling bands. As the ball is rolling around y-axis, the curved shape of the surface leads to a different radial velocity of points a-b and c-d with respect to y-axis. Unless the rolling element is highly elastic, which rarely is the case, an interfacial slip must occur at various points on the surface. The three arrows indicate the direction of this slip (Fig. 2.1). According to Heathcote [18], the force required for rolling the ball is equal to the friction caused by this interfacial slip.

The direct contact of the rotating elements causes heat dissipation and deformation in the material, due to the weight of the rollers/balls in combination with the applied load.

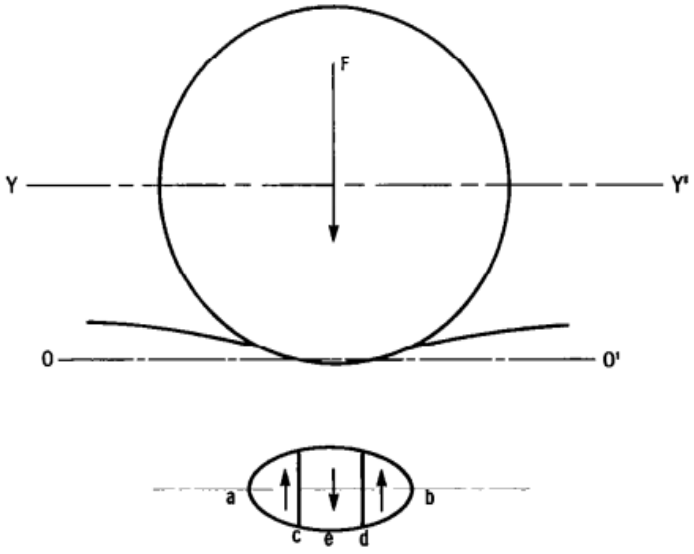

Figure 2.1: Interfacial slip in roller bearings [17]

All materials are elastic, and some sort of compression will occur on either the rolling element, or the guiding surface. Unless prevented by friction, the variation in stresses of the two contacting surfaces will result in additional slip loss. This is known as hysteresis losses, with a limiting friction force defined by Tabor [20] in Equation (2.1):

$$T = \frac{0.2\mu D_y^2 F}{r_{ax}^2} \quad [N] \tag{2.1}$$

Where μ is the friction coefficient, D_y is the diameter of the elliptic contact surface, F is the applied force and r_{ax} is the ball radius.

Including the elastic energy lost in the compression, the following equation is obtained:

$$T = c_4 \curlywedge \frac{F D_y}{r_{ax}} \quad [N] \tag{2.2}$$

Where

$$\curlywedge = \frac{\pi D_y^2 E'}{4 \mu r_{ax}^2 p_m} \quad [-] \tag{2.3}$$

p_m – Mean pressure

E' - Effective modulus of elasticity

c_4 is a constant dependent on the shape of contacting surfaces. Tabor [20] defines it as $1/3$ for rectangular contacts, and $3/32$ for elliptical contacts.

In case of angular ball bearings under thrust loads, additional spinning friction is present. This is due to the tendency of the balls to rotate about an axis perpendicular to the leading contact surface. Furthermore, lubricated bearings have seals, and frictional forces will be present between the sealing element and its counterface. Inadequate lubrication or high viscosity of the fluid will increase the magnitude of these friction forces, especially at startup phases when the fluid temperature is low. Finally, there is the viscous drag forces of the lubricant, which are dependent on the amount and viscosity of the fluid as well as the rotational speed of the shaft.

It is also important to note that roller bearings are very stiff. Any misalignment or thermal expansion will result in additional loads on the unit.

To sum it up, there are several factors affecting the magnitude of the frictional forces [17]:

- Bearing Size
- Bearing Design
- Forces
- Shaft speed
- Lubricant properties
- Lubricant quantity

This complex nature of friction forces complicates accurate estimation of friction coefficient, μ. As per today, this parameter is estimated using numerical computations.

Assuming good lubrication and normal operating conditions, the coefficient of friction can be approximated constant, and moment, M, is calculated using Equation (2.4).

$$M = 0.5 \cdot \mu \cdot P \cdot d \quad [Nmm] \tag{2.4}$$

When it comes to forces on a bearing unit, it is distinguished between static and dynamic loads. The static loads are mainly due to the magnetic pull caused by the eccentric rotor position in the generator stator [27], uneven properties of the flow and poor bearing alignment [26]. The dynamic loads are caused by the unsymmetrical design of the turbine and generator rotors, as well as the turbulent flows in the turbine [26]. In Equation (2.4), P is the dynamic bearing load and d is bearing bore diameter.

For calculation of start-up friction, it is suggested use of a friction coefficient 60 % higher than the running value [19].

2.3.2 Hydrostatic bearings

The power loss in a hydrostatic bearing is less than for contact bearings, due to a lower friction coefficient. Unlike the contact bearings, which are forced to overcome the static friction at start-up, hydrostatic bearings have zero static friction. The dynamic friction will depend on the fluid viscosity and effective gap area, h_0, illustrated in Figure 2.2. The pressure in this gap will reduce gradually due to the viscous friction, this being a result of shear stresses between the fluid and surface wall, and internal viscous forces of the fluid. The gap area is in turn controlled with flow rate of the external pump, Q. Counteracting this movement is the load from the shaft, W, which, under steady conditions, equal the external thrust load on the shaft.

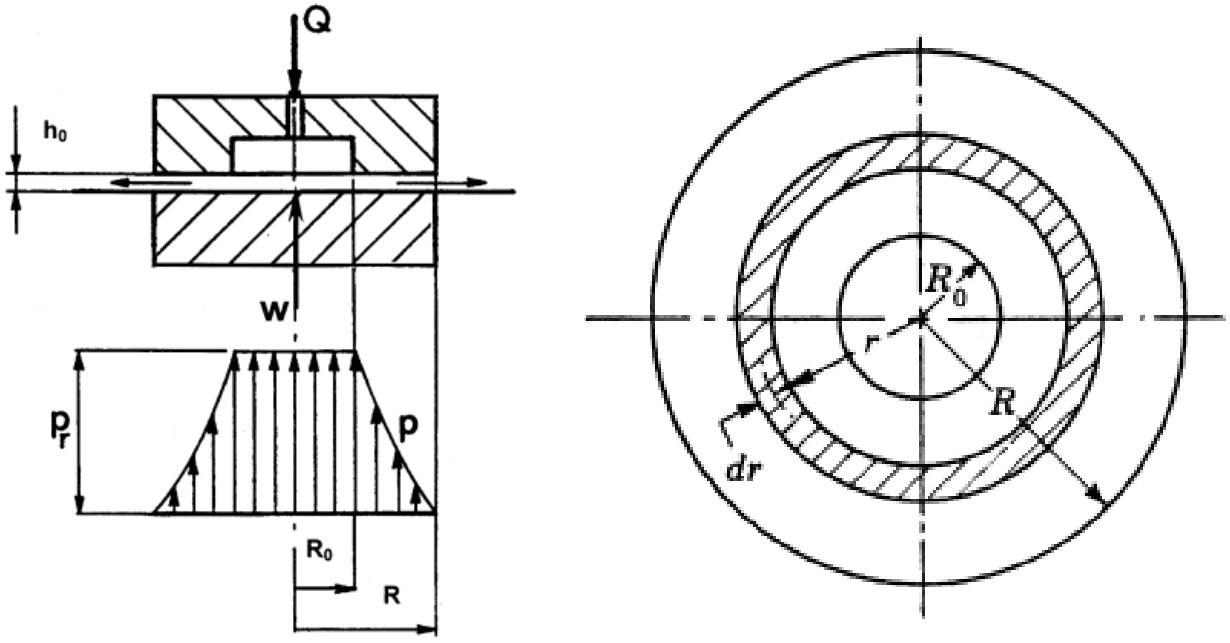

Figure 2.2: Hydrostatic bearing, with lubrication and pressure distribution [8]

The power consumption in the hydrostatic bearing is defined as the combination of mechanical and hydraulic power required to overcome the viscous forces of the lubricant, given in Equation (2.5).

P_m – Mechanical power required to overcome the frictional torque resulting from viscous shear of the lubrication fluid.

$$P_m = T_m \omega \quad [W] \tag{2.5}$$

$$T_m = \frac{\pi}{2} \mu \frac{R^4}{h_0} \left(1 - \frac{R_0^4}{R^4}\right) \omega \quad [Nm] \tag{2.6}$$

$$P_m = T_m \omega = \frac{\pi}{2} \mu \frac{R^4}{h_0} \left(1 - \frac{R_0^4}{R^4}\right) \omega^2 \quad [W] \tag{2.7}$$

Where

R – Radius of the circular pad

R_0– Radius of the recess

ω – Angular speed of the shaft

T_m– Mechanical torque

P_h is the hydraulic power required to pump the fluid through the gap. Neglecting power loss in inlet pipes, this power can be expressed as:

$$P_h \approx Q p_r \quad [W] \tag{2.8}$$

Which gives a total power consumption:

$$P_t = P_h + P_m \, [W] \tag{2.9}$$

$$P_t = Q p_r + \frac{\pi}{2} \mu \frac{R^4}{h_0} \left(1 - \frac{R_0^4}{R^4}\right) \omega^2 \quad [W] \tag{2.10}$$

Substituting flow rate Q and dividing by the efficiency of the drive, η_1, and the pump, η_2, the power consumption in form of consumed electricity is obtained:

$$P_t = \frac{1}{\eta_2} \frac{1}{6} \frac{\pi h_0^3}{\mu ln(R/R_0)} p_r^2 + \frac{1}{\eta_1} \frac{\pi}{2} \mu \frac{R^4}{h_0} \left(1 - \frac{R_0^4}{R^4}\right) \omega^2 \quad [W] \tag{2.11}$$

Similar to contact bearing theory, the friction coefficient of hydrostatic bearings depend on several factors, and can be estimated only with the help of numerical computations.

2.4 IEC 60193 "Hydraulic turbines, storage pumps and pump-turbines – Model Acceptance tests"

The international IEC 60193 standard [2] provides rules and recommendations for conduction of model acceptance tests in laboratory applications. The guidelines apply for both impulse and reaction turbines, covering every aspect of relationship between the prototype and the model. Main objective of the standard is to provide the reader with information on correct measurement of the involved quantities, in order to ascertain the hydraulic performance of the model. In addition to the experimental conduction, the standard also provides valuable information on processing, analysing and reporting of data.

For this report, the guidelines on measurement of shaft torque, section 3.6 [2], and axial and radial thrust forces, section 4.5 [2], have been frequently utilized for solving the tasks. The standard has also been an essential tool during material selection, equipment study and conducting uncertainty analysis.

2.5 PTC Creo Parametric 3.0.

PTC Creo Parametric 3.0 is a Computer Aided Design (CAD) software for three-dimensional modelling. This is a new software, released in 2011, with a highly expanding popularity. PTC Creo is developed for windows software, and build around a number of key C modules of different Application Programming Interfaces (APIs). This design software offers numerous application capabilities, from simple sketching to the complete design for Additive Manufacturing, 3D printing.

For this project, PTC Creo Parametric is mainly used for modelling of solids, as well as producing the machine drawings.

2.6 Ansys Workbench

Ansys Workbench is a platform for advanced engineering simulation. The software consists of a number of simulation and stress analysis tools, and can be utilized in every aspect of structural analysis.

With a build in bi-directional connectivity to Creo Parametric, the software can be used to conduct simulations on imported geometries. Static Mechanical, which is a subsection of the Workbench accessories, is used in this thesis for stress analysis of the designs.

Chapter 3
Background and Previous Work

Waterpower laboratories around the world have played an important role in research and development of hydropower. One of the main applications is performing model tests for prototypes. This is more cost efficient, as the efficiency of the runners can be improved substantially before the actual production. Numerical analysis of flow characteristics is not sufficient enough, and require additional model testing in order to accurately map the performance of the turbine.

3.1 Waterpower Laboratory, NTNU

The Waterpower Laboratory at NTNU is a certified model testing facility, following the guidelines of IEC 60193 [2]. The laboratory was built in 1916, with a complete refurbishment in 2006. The current lab arrangement consists of two water reservoirs, a pressure tank, a surge tank and two pumps with a power output of 350 kW each. Thee turbine test rigs can be operated in the laboratory, Francis turbine, Pelton turbine and a small turbine loop. All the rigs are in accordance to IEC 60193 [2]. The piping and reservoir arrangement allows for operation of the turbines in both open and closed loops. The pressure tank, which can sustain a maximum pressure of 10 bar, can provide a head of 100 meter water column (mwc) in closed loop operation. This gives the laboratory a large range of testing abilities when it comes to model testing.

The Francis turbine at Waterpower Laboratory is mounted vertically, with the generator located on top of the rig, as shown in Figure 3.1. The turbine consists of following main components [5]:

- Draft tube (1)
- Runner (2)
- Guide vane cascade (3)
- Regulating mechanism (4)
- Spiral casing (5)
- Turbine housing (6)
- Shaft (7)
- Shaft seal (8)
- Bearing block (9)

The bearing block constitute for one of the most critical components in a turbine. The main purpose of the block is to support the weight of the runner and shaft arrangement. In general, the design of the block can vary significantly in both shape and size, and is often supplied with auxiliary lubricant, such as oil or grease.

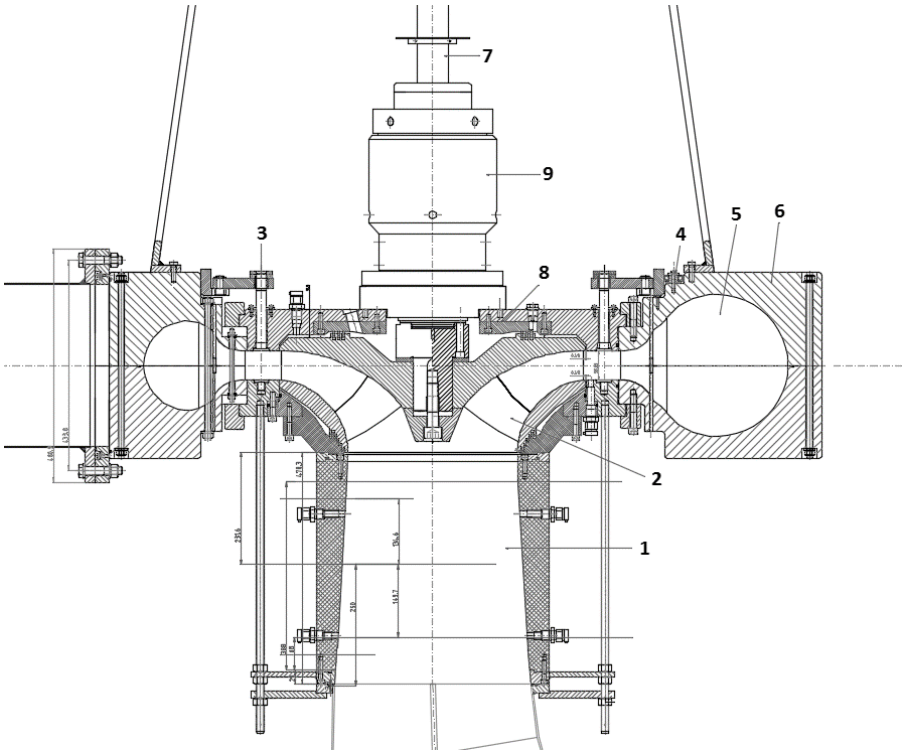

Figure 3.1: Model Francis turbine, Waterpower Laboratory, NTNU.

3.1.2 Bearing block

In order to understand the problem of friction torque measurement in hydrostatic bearings, the design of the bearing block has to be examined. The block connects the rotating parts of a turbine with the stationary structure surrounding the unit. In a vertically aligned turbine, the block acts as a hydrostatic bearing, supporting the axial and radial loads of the turbine. This type of solution is often found in large hydropower units, where the unit is exposed to high loads, while at the same time having to satisfy high demands for accuracy in axial positioning of the shaft. There are numerous advantages coming with this design. The wear due to direct contact at the start up is minimal, higher precision in comparison to other designs, and prevention of overheating of the bearing due to the constant circulation of oil [8]. As mentioned in section 2.2.2, the unit is highly sensitive to dust and grit, and a proper oil filter is a requirement for safe operation.

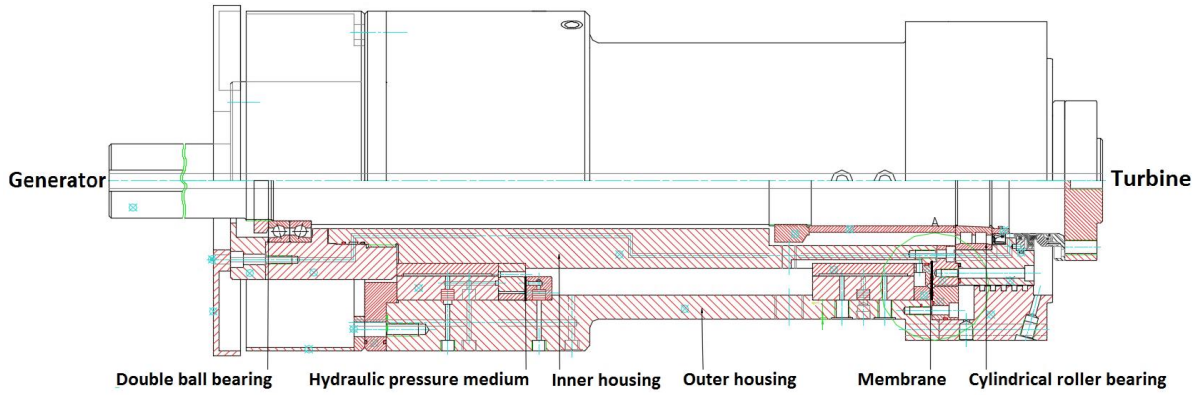

Figure 3.2: CAD-drawing of the bearing block, Water Power Laboratory, NTNU.

Figure 3.2 shows the hydrostatic bearing block at the Waterpower Laboratory. The 786 mm long vertical shaft is enclosed in a thrust block, consisting of an inner and outer housing unit. The outer unit is stationary, while the inner unit is only affected by the frictional forces of rolling elements. Two bearing units are used to connect these two housing components. The upper bearing is a double ball bearing with a back-to-back arrangement, shown in Figure 3.3. In this arrangement, the bearing is preloaded due to the small gap between the inner races, providing it with a higher moment stiffness than regular units. It can, if necessary, ensure the shaft retention on its own due to the rigidity. The axial loads on the thrust block are transferred through the ball bearing, to the inner

bearing house and downwards to the cavity between the two housing, supported by hydraulic pressure medium (Fig. 3.2). The pressure in this section is measured with several pressure taps located around the block. Knowing the pressure, p, and area supported by the fluid, the force is calculated using Equation (3.1):

$$\mathrm{F} = \frac{\pi \mathrm{d}^2}{4} \cdot \mathrm{P} \quad [N] \tag{3.1}$$

A double-row, cylindrical roller bearing is used for lower connection of the block, shown in Figure 3.4. This bearing is well suited for high speed and accuracy requirements due to its excellent rigidity. As it is located close to the runner, the main purpose of the bearing is to absorb radial forces of the turbine.

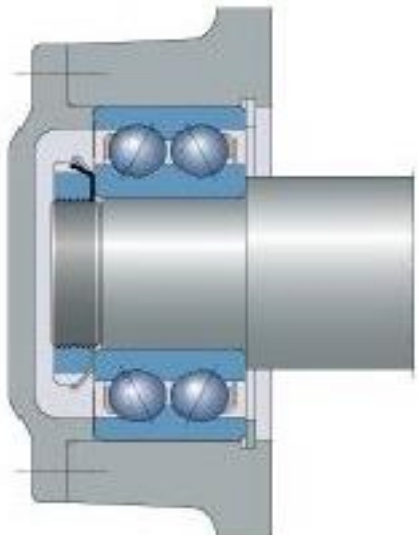

Figure 3.4: Angular contact ball bearing [10]

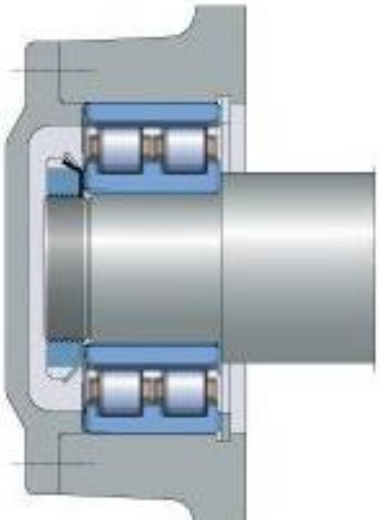

Figure 3.3: Cylindrical roller bearing [10]

During operation, the radial movement of the shaft is retained by the external pressurized oil surrounding it. The fluid flow to each side of the bearing creates a pressure differential proportional to the displacement of the rotating element. The total friction in this hydrostatic bearing is the sum of the static friction of the rolling bearings, and the dynamic friction of the fluid, which in turn is dependent on the gap and viscosity of the oil.

Ideally, the two bearing units would be the only connection between inner and outer housings, where bearing friction is the only mechanical friction present.

The friction forces may be determined by using an arm and a load cell mounted on the inner and outer housing covers respectively. This method is closer described in Chapter 4. However, hydraulic units require some type of sealing connection in order to retain/separate the fluids, which gives a second source of direct contact. In Figure 3.2, a membrane is located at the lower section of the block, separating the cooling water from the exiting oil. The elastic membrane provides a slight movement when exposed to radial forces. The outer housing cover of the block, which should only experience the mechanical forces of the bearing connections and the viscous forces of the fluid, has an additional restriction in movement perpendicular to the elasticity of the membrane. For a turbine in operation, this introduces counteracting forces in the membrane due to the movement of the inner housing cover caused by friction in bearings. The current friction torque measuring system at Waterpower laboratory does not account for the counterforces in the membrane, and measurements are often characterized with high uncertainty.

3.1.3 Generator torque measurement

The generator torque of the Francis test rig at NTNU is measured with a Hottinger Z6FC3 type load cell attached to an arm, which in turn is mounted on the generator [1]. The load cell is based on strain-gauge sensing element, producing voltage signal proportional to the stretching/compression of the sensing material. An external amplifier with a range of 0-10 V is used for signal amplification.

According to IEC 60193 Section 3.6.2.2 [2], this is a secondary method of measuring generator torque and requires calibration by the primary method. This is done with use of calibrated weights, where the load cell produces a voltage signals proportional to the applied force of the weights. This is, in turn, used to obtain calibration curve for the load cell mapping the uncertainty of the cell.

3.1.4 Friction torque measurement

Friction torque is measured similarly, with a HBM load cell attached to an arm [1]. The arm is mounted on the inner housing cover of the bearing block, moving proportionally to the friction forces of the bearing and seals. The force cell senses this movement as force, and the torque is calculated by multiplying the force with arm length. This torque measuring method is described as

"Bearing of rotating parts not in balance" in IEC 60193, section 3.6.1 [2]. An important aspect of this method is that the friction torque is measured separately, distinguishing between generator torque T, and friction torque, T_{Lm}.

Calibration process described in section 3.1.3 is used for calibrating the friction torque measuring load cell as well. Calibrated weight, ranging from 0-10 kg, are used to obtain the calibration curve and uncertainty percentage of the cell. The procedure is provided in Appendix G.1.

3.1.5 Axial thrust measurement

Axial thrust force is measured using differential pressure transducers inside the bearing block [1]. The oil pressure is supplied to the transducers from the two section of the axial thrust bearing, and an output signal of 4-20 mA is produced. The range of the differential pressure transducers is 0 to 3000 kPa, corresponding to 1230 kg.

The transducers are calibrated using high load calibration weights. These weights are supported with a hanging fixture secured to the shaft, and the relation between the measured pressure and the applied weights is given by equation (3.2):

$$F = W \cdot g = \frac{p}{A} \quad [N] \tag{3.2}$$

Where F is the force $[N]$, W are the weights $[kg]$, P is the pressure $[N/mm$], A is the effective area $[m^2]$ and g is gravitational constant $[m/s^2]$. Full calibration procedure is provided in Appendix G.2.

3.1.6 Previous work – Waterpower Laboratory

There is no documented work available on the design of the specific friction torque measurement system of the Francis test rig. The apparatus was manufactured and installed by the staff at the Waterpower Laboratory, and no specifications or drawings are available from the procedure.

A former master student, Kyrre Reinertsen, wrote his thesis on design and manufacturing of the bearing block and friction torque measurement system for the Pelton turbine test rig [13]. The design is based on existing bearing block at Hochshule Luzer Laboratory in Zurich. The bearing block, along with the friction torque calibration and measurement setup can be viewed in Figure 3.5.

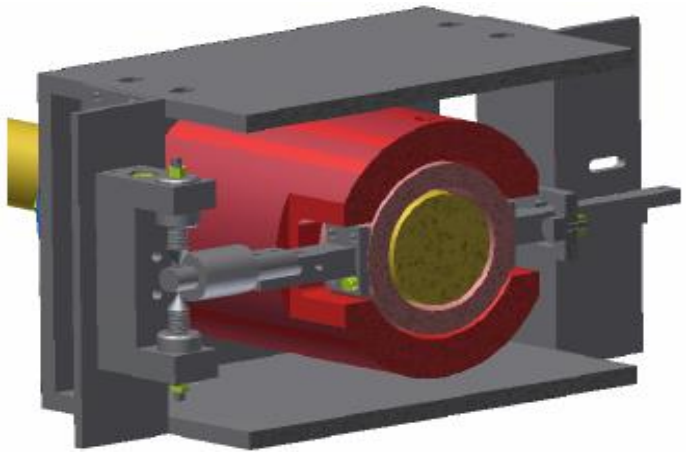

Figure 3.5: Pelton turbine friction torque calibration setup

The concept consists of four main elements: An inner and outer cylinder, the shaft and a bearing enclosure. Six roller bearings are used for connection of the components. The shaft is connected to the inner cylinder with two bearings, one on each side of the enclosure. The inner cylinder is in turn connected to the outer cylinder with additional four bearings. Inner cylindrical part is in free rotation, only affected by the mechanical friction of the rolling elements. Friction torque in bearings can be determined by applying a force cell to this freely rotating part. On the far right side of the block (Fig. 3.5), a beam is located for calibration of the force cell. Such designs are frequently used in rotating machinery where application requires regular calibration of the measuring equipment. Reinertsen concludes the paper highlighting at a total uncertainty of 2.5% for operation at best efficiency point (BEP) using this method of measurement.

3.2 Turbine Testing Laboratory, Kathmandu University

The building of Turbine Testing Laboratory at Kathmandu University started in year 2000, with a purpose of creating a facility for performance testing of model hydropower turbines. The goal is to build the laboratory similar to the Waterpower laboratory, with respect to the requirements of IEC 60193 [2].

The complete design of the Turbine Testing Laboratory includes two reservoirs, two pumps, piping arrangement, pressure and surge tanks, calibration tank, electric overhead travelling cranes (EOT) and a Francis and Pelton test rigs. As of today, the reservoirs, pumps, EOT crane and the Pelton rig are in place. The reservoirs are positioned such that a natural head of 30 m is obtainable. The lower reservoir is located beneath the building, and has a storage capacity of 300 m^3, while the upper reservoir is situated on a hill outside the laboratory, with a storage capacity of 100 m^3 [15]. Two pumps, slightly smaller than those at Waterpower Laboratory, with a power output of 250 kW each, are able to provide the system with a flow of 0.25 m^3/s.

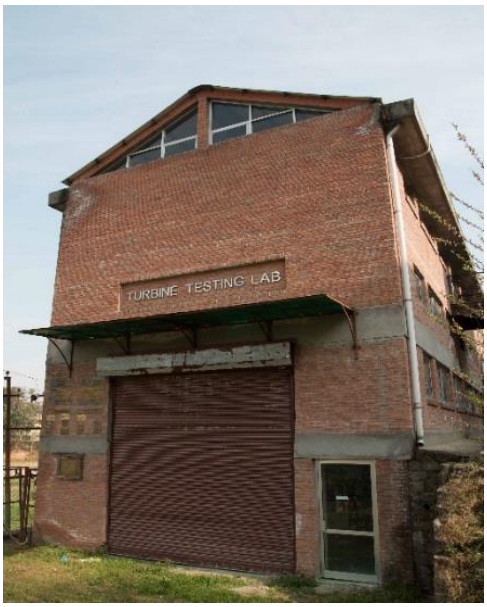

Figure 3.7: Turbine Testing Laboratory

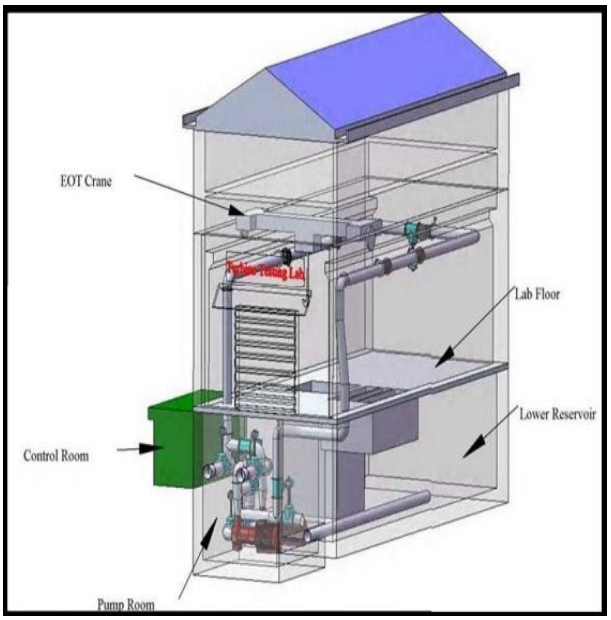

Figure 3.6: Schematic presentation of TTL [16]

The

The Pelton test rig is complete, with inlet/outlet piping, generator, shaft connection and the runner. The Francis rig lacks all of its essential components. As per today, the rig consists of a stationary frame, along with a simplified test arrangement implying the design and location of the turbine. As part of this thesis, a suggestion is made for the design of a shaft coupling that will, in addition to connecting the generator and turbine, prevent the axial and radial forces from propagation to the essential parts of turbine. The design includes measurement and calibration of friction torque, generator torque and axial/radial thrust forces.

Figure 3.8: Simplified Francis turbine test rig, TTL

3.2.2 Previous work – Turbine Testing Laboratory

In cooperation with NTNU, several projects have been conducted on development of TTL in recent years. Bidhan Rajkarnikar Halwai, a master student at NTNU, developed as part of his thesis a design of the Francis turbine test rig for TTL [15]. The design was modified somewhat by the staff at TTL, before manufacturing and installing the arrangement seen in Figure 3.7. For measurement of generator torque, friction torque and axial thrust forces, Rajkarnikar suggested use of methods similar to the Francis test rig at NTNU, including a hydrostatic bearing block with external oil suppling pump.

Inger Johanne Rasmussen did, in her master thesis, a complete design of the Francis test rig at TTL [4], including the bearing block and friction torque measuring systems. For the shaft connection, Rasmussen suggests use of two bearing units from SKF, a double row angular ball bearing in the upper section, and a single row deep groove ball bearing in the lower section of the shaft. The angular contact ball bearing is a thrust bearing, taking up the axial loads in both directions. This results in minimal forces and extended lifetime of the lower bearing, leading to a simple and cost efficient solution.

Strain gauge based setup is suggested for measurement of axial loads on the shaft. The method is based on a test rig of *General Electric Canada Inc.* in Montreal. The concept is simple and cost efficient, and can provide, with use of correct excitation equipment, highly accurate results.

For measurement of friction torque in bearings, it is recommended to run the generator and turbine without load, and measure the combined generator and friction torque with a torque meter. This method assumes that the forces will be the same with the turbine in place.

Chapter 4

Method and Calculations

This chapter presents the method and calculations utilized for this thesis. The first section provides an insight into the model testing procedure as described in IEC 60193 [2], with the concepts of hydraulic efficiency, power and torque in particular.

Section 4.2 covers different strain gauge applications for measurement of forces acting on a turbine shaft. Strain gauges are frequently used in hydro turbine industry, and can, with correct accessories, measure axial, radial and torsional forces with high accuracy.

IEC 60193 [2] provides guidelines on uncertainty analysis in model turbine measurements. Section 4.3 covers the procedure for this analysis, with a review on how the analysis are performed and what factors are to be considered.

In section 4.4, the hydraulic forces of the Francis turbine at Waterpower laboratory are calculated in order to map the necessary calibration range of axial force measuring pressure transducers. The calculation procedure provides a quite accurate estimation of the hydraulic forces, with an approximate uncertainty of 10 % in the resulting values. These calculations also apply for the Francis test rig at Turbine Testing Laboratory, as it is assumed dimensional similarity of these two turbines.

The terms and abbreviations used in this chapter are as defined in IEC 60193 [2].

4.1 Efficiency, power and torque

When doing model testing of a turbine, a main objective is to estimate the hydraulic efficiency of the unit. This is defined as mechanical power divided by the hydraulic power, given in Equation (4.1):

$$\eta_h = \frac{P_m}{P_h} \quad [-] \tag{4.1}$$

Where P_m is the mechanical power of the runner and P_h is the available hydraulic power. The mechanical power is the power generated by the turbine runner on the shaft, and is dependent on the rotational speed, n, and the mechanical torque on the shaft, T_m.

$$P_m = 2 * \pi * n * T_m \quad [W] \tag{4.2}$$

IEC 60193 [2] describes two main methods of measuring the mechanical torque:

1. "*Bearing of rotating parts in balance*" – Here, the friction torque due to guide bearing, thrust bearing and seals, T_{Lm}, is considered as inner torque taken into account by the system itself. The shaft torque, T, and friction torque, T_{Lm}, are measured as one: $T_m = T$.
2. "*Bearing of rotating parts not in balance*" - T and T_{Lm} are measured separately, and added for determination of total torque transmission.

$$T_m = T + T_{Lm} \quad [Nmm] \tag{4.3}$$

4.2 Force and torque measurement with strain gauges

Strain gauges are used in numerous applications, and measurement of forces in hydro units is no exception.

The strain gage is a sensing element, which measures strain based on the increase or decrease in resistance of the sensing element [24]. Strain is defined as fractional change in length after a force is applied [24].

$$\epsilon = \frac{\Delta L}{L} \tag{4.4}$$

The main idea is to measure the exerted force electronically, and convert it into an electrical signal. The simple installation, low maintenance requirements and long lifetime, make strain gage sensors an attractive method for measurement of stresses on a turbine shaft.

In most applications, the strain, and the corresponding electric signal output of the gauges is too low to be perceived by the measuring equipment. Bridge configurations are utilized for the purpose of increasing the signal to readable magnitude by driving an input voltage over a set of resistors. The gauges are connected in either series or parallel, depending on the application. A common configuration is the Wheatstone bridge, illustrated in Figure 4.1 [25].

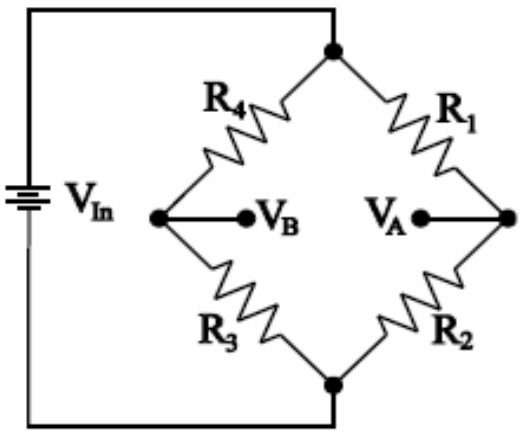

Figure 4.1: Wheatstone bridge circuit [25]

The arrangement consists of four resistors connected in a quadratic formation. R_1 and R_2, along with R_3 and R_4 are connected in series, while R_1 and R_3, and R_2 and R_4 are connected in parallel. The arrangement is utilized for measurements of small strains. The slight change in one of the resistors is increased with two wires driving excitation voltage, and two other wires measuring the voltage difference. V_{in} is the excitation voltage across the bridge, whilst the difference between V_A and V_B determines the output voltage V_{out}. The small change in resistance is turned into voltage difference with an excitation value of 4. Equation (4.5) shows the voltage output for a Wheatstone bridge circuit [25].

$$\frac{V_{out}}{V_{in}} = \frac{V_A - V_B}{V_{in}} = \frac{R_2}{R_1 + R_2} - \frac{R_3}{R_3 + R_4} \tag{4.5}$$

In addition to the excitation, the full bridge configuration also provides linear output exactly proportional to the applied force. In case of different material of the strain gauge and the measuring object, the measurements are exposed to errors if temperature variation is a factor. Different materials will expand at different temperatures, which disrupts the linear output. This is again an advantage of bridge configurations with more than 1 resistor, as the second resistor can be used to compensate for temperature variations. This compensation process requires correct positioning of the gauges, detailed in Chapter 6.4.

An important parameter of strain gauges is the sensitivity. This parameter, expressed as Gage Factor (GF), is the sensing materials ability to react to small strains.

$$GF = \frac{\Delta R/R}{\epsilon} \tag{4.6}$$

The gage factor is the main parameter considered when differentiating between the strain gauges. Silicon piezoresistive gauges for example, have a significantly higher gage factor than metal-foil wire based elements, due to the higher strain sensitivity of silicon. These high sensitivity measuring devices, known as semiconductors, depend on the piezoresistive effects of silicon, and are a preferred choice when measuring small strains. Similar to standard gauges, semiconductors measure the change in resistance with stress as opposed to strain.

Strain gauges are regularly used to measure strain and/or torque acting on a turbine shaft. For measurement of deflection in axial direction, four gauges are mounted perpendicular to the shaft axis, as illustrated in figure 5. Only two gauges are visible on the figure, gauge 3 and 4 are mounted 180 degrees apart. Element 1 and 3 are similar in axial orientation, but located on each side of the shaft. Same goes for element 2 and 4, having same axial positioning, but a 180 degree offset in the radial direction.

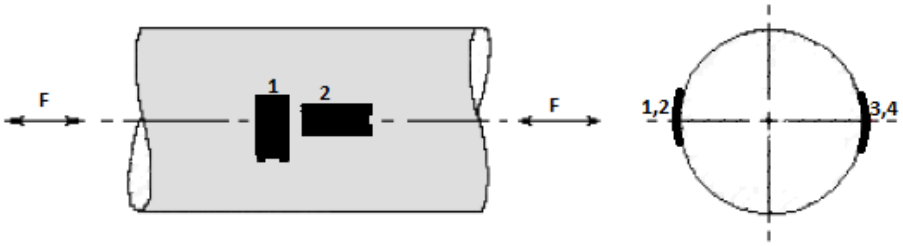

Figure 4.2: Strain gauge placement for measurement of axial deflection on a shaft

Looking at Figure 4.2, the strain in shaft due to the axial force F is measured with strain gauge 2. The placement of gauge 1, with a transverse orientation is done to compensate for possible temperature variations in the material. As the thermal outputs are equal in size and magnitude, the change in the corresponding resistances is doubled, increasing the errors of thermal expansion. As the gauge 1 and 2 are connected to the adjacent connection in the bridge circuit, shown in Figure 4.2, these temperatures induced resistances will cancel each other out.

Strain gauge 4, having same axial orientation as 2, is required due to the algebraic characteristics of the circuit relative to the resistance in each element. In case of a uniform axial force F stretching the shaft, gage 1 and 2 would measure the same strain value. But due to the same adjacent connection in the bridge, these two strains will also cancel each other out, resulting in zero output. Instead, they are connected in opposite bridge arms, 1-3 and 2-4, adding the resistance and thus doubling the output.

An important requirement when measuring stress and torque with strain gauges is that the sensors have to be placed at area of maximum occurrence. Measurements at less exposed areas are erroneous readings. Figure 4.3 shows the ideal orientation of strain gauges when measuring the

shaft torque. The transducers are placed 45° to the thrust axis, as the maximum tensile and compressive strain lie with an inclination of 45° to the shaft axis [24].

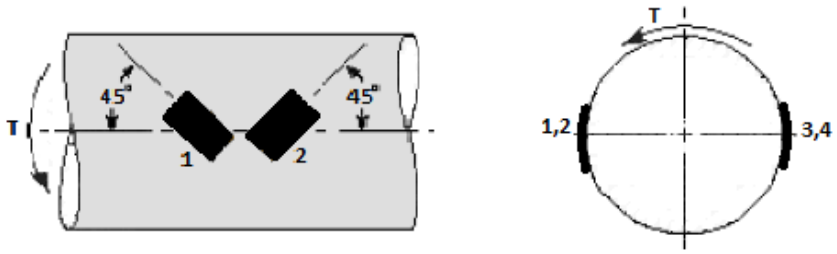

Figure 4.3 Strain gauge placement for measurement of torque on a shaft

Exposed to pure torsion, the axial and radial stresses are of equal magnitude, and the difference between these two normal strains is the maximum shear strain measured at 45° to the shaft axis. A second gauge, 2, is introduced to double the output and compensate for possible bending or direct stresses. The reasoning behind elements 3 and 4 is the same as for measurement of normal stresses, to compensate for temperature variations, while maximizing the signal output.

4.3 Uncertainty analysis

Uncertainty analysis of the measurements is an important step in accurately estimating the hydraulic performance of a turbine. All measurements are to some degree exposed to errors, and this should be accounted for when estimating the uncertainty of the results. IEC 60193 [2] defines errors in the measured quantity as: *"the difference between that measured and the true value of the quantity".* The uncertainty of the measurement is then defined as *"the range within which the true value of a measured quantity can be expected to lie, with a suitable probability"*. For IEC 60193, this probability is a 95 % confidence level. The relation between the uncertainty and error for measurement x, is given in Equation (4.7):

$$f_x = \frac{e_x}{x} \tag{4.7}$$

For combination of n uncertainties, Equations (4.8) – (4.10) are utilized:

$$f_{x^n} = n \cdot f_x \tag{4.8}$$

$$f_{xy} = \sqrt{f_x^2 + f_y^2} \tag{4.9}$$

$$f_{x+y} = \frac{\sqrt{e_x^2 + e_y^2}}{x + y} \tag{4.10}$$

4.3.1 Types of errors

There is distinguished between three main sources of measurement errors [2]:

Spurious errors

Spurious errors deal with human errors and instrument malfunction. The usual source of these occasions is the incompetence, or lack of knowledge of the personnel. In most cases, when this type of error is present, the data is disregarded, and the measurements have to be repeated.

Random errors, e_r

This is a result of a numerous unpredictable and independent factors that affect the measurements. For several measurements, the values will deviate from the mean and can be assumed to form a normal distribution. One way of reducing the effect of random errors is to increase the sampling rate of the equipment. For smaller sampling rates, however, the uncertainty resulting from random errors will increase, due to the decreased sample data. According to IEC 60193 [2], this can be compensated for by using the Student's t factor. Equation (4.11) describes the random uncertainty of secondary instrument during a calibration. n is the number of measurements, s_c is the standard deviation and t is Student's factor. The standard deviation is in turn a function of the measurement value, x_i and its mean value x_i, Equation (4.12).

$$f_d = \pm \frac{t s_c}{\sqrt{n}} \tag{4.11}$$

$$s_c = \pm \sqrt{\frac{\sum(\bar{x} - x_i)^2}{n - 1}} \tag{4.12}$$

Systematic errors, e_s

Systematic errors describe factors concerning the equipment performance, environmental influence or other external sources of recurring error. The most common source of this type of error is the calibration process of secondary instrument, along with the physical properties. Unlike random and spurious errors, the repeatability of a measurement is not affected by systematic errors. Another beneficial characteristics of systematic errors is that they are statistically occurring, which means they can be compensated for if the deviation is known. If the error consists of several components, the total value is estimated with the root-sum-square method given in Equation (4.13).

4.3.2. Total uncertainty

Knowing the random and systematic errors present, the total relative uncertainty in any measured quantity is calculated using the root-sum-square method:

$$f_t = \pm\sqrt{f_s^2 + f_r^2} \tag{4.13}$$

Whereas f_r and f_s are the uncertainties resulting from random and systematic errors respectively. Similar approach is used to determine the total random or systematic uncertainty of the hydraulic efficiency, by adding up the systematic and random error related uncertainties for all the measured quantities. For testing of a Francis model, this includes: discharge $(f_{\mathbf{Q}})_s$, specific energy $(f_{\boldsymbol{E_s}})_s$, torque $(f_{\mathbf{T}})_s$, speed of rotation $(f_{\mathbf{n}})_s$ and density of water $(f_{\boldsymbol{\rho}})_s$.

$$(f_{\mathbf{h}\eta})_s = \pm\sqrt{(f_{\mathbf{Q}})_s^2 + (f_{E_s})_s^2 + (f_{\mathbf{T}})_s^2 + (f_{\mathbf{n}})_s^2 + (f_{\boldsymbol{\rho}})_s^2} \tag{4.14}$$

$$(f_{\mathbf{h}\eta})_r = \pm\sqrt{(f_{\mathbf{Q}})_r^2 + (f_{E_s})_r^2 + (f_{\mathbf{T}})_r^2 + (f_{\mathbf{n}})_r^2 + (f_{\boldsymbol{\rho}})_r^2} \tag{4.15}$$

IEC 60193, section 3.6 [2] provides strict requirements to the allowable uncertainties. For measurement of friction torque using secondary method, the systematic uncertainty should be within:

$$f_{TLm,s} = \pm \text{ 0,02 to 0,05 \% of } T_{m,max} \tag{4.16}$$

When it comes to random uncertainty, the standard states no clear limitations. It is suggested that an agreement between the parties prior to the measurements should be made specifying the maximum permissible value of $f_{TLm,r}$. However, in absence of such, as reasonable limit is set to $\pm 0{,}1$ near the optimum point.

4.4 Hydraulic Axial Forces on the Francis Turbine Runner

The following section includes calculation procedure of the hydraulic axial forces in a Francis turbine according to "*Pumper & Turbiner" [5]*. The necessary dimensional and operational data of the turbine are shown in Appendix F.

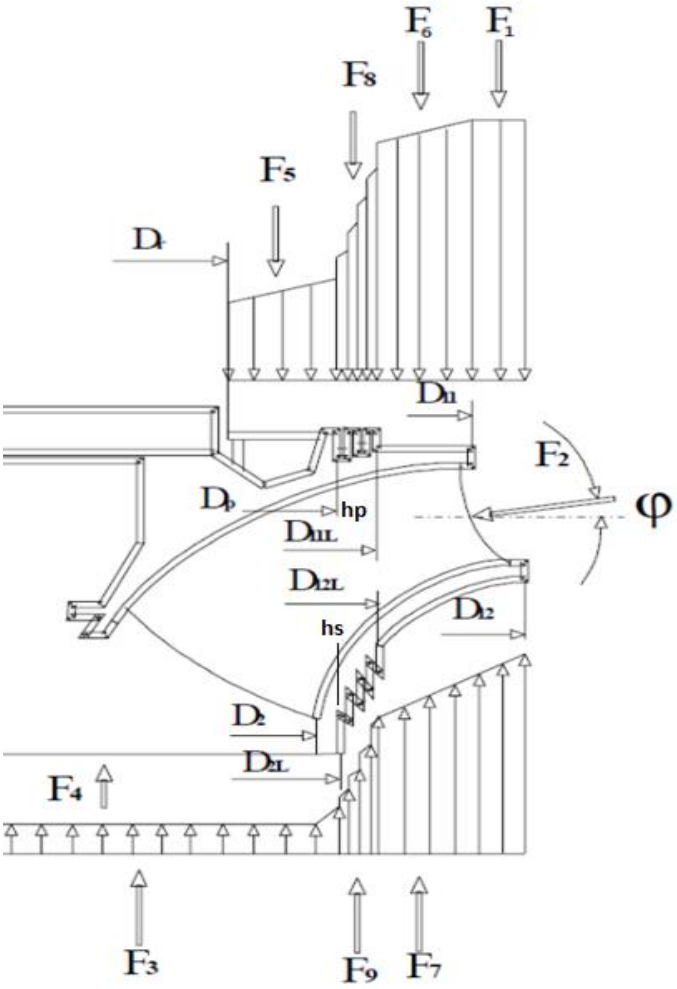

Figure 4.4: Hydraulic axial forces on a Francis turbine [5]

- F_1 - Forces caused by the difference in diameter between hub and shroud at the inlet.
- F_2 - Reaction forces caused by the axial components of inlet flow.
- F_3 - Forces caused by the pressure in the draft tube.
- F_4 - Reaction forces caused by the axial components of outlet flow
- F_5 - Forces caused by pressure difference inside the upper labyrinth sealing
- F_6 - Forces due to pressure difference outside the upper labyrinth sealing
- F_7 - Forces due to pressure difference outside the lower labyrinth sealing
- F_8 - Forces acting on the upper labyrinth sealing
- F_9 - Forces acting on the lower labyrinth sealing

The purpose of the calculation is to approximately estimate the hydraulic forces the turbine will experience during operation. It is important to note that the friction and gap losses are not included in the calculations. According to Brekke [5], the following procedure provides results with an accuracy of approximately 90 %.

The forces are calculated based on the pressure at the inlet and outlet of the runner. The inlet pressure, given in meters of water column, is assumed to have a 50% reduction from the initial net head, H_n.

$$h_1 = H_n - \frac{c_1^2}{2g} - losses \approx 0.5 \cdot H_n \ [m] \tag{4.17}$$

The outlet pressure, h_1, is estimated using Bernoulli equation between two points in the lower section of the system; runner outlet and free water surface of the surge pressure tank. In this case, two essential significations are necessary in order to estimate the outlet pressure:

- Atmospheric pressure in the vessel
- Zero velocity at the free water surface

The inlet and outlet meridional velocities, c_{m1} and c_{m2}, are given by Equations (4.18) and (4.19), with the assumption of constant and uniform flow at both sections of the turbine.

$$c_{m1} = \frac{Q}{\pi D_1 B_1} \ \left[\frac{m}{s}\right] \tag{4.18}$$

$$c_{m2} = \frac{4 \cdot Q}{\pi D_2^2} \ [\frac{m}{s}] \tag{4.19}$$

Where Q is the flow rate, B_1 is the inlet height and D_1 and D_2 are the inlet and outlet diameters respectively.

Further, the Bernoulli equation is used to calculate the pressure at the outlet of the turbine.

$$h_2 = h_3 + z_3 + \frac{v_3^2 - v_1^2}{2 * g} - z_1 \ [m] \tag{4.20}$$

Where h_3 is the atmospheric pressure in the surge tank.

Additionally, the air supplying tap on the left side of upper labyrinth, is also considered to have atmospheric pressure. With these three pressure points known, the remaining relations are derived based on change in the diameter.

The absolute velocity in the upper section of the turbine, between the cover and the runner, is assumed to be between 50% and 55% of the peripheral velocity in that section. Using the definition of peripheral velocity, Equation (4.21) is obtained:

$$u = r * \omega \quad \& \quad c_u = k * u \quad \rightarrow \quad c_u = k * r * \omega \ [\frac{m}{s}] \tag{4.21}$$

$$Where \ \ \omega = \frac{\pi * n}{30} \quad and \ \ 0.5 < k < 0.55 \tag{4.22}$$

Using Newton's second law for force balance on a fluid element, the following relation is obtained:

$$\frac{\partial h}{\partial r} dr = \frac{c_u^2}{gr} dr \quad \rightarrow \quad \frac{\partial h}{\partial r} = \frac{r * k^2 * \omega^2}{g} \ [-] \tag{4.23}$$

Integrating equation (4.24) with respect to h and r:

$$\int_h^{h_i} dh = \frac{\omega^2 * k^2}{g} \int_r^{r_i} r dr \quad \rightarrow \quad h_i - h = \frac{k^2 * \omega^2}{2g} (r_i^2 - r^2) \ \ [m] \tag{4.24}$$

This pressure relation can be applied to any point in the turbine where the pressure difference is only based on the change in diameter. This includes both inner and outer sections of the upper and lower labyrinths.

With all necessary pressure points mapped, the equations for the different forces are derived. The background for each derivation is the definition of force, pressure times area, with small adaptions to the individual case. The hydraulic axial forces can be divided in three sections:

1. Pressure and reaction forces at the inlet and outlet (F_1, F_2, F_3 and F_4)
2. Axial pressure forces between the cover and runner (F_5, F_6 and F_7)
3. Axial pressure forces in the labyrinth seals (F_8 and F_9)

Pressure and reaction forces at the inlet and outlet

Equation (4.26) describes the force due to the difference in diameter between hub and shroud at the inlet area.

$$F_1 = \frac{1}{2}\rho g(h_{11} + h_{12})\frac{\pi}{4}(D_{12}^2 * D_{11}^2) \ \ [N] \tag{4.25}$$

Where $\frac{1}{2}\rho g(h_{11} + h_{12})$ is the approximated pressure distribution on the hub, ρ is the density of water and g is the standard gravity acceleration.

$$F_2 = \rho Q c_{m1} sin\theta \ \ [N] \tag{4.26}$$

$$F_3 = \rho g h_2 \frac{\pi D_{2L}^2}{4} \ \ [N] \tag{4.27}$$

$$F_4 = \rho Q c_{m2} \ \ [N] \tag{4.28}$$

Axial pressure forces between the cover and runner

Forces caused by pressure difference inside the upper labyrinth sealing can be found by integrating across the respective area:

$$F_i = \rho g \int_{r_i}^{r_p} 2\pi r h \, dr = 2\pi\rho g \int_{r_i}^{r_p} \left(h_p - \frac{k^2\omega^2}{2g}\left(r_p^2 - r^2\right)\right) r \, dr \tag{4.29}$$

Rewritten and integrated:

$$F_i = 2\pi\rho g h_p \int_{r_i}^{r_p} r\,dr - \rho\pi k^2\,\omega^2 r_1^2 \int_{r_i}^{r_p} r\,dr + \pi\rho k^2\omega^2 \int_{r_i}^{r_p} r^3\,dr \tag{4.30}$$

$$F_i = \pi\rho g h_p\left(r_p^2 - r_i^2\right) - \frac{1}{4}\rho\pi k^2\omega^2\left(2r_p^4 - 2r_p^2 r_i^2\right) - \frac{1}{4}\rho\pi k^2\omega^2\left(-r_p^4 + r_i^4\right) \tag{4.31}$$

$$F_5 = F_i = \rho\pi g h_1\left(r_p^2 - r_i^2\right) - \frac{\rho\pi k^2\omega^2}{4}\left(r_p^2 - r_i^2\right)^2 \quad [N] \tag{4.32}$$

Similarly, forces due to pressure difference outside the upper and lower labyrinths are derived by integration across an area:

$$F_6 = \rho\pi g h_{11}(r_{11}^2 - r_{11L}^2) - \frac{\rho\pi k^2\omega^2}{4}(r_{11}^2 - r_{11L}^2)^2 \quad [N] \tag{4.33}$$

$$F_7 = \rho\pi g h_{12}(r_{12}^2 - r_{12L}^2) - \frac{\rho\pi k^2\omega^2}{4}(r_{12}^2 - r_{12L}^2)^2 \quad [N] \tag{4.34}$$

Axial pressure forces on the labyrinth seals

Lastly, forces acting on the upper and lower labyrinth seals are given in Equations (4.35) and (4.36).

$$F_8 = \frac{\rho g(h_{11L} + h_p)}{2} \cdot \frac{\pi(D_{11L}^2 - D_p^2)}{4} \quad [N] \tag{4.35}$$

$$F_9 = \frac{\rho g(h_{12L} + h_s)}{2} \cdot \frac{\pi(D_{12L}^2 - D_{2L}^2)}{4} \quad [N] \tag{4.36}$$

The total axial forces acting on the turbine under operation are summed up in Equation (4.37):

$$F_{tot} = F_1 + F_2 - F_3 - F_4 + F_5 + F_6 - F_7 + F_8 - F_9 \quad [N] \tag{4.37}$$

The axial thrust forces for maximum operating condition is estimated to $8700\ N$. A design load of $10\ kN$ is used as the dimensioning load in further calculations. The details of the calculations can be viewed in the Matlab script provided in Appendix F.

Chapter 5

Design, Waterpower Laboratory, NTNU

This chapter covers the design work for the Francis turbine rig at NTNU. The main goal has been to suggest a setup that is reliable, simple in design and use, and satisfies the requirements of IEC 60193 [2]. Low uncertainty in the measurements has also been a dimensioning factor of the task.

The first section presents a setup for calibration of the axial thrust force measuring devices, along with basic stress analysis of the critical parts and an uncertainty estimation procedure.

The second section of this chapter covers the design for the friction torque calibration and measurement setup. The design is a further development of the existing arrangement, with similar base structure, but with important changes to the measurement process.

The systematic uncertainty of each setup is estimated along the way. The estimation is merely a theoretical description on how to perform the analysis, and what magnitude to expect the error to be within. True scale of the uncertainty that will be present is impossible to calculate without performing the actual measurements. Complete uncertainty analysis of the test rigs have been performed previously by the students and staff at the Waterpower Laboratory. Among them are Pål-Tore Storli [6], who did a complete model test of the Francis turbine, and Kyrre Reinertsen [13] performing uncertainty analysis of the Pelton test rig. When estimating the errors related to measurements, the value presented in [13] and [6] have been assumed for this project.

5.1 Axial load measurement and calibration setup

As mentioned in section 3.1.5, the thrust loads are measured with help of pressure transducers located at various sections of the hydrostatic bearing. According to IEC 60193 [2], this is a direct type measurement, and a typical calibration procedure is the use of certified masses to apply force perpendicular to the impeller/runner.

When designing a calibration setup, the simplicity of the procedure is essential. For obvious reasons, it is desirable to calibrate the pressure transducers without having to remove the bearing block from the shaft arrangement. Calibrating the load in positive axial direction (downwards) is a straightforward procedure, by applying the desired weight loads on a frame attached to the generator shaft. However, calibrating forces in the negative axial direction (upwards) requires some sort of conversion of the load direction. The limited available space above the turbine prevents solutions such as use of a pulley to redirect the weight loads. The design presented in this chapter takes advantage of lever principle, with a loaded beam rotating around a fixed point. The basic concept is presented in Figure 5.1. Positive load applied at point A is transferred to opposite direction at point B through a rolling support.

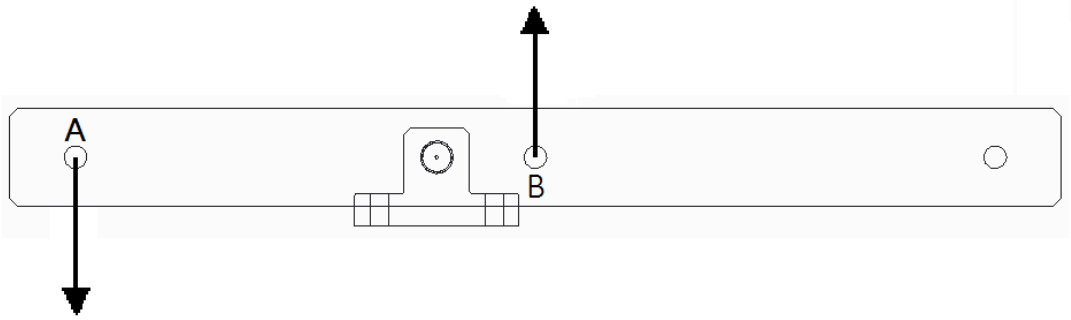

Figure 5.1: Lever beam concept with rolling support.

Idea for this design was developed after conversations with Professor Ole Gunnar Dahlhaug [31]. The arrangement consists of two steel frames attached to a beam with basic screw joints. The beam is in turn connected to the shaft at centre point, with an arrangement of adjustable length. Two single row ball bearings are used to reduce friction in the rotating support. The arrangement is

resting on a circular plate, fixed to the turbine housing with four hex bolts. A 3D representation of the design can be viewed in Figure 5.7.

Detailed machine drawings of the consisting parts are provided in Appendix C.1. The existing calibration procedure provided in Appendix G.2 is still valid, with the only change being an additional implementation of the same process for forces in the upward direction.

5.1.1 Safety factor of the threaded fasteners

The present outer turbine housing contains four threaded holes centred around the shaft axis. It is suggested to utilize these connection points for fixing the calibration setup to the stationary frame. The summetrical holes are 14 mm in diameter, located in a distance of 502,05 mm relative to each other.

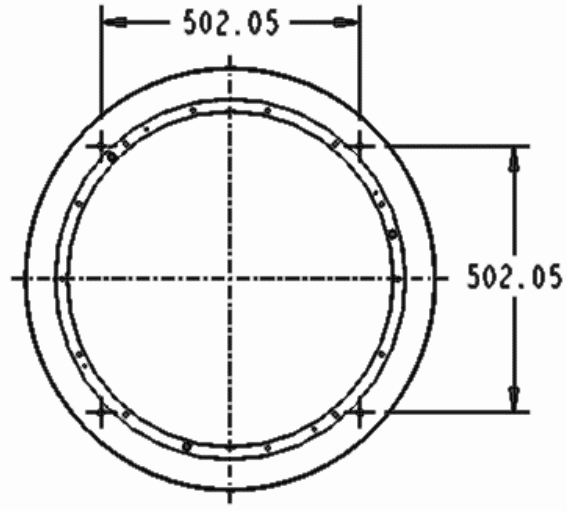

Figure 5.2: Turbine lower head cover of the Francis turbine at Waterpower Laboratory.

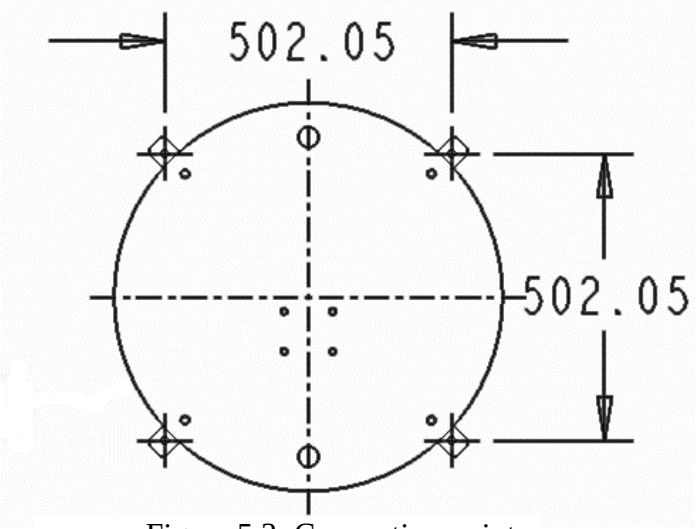

Figure 5.3: Connection points of the calibration Setup

The four threaded connections are supporting the total weight load and are the most critical part of the setup.

The hole threads are for standard metric M14 bolts. Dimensioning factor is considered to be the yield strength of the unit, σ_y. The dimensional values and calculation procedure as described in *"Styrkeberegning: Skrueforbindelser"* [32], is used when calculating the equivalent stress of a standard M14x1.5 metric bolt. Due to the off-centered location of the bearing support, the loads

are asymmetrically distributed on the four bolts. The calculations are performed for the worst case scenario of a load of 10 kN acting on a single unit.

The equivalent stress in the threads is a combination of tension and torsion.

$$\sigma_{eq} = \sqrt{\sigma_t^2 + 3 * \tau_v^2} \tag{5.1|}$$

Bending moment is neglected to simplify the calculations. The preload of the torsion component is equal to the axial load: $F_i = F_a = 10000\ N$.

Component of tension:

$$\sigma_t = \frac{F_a}{A_t} \tag{5.2}$$

Component of torsion:

$$\tau_v = \frac{F_i \cdot tan(\varphi + \varepsilon) \cdot 0.5\, d_m}{\frac{\pi}{16} d_i^3} \tag{5.3}$$

A standard ISO profile of metric bolts is shown in Figure 5.4.

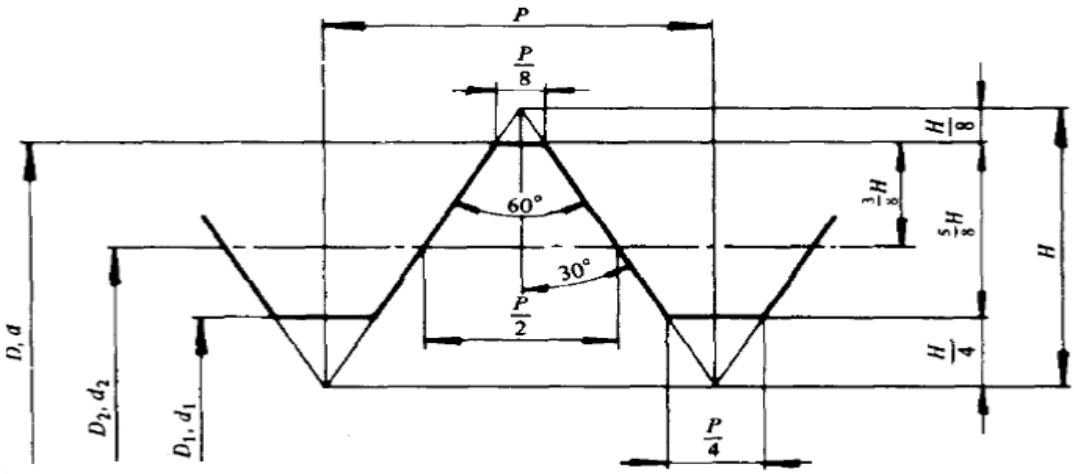

Figure 5.4: Standard profile of ISO-threads [32].

Following dimensions are obtained based on the data table of ISO metric threaded connections [32], and the dimension classes for M14x1.5 bolts according to NS 1873-ISO 724 [33].

Table 5.1 M14x1.5 ISO metric bolt data, [32] and [33].

Property	Notation	Value	Unit
Major diameter	d	14	mm
Pitch diameter	$d_1 = d_i$	12,376	mm
Minor diameter	$d_2 = d_m$	13,026	mm
Pitch	P	1,5	mm
Friction coefficient	μ	0,2	–
Thread angle	α	30	–

A_t is the tensile stress area, given by Equation (5.4):

$$A_t = (\frac{d_2 + d_1}{2})^2 \frac{\pi}{4} \approx 125\ mm^2 \tag{5.4}$$

ε and φ are the friction and thread dependent angles respectively. These angles, along with the axial force on the unit, are used to estimate the tangentialforce required to rotate a scew in frictional contact. The angles are calculated from trigonometrical relation of the threaded section as shown in Figure 5.4.

$$tan\ (\varepsilon) = \frac{\mu}{cos\ (\alpha)} \qquad and \qquad tan\ (\varphi) = \frac{P}{\pi * d_m} \tag{5.5}$$

Solving Equation (5.5) for tension and torsion components of the total stress:

$$\sigma_t = 78{,}7\ MPa,\ \ \tau_v = 47{,}2\ MPa$$

Inserted in equation 5.1, this gives:

$$\sigma_{eq} = \sqrt{\sigma_t^2 + 3 * \tau_v^2} = 113{,}5\ MPa \tag{5.6}$$

The safety factor, SF, is determined based on the mechanical properties of the metric fastener, which are in turn given by the property designation class.

$$SF = \frac{\sigma_y}{\sigma_{eq}} \quad [-] \tag{5.7}$$

The property designation class of metric fasteners describes the tensile and yield strenghts of the material. As an example, a property class of 4.6 means tensile ultimate strenght (TUS) 400 MPa and tensile yield strenght of 0,6 times TUS; $\sigma_y = 0.6 * 400 = 240\ MPa$. In general, for static load applications a safety factor of 2.5 to 3 is considered sufficient. Based on the calculation above, a property class of 5.8 or higher will provide a safety factor above 3.

5.1.2 Stress Analysis in Ansys Mechanical

Simple stress analysis are performed to verify the dimensions of the consisting parts. Structural steel with yield and tensile strengths of 250 and $460\ MPa$ respectively is used in the study. The results are shown in Figures 5.5 and 5.6.

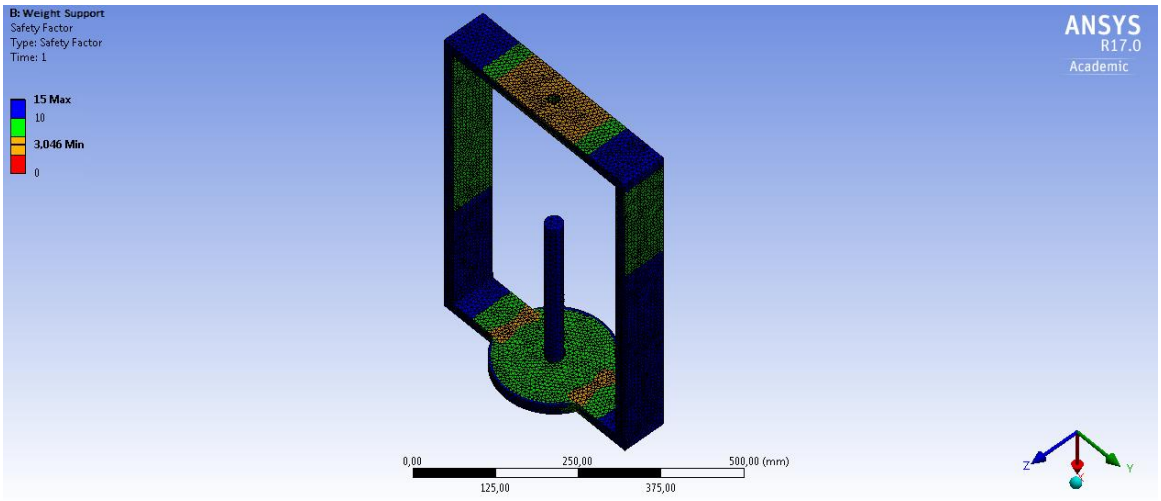

Figure 5.5: Weight holder, Ansys analysis.

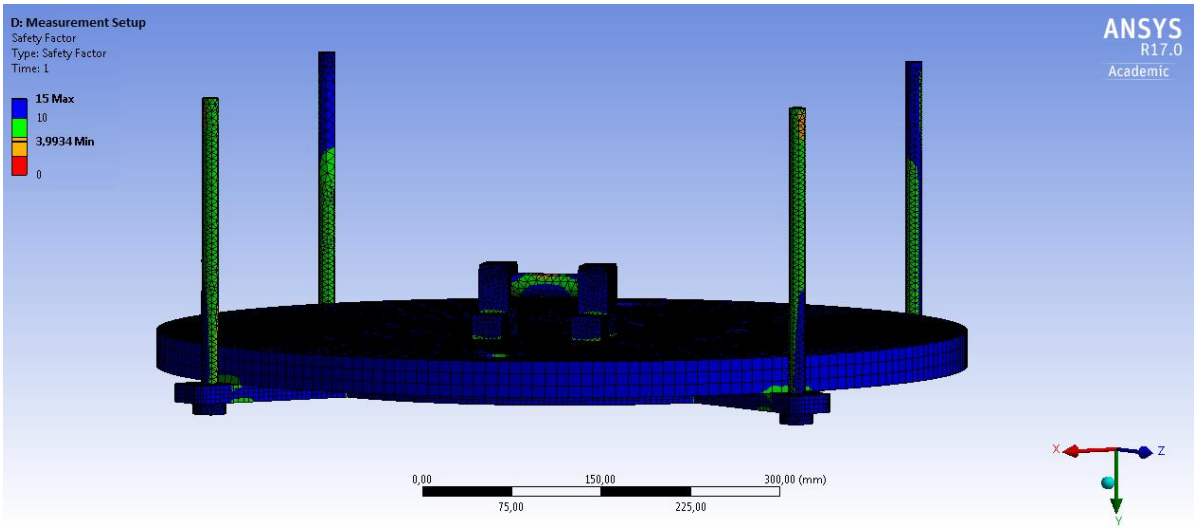

Figure 5.6: Circular plate, Ansys analysis

Safety factor above 3 is observed for all consisting parts. According to the results, certain sections of the design are over dimensioned in terms of material thickness. This concern in particular the circular plate, with plenty room for optimization of the 30 mm thick steel.

3D representation of the axial force calibration setup is shown in Figure 5.7 and 5.8.

Figure 5.7: 3D representation of the axial force calibration setup.

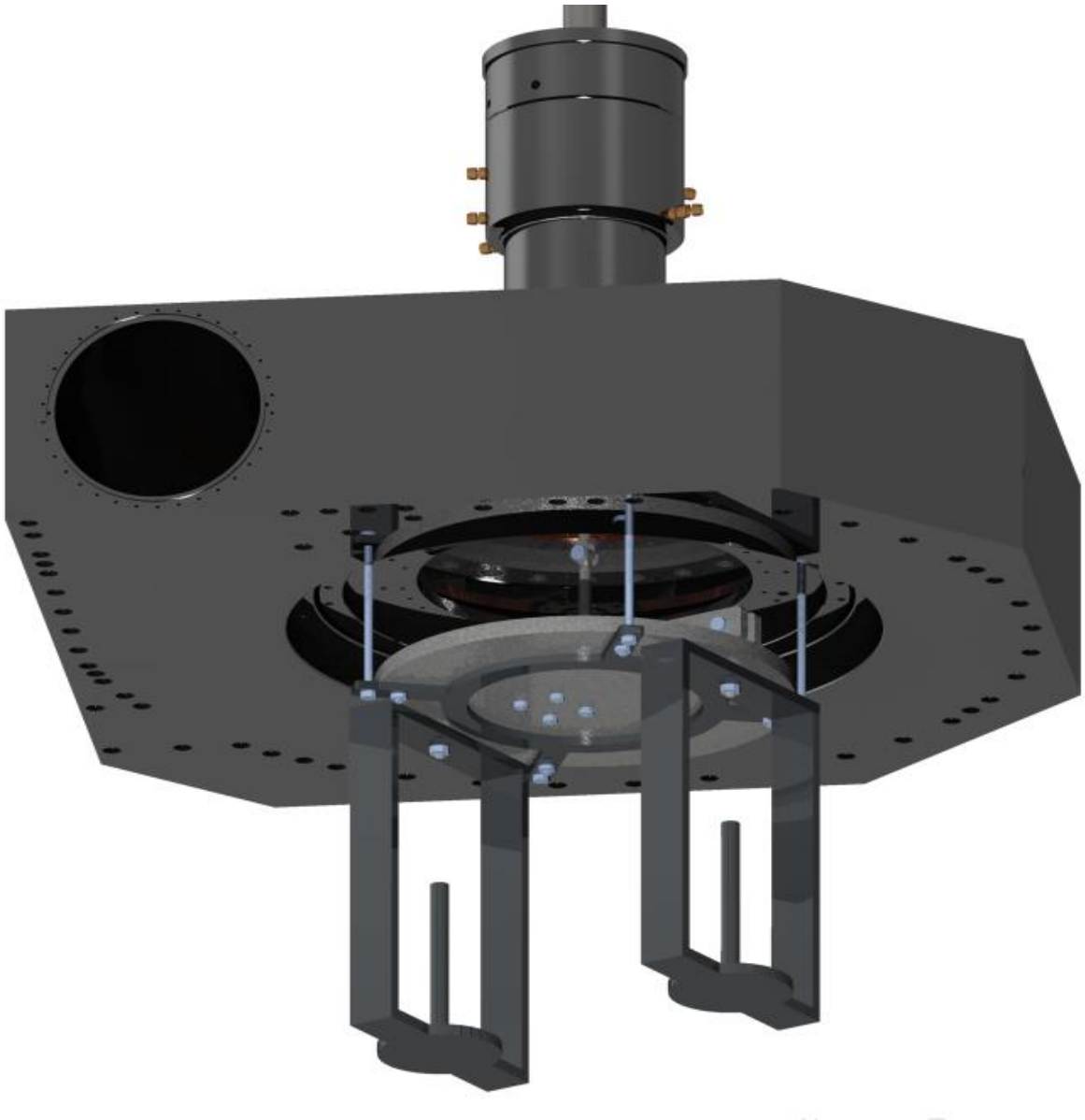

Figure 5.8: 3D representation of the calibration setup, the thrust block and the turbine housing.

5.1.3 Uncertainty analysis

As the calibration setup was not manufactured, the total uncertainty of the procedure is difficult to map. It is, however, possible to estimate the level of systematic uncertainty, by individually considering the contributing factors. The uncertainty $(f_{F_a})_s$ is given as the sum of:

- Uncertainty in calibration weights, f_{W_1}
- Regression error, f_{reg}
- Uncertainty due to the weight contribution of the setup, f_{W_2}
- Uncertainty caused by the friction in roller bearing, f_f

The total systematic uncertainty is given by equation (5.8):

$$(f_{F_a})_s = \pm\sqrt{(f_{W_1})^2 + (f_{reg})^2 + (f_{W_2})^2 + (f_f)^2} \tag{5.8}$$

Equation (5.8) expresses the relative systematic uncertainty, whereas the absolute value can be obtained by multiplying the equation with the quantity of interest:

$$(e_{F_A})_s = \pm F_A\sqrt{(f_{W_1})^2 + (f_{reg})^2 + (f_{W_2})^2 + (f_f)^2} \tag{5.9}$$

The calibration weights are known to contain small error, which was estimated by Storli [6] to 75 grams for each weight.

The regression error is a result of the uncertainty in measured points, and the utilized method for point fitting along the regression line. This error is strictly limited to the uncertainty of each measured value, and can only be estimated after the calibration process. IEC 60193 section 3.9.2.2.2 [2] states that although the regression error can be evaluated in accordance with ISO 7066, a conventional value of $\pm 0{,}05$ % can be assumed.

As the calibration setup is fixed to the turbine housing, the weight contribution to the axial force measurement will be marginal. The similar design of the two steel frames is also contributing to equalizing the loads on each side of the bearing support. The off-centred location of the support

however, will result in a slight error if not compensated for. With no loads applied, the difference in weight balance will tip one section of the beam with force F_3, as illustrated in Figure 5.9.

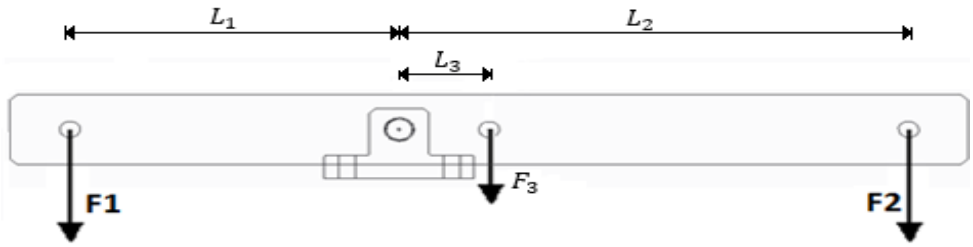

Figure 5.9: Forces acting on the freely supported beam

With the lengths and masses of beam structure knows, F_3 is calculated by applying moment balance on the beam.

$$F_3 = \frac{F_1 L_1 - F_2 L_2}{L_3} = \frac{F(L_1 - L_2)}{L_3} \quad [N] \tag{5.10}$$

The design load acting on distance L_1 from the support, exerts a torque on the bearings equalling:

$$T = F_1 \cdot L_1 \tag{5.11}$$

The friction forces counteracting this torque is another source of uncertainty. Anti-friction ball bearings are used specifically for the purpose of reducing this effect. The moment is estimated using the SKF model [10], detailed in Appendix B.2.

Total relative systematic uncertainty of the axial force calibration setup is calculated in Appendix A. The results are presented in Table 5.2.

Table 5.2: Systematic uncertainties of the axial force calibration setup.

Uncertainty	**Notation**	**Value [%]**
Calibration weights	f_{W_1}	0,01061
Regression	f_{reg}	0,05
Weight of the setup	f_{W_2}	0,0025
Friction in bearings	f_f	0,011

Inserted into equation 10, this gives:

$$(f_{F_a})_s = \pm\sqrt{0{,}01061^2 + 0{,}05^2 + 0{,}0025^2 + 0{,}011^2} = 0{,}0523\ \% \tag{5.12}$$

In addition to the systematic uncertainties listed above, the random error has to be accounted for as well, given by Equation (5.13):

$$f_d = \pm\frac{ts_c}{\sqrt{n}} \tag{5.13}$$

Where n is the number of measurements, s_c is the standard deviation and t is Student's factor.

It is worth noting that both random and systematic uncertainties will vary for each measurement, and can be mapped accurately only after completion of the tests. $0{,}0523\ \%$ is a rough estimation, but it provides an idea of the scale the systematic uncertainty will represent.

5.2 Design of the frictional torque measurement and calibration setup

The friction torque is measured as before, with the arrangement described in Chapter 3.1.4. An arm is attached to the swinging frame, moving in line with the frictional forces of the hydrostatic bearing. This arm is in turn in contact with a load cell, which senses the movement and converts it to a voltage output.

As described in section 3.1.2, the membrane located inside the bearing block is in tension during the operation of the turbine, resulting in false reading of the load transducer. According to IEC 60193 section 3.6.4.5 [2], if the sealing is made by the means of friction or membrane seals, these should be calibrated. How much moment the membrane exerts on the load cell is unknown. Based on the characteristics of friction it can be assumed to have an increasing moment as the speed of the shaft is increasing.

The following friction torque measurement setup is designed to counteract the moment caused by the membrane. Main components of the setup are a straight beam, roller bearing, load cell, and two weight loads of 2 kilograms each. Due to time constraint and available lab personnel, the parts were not manufactured during this thesis.

The design utilizes the concept of weight balance, illustrated in Figure 5.10.

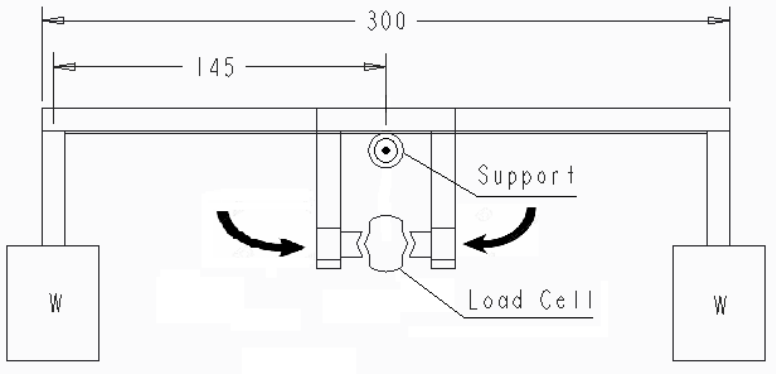

Figure 5.10: Weight balancing concept of the friction torque measurement setup.

When in perfect balance, $L_1 = L_2$, the beam exerts no forces on the sensing element. The torque is equal on both sides of the resting point.

$$T_1 = T_2 \tag{5.13}$$

$$WL_1 g = WL_2 g \tag{5.14}$$

As the roller bearing is moved to one of the sides the beam loses its equilibrium proportionally to the movement. The load cell is then exerted to the differential torque, ΔT, defined in equation (5.15):

$$\Delta T = \sqrt{(T_1 - T_2)^2} \tag{5.15}$$

High frictional contact between the roller bearing and the contact surface of the beam is required to avoid slip errors during operation. It is suggested to use a material combination that provides high frictional coefficient. Two aluminium surfaces are preferable, as the coefficient of friction between these two faces can reach up to 1.35 for dry surfaces. An electric motor is used to regulate the horizontal movement of the bearing support. The motor is a stepper type, which means the rotation of the shaft can be controlled in movement of selected degrees. Rather than making a whole spin, the rotation is divided in small parts. For normal, full step motors, this mean a movement of 1,8 degrees, which equals 200 steps for a full rotation. An apparent requirement is to convert the rotational motion of the motor shaft into linear motion. This type of mechanisms can be found in various types of engineering solutions. The original idea was to use rack and pinion concept. A gear rack resting on a pinion, moving in the same direction as the rotating shaft. The concept is illustrated in Figure 5.11. The idea was, however, disregarded at an early stage due to the uncertainties linked to gearing mechanism.

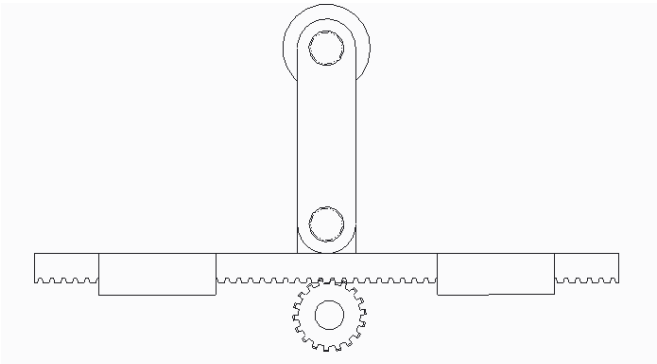

Figure 5.11: Rack and pinion concept for conversion of rotary motion to linear motion

Other practical solutions that do not include gearing arrangements are available as well. As the repeatability and accuracy of the drive is essential in this case, a roller screw based solution is chosen. The concept is simple, cost efficient, and the high precision positioning and increased load capacity makes it ideal for current application. The concept, illustrated in Figure 5.12, consist of a linear stepper motor with integrated screw mechanism for linear to rotary motion conversion. A lead screw is rotating with motor shaft, providing the slide block with horizontal movement. The block is operated through guiding rails, and available length of the linear motion can be adjusted by extending/reducing the lead screw.

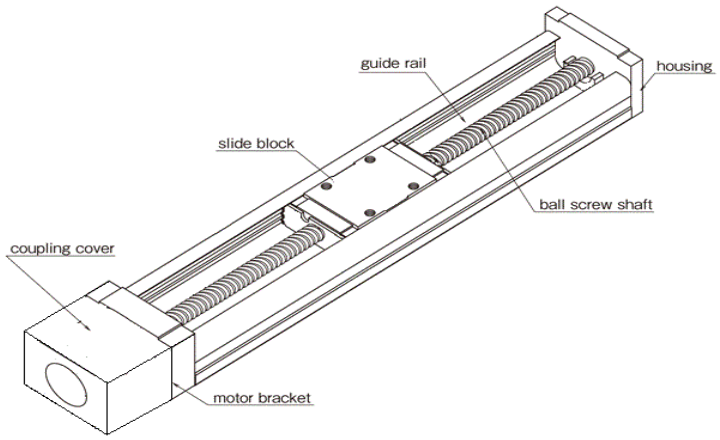

Figure 5.12: Schematic representation of the motorized linear actuator

The unit is provided by *Thomson Linear Motion* [35]. The dc motor is a ML11 type, with technical data given in Appendix E. A stroke length of 100 mm, with minimum step length of 0,05 mm, is provided by the driving mechanism. The motor operates at steps of 1,8 degree with 95 % accuracy.

Using Equation (5.16), the minimum torque exerted on the load cell by the balancing beam can be determined. A $0{,}05\ mm$ change in lengths L_1 and L_2 results in $1{,}962\ Nmm$ torque. Adding the uncertainty span of ± 5 %, the minimum friction torque that can be provided to counteract the frictional forces of the membrane is found:

$$T = 1{,}962 \pm 0{,}0981\ Nmm \tag{5.16}$$

Similarly, the maximum stroke of 100 mm, meaning 50 mm change in L_1 and L_2, gives the maximum torque available:

$$T = 1962 \pm 98{,}1\ Nmm \tag{5.17}$$

The weight blocks are designed with threaded connections, to make it possible to change the weights if higher or lower torque values are required. This also simplifies the calibration process, where the blocks are replaced with a steel frame that can hold the certified calibration weights. The existing calibration process for friction torque measuring equipment is used for the setup, with detailed procedure provided in Appendix G.1.

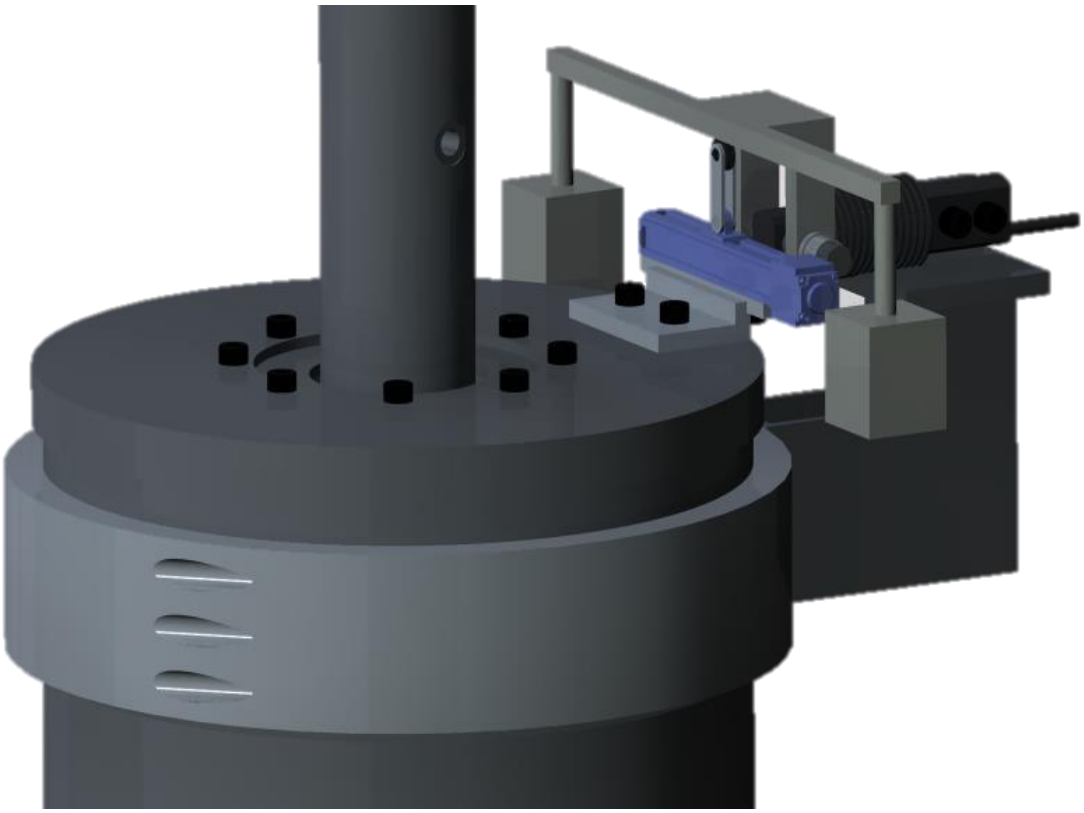

Figure 5.13: 3D model of the friction torque measurement setup.

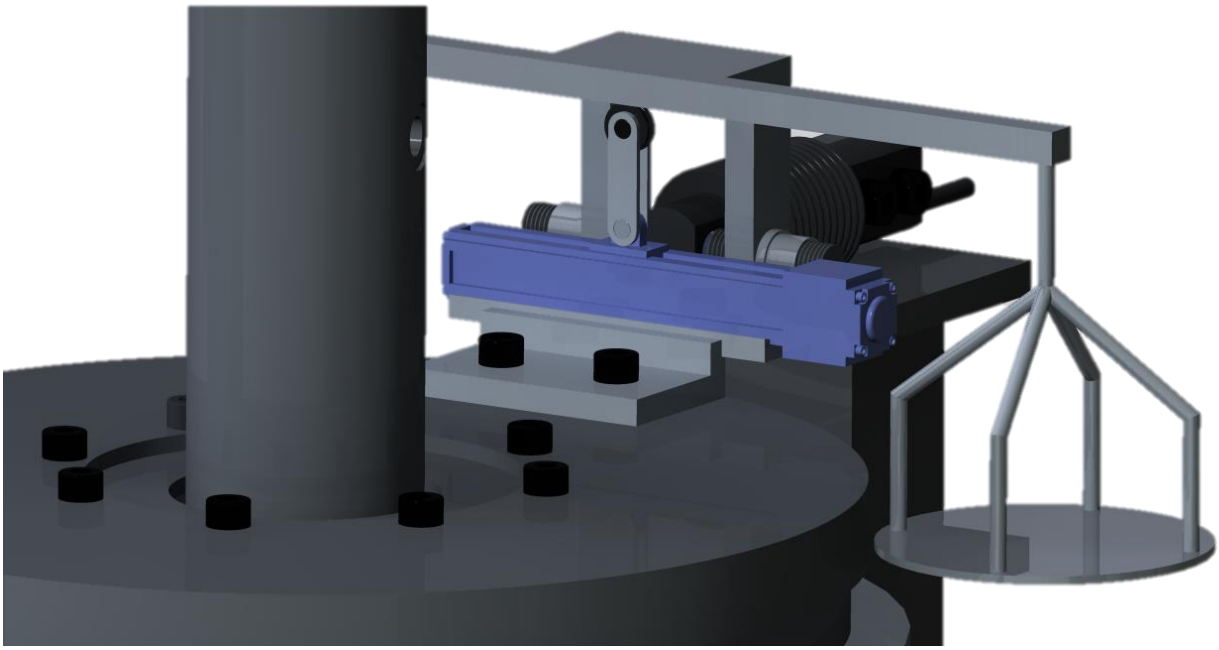

Figure 5.14: 3D model of the friction torque calibration setup.

5.2.1 Uncertainty analysis

For calibration of the existing friction torque measurement setup at NTNU, the relative systematic error is found as the sum of the individual uncertainties of the calibration arm, f_{arm}, calibration weights, f_W, and the regression error, f_{reg}. In addition to these, the new design introduces a fourth source of uncertainty, f_m, that expresses the accuracy of the electric motor and the associating equipment.

$$(f_{T_{Lm}})_s = \pm\sqrt{(f_W)^2 + (f_{arm})^2 + \left(f_{reg}\right)^2 + (f_m)^2} \tag{5.18}$$

With a corresponding absolute uncertainty:

$$(e_{T_{Lm}})_s = \pm T_{Lm}\sqrt{(f_W)^2 + (f_{arm})^2 + \left(f_{reg}\right)^2 + (f_m)^2} \tag{5.19}$$

Reinertsen [6] used the same calibration weights in his analysis of the friction torque measurement procedure of the Pelton test rig, and uncertainty was found to 0,11 %.

The uncertainty related to calibration arm is originating from the errors in measurements of the consisting lengths. Storli [6] estimated this value to 0,00437 %.

Referring to IEC 60193 section 3.9.2.2.2, the uncertainty caused by the regression process is assumed to 0,05 %.

The motor accuracy is affected by several factors. Friction forces between the mechanical components such as the lead screw and linkages is one of them. The loss in friction affects directly the torque and power transmitted by the motor. The components also contain design errors, such as tolerance requirements. The total combined error of the motorized unit is given to 5% in the data sheets. In order to estimate the resulting uncertainty f_m, it is necessary to know how much torque the membrane exerts on the load cell. As this step was not performed during the project, the uncertainty related to the motor motion is unknown.

Chapter 6

Design, Turbine Testing Laboratory, KU

This Chapter covers the design aspects of the shaft and bearing block for the Turbine Testing Laboratory. The objective has been to suggest a solution that is simple and cost efficient, while satisfying the operational requirements of the turbine, as well as the requirements of the international IEC 60193 [2] standard. The preliminary sections of this chapter cover the selection of bearings, bearing accessories and couplings. The second part includes the suggested methods for measurement and calibration of friction torque and axial force for the Francis turbine at TTL.

The existing drawing of the Francis test rig, along with a presumed design of the remaining components were provided by Biraj Singh. In order to comply with the measurement setups, some changes have been imposed to the shaft and bearing components. A complete 3D model of the Francis turbine test rig at TTL is provided in Appendix H.

6.1 Shaft coupling

Hard, preferably heat treated, structural steel is the suggested material for shaft design. For smaller turbines, a consistent shaft can be used, with the generator rotor and turbine runner connected at each end. This is, however, not desirable as it exposes the shaft to extension and compression as the axial forces in the turbine increase. The radial loads on the essential components of the machinery will also increase, as there is no elastic motion in the connecting parts to absorb it.

A flanged connection is suggested for connecting the generator and turbine shafts. The strength of the material used in flanged connection is necessarily lower than the shaft material, to avoid the distortion of the shaft caused by the axial and radial loads of the system. This way, the turbine and generator can be considered as two separate parts when designing the axial force and shaft torque measurement setups. With use of proper bearing units, absorbing the axial and radial loads on the

shaft unit, the shaft connection should consist of a flexible coupling with enough elasticity to resist the distorting stress forces.

6.2 Bearings and bearing accessories

During the operation, the turbine components are constantly exposed to high loads in both axial and radial directions. These loads propagate from the rotating shaft and into the stationary parts of the turbine. As the connection point between the rotating and stationary parts, the correct selection of bearing is essential. The suggestions and guidelines for bearing selection by the Swedish ball bearing company [10], are utilized when choosing the thrust and guide bearings.

The dimensioning data is given in Table 6.1. The maximum generator speed and design thrust load are based on the performance data of Francis test rig at NTNU.

The radial forces of the turbine are unknown. According to IEC 60193 [2] they are determined by measuring one of the following quantities:

- Reaction forces in the shaft bearings
- Supporting forces of the bearing block
- Deflection of the shaft
- Multidirectional strain measurement of the turbine shaft

The shaft at the waterpower laboratory at NTNU is 90 mm at its largest, with decreasing diameter towards the coupling. This design is slightly modified, to fit the current application. The machine drawings of the Turbine Testing Laboratory show a shaft diameter of 50 mm on Francis rig. This has been used in further design.

Table 6.1 Dimensioning data for the Francis turbine at TTL.

Property	Notation	Value	Unit
Max. generator speed	n_{max}	1500	rpm
Axial loads	F_a	10000	N
Radial loads	F_r	–	–
Shaft Diameter	D	50	mm

There are four bearings assigned for the rotating components. The generator has upper and lower guide bearings, with a task of taking up the radial loads and keeping the generator shaft aligned. The lower bearing is also supporting the axial loads, including the weight of the rotating parts of the generator. Due to the time constraint and relevance to the thesis, the selection of generator bearings is not included in this project.

For turbine shaft, a bearing house with two rotating elements is used. A thrust bearing is located closest to the turbine, resting on a flat, annular plate. The axial forces exerted on this bearing are transferred through the surface of the bearing block, and down into the flat plate. The idea is to measure these forces based on the deflection of the annular plate. The process is detailed in section 6.3.

The upper section of the bearing block is kept aligned with a second bearing, which is mainly guiding the shaft in radial direction.

Following factors were considered for proper selection of turbine shaft bearings:

Size limitations

There are no given size limitations restraining the axial or radial dimensions of the bearing. The only consideration is the bore diameter, as it is determined by the shaft size.

Loads

As the lifetime of the bearing is mainly dependent on the loading conditions of the turbine, this is a dimensioning aspect of the selection procedure. This also includes entrainment of the shaft against axial and radial displacements. For ball and roller bearings, minimum radial loads is also a

requirement, as the inertia forces of the bearing unit as well as the friction in lubricant may cause damaging slide movement if the forces are too low [10].

Friction

Friction in bearings directly contribute to reduced efficiency. It is, therefore, desirable with as little friction as possible.

Seals

Use of lubricants is an effective way of reducing friction in bearings. As a result, sealing solutions are required. In addition to keeping the lubricant in, the seals also keep the contaminants out, which is another contribution to lower friction losses.

Misalignment

Misalignment is a common occurrence in hydro turbines, and has to be considered when selecting bearings. Even if the shaft is perfectly aligned with the housing when installed, the unit will still deflect when radial loads are applied. Self-aligning bearings are available for such application.

Precision

There are no significant precision requirements for current application.

Speed

Due to the frictional heat generation, the bearings usually have a limitation on operating temperature, and thus a maximum permissible speed. For current case, it is important that the bearing can manage the maximum rotational speed of the generator.

Stiffness

Stiffness defines the scale of elastic deformation of bearing elements. It has previously been shown that a higher stiffness of the bearing, or preloading, which gives the same effects, reduces the shaft vibration and bearing metal temperature [22]. Stiffness of the material has been considered when selecting the bearing.

Quiet running

There are no design requirements of quiet running of the bearing.

The bearing housing will be exposed to high axial thrust forces, and a stable and rigid connection is essential. The bearings are to be lubricated and sealed, in order to reduce the costs of having an external lubrication system. The loads in axial direction are exerted on the upper bearing, through the housing and into the cylindrical flat plate. A double row angular contact ball bearing is chosen for this section. The bearing is simple in design, has low maintenance necessities and fits the current application in terms of the requirements listed above. In addition to forces in radial and axial directions, the bearing also accommodates tilting moments, due to its stiff arrangements [10].

Theoretical calculations prove long lifetime, good performance characteristics and low frictional moment. The results are given in Table 6.2. It is worth noting that these values are based on simplified calculation, only meant for rough estimation of the bearing characteristics. As stated in the theory Chapter 2.3, accurate calculations would require complex computational analysis of the bearing units, which is beyond the scope of this thesis. The description of the SKF estimation model is provided in Appendix B.2.

Table 6.2: Turbine thrust bearing data.

Property	**Notation**	**Value**	**Unit**
Total frictional moment	M_{tot}	1321.9	Nmm
Starting Torque	M_{start}	1687.1	Nmm
Power loss	N_r	210	W
Bearing life	L_{10m}	19800	$hours$
Limiting speed	n_{max}	6000	rpm

For lower section of the turbine shaft, a single row, deep groove ball bearing is chosen. The unit is only supporting the shaft alignment in the radial direction, and is not exposed to any prominent forces. A simple and cost efficient design has been the main purpose of this selection. Similar calculations are applied for this bearing unit, and resulting data is given in Table 4.

Table 6.3: Turbine radial bearing data.

Property	Notation	Value	Unit
Total frictional moment	M_{tot}	492,4	Nmm
Starting Torque	M_{start}	444,7	Nmm
Power loss	N_r	93	W
Bearing life	L_{10m}	$> 10^5$	$hours$
Limiting speed	n_{max}	4300	rpm

The theory behind the calculation model used for selection of the bearings is described in Appendix B.2.

6.3 Axial loads measurement setup

It is suggested to measure the axial forces using silicon strain gauges. These semiconductors are preferred over metal wire based gauges due to the accuracy, sensitivity to strain and fatigue life. The full comparison of the gauges is provided in Appendix D.2.

Both the static and dynamic axial loads of the turbine are transmitted through the thrust bearing and into the bearing house. According to the specification data of the semiconductors [25], gage factors up to 3000 are available. In theory, the gauges could be mounted on the bearing house, or even the shaft, and still measure low strains with high accuracy. The fatigue life of silicon gauges is infinite for load application below 500 strain. The bearings, however, require regular maintenance in terms of either lubrication or replacement of the units. It is therefore desirable to have a separate section for measurement of thrust forces, independent of the bearing accessories.

A circular flat plate with centred hole is used to support the bearing block, absorbing the axial forces of the turbine. The plate, shown in yellow in Figure 6.1, is mounted to the stationary frame with eight bolts. The red lines indicate placement of the gauges.

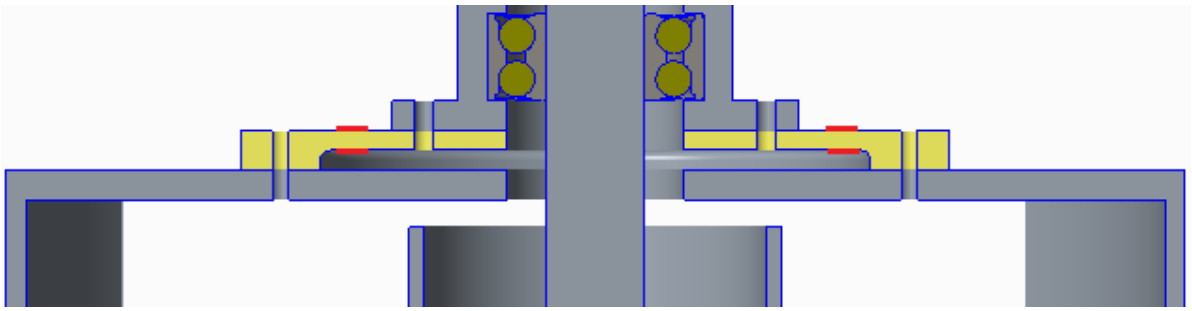

Figure 6.1: Annular plate design with four strain gauges.

Four silicon semiconductors of type C, with gage factor 100 and a resistance of 120 Ω, are used to measure the strain [25]. A full bridge configuration is utilized to ensure maximum signal output and compensation for bending stresses and temperature variations. The equipment is provided by the same vendor to avoid deviation in gage properties. Sensing ability of C-type semiconductors is given to a minimum and maximum strain values of 10 and 1000 respectively. A fellow master student at the Waterpower Laboratory, Einar Agnalt, used semiconductors for his measurements on the turbine runner, and solid performance, with low noise affection and data measured down to 2 microstrains was observed for the sensors. The characteristic data of the semiconductors along with comparison of metal wire based and silicon based strain gauges is provided in Appendix D.

By reducing the thickness towards the centre, the maximum stresses are ensured to occur at the thickness transition area, proportionally to the applied force. The plate is manufactured from stainless steel. Dimensions of the annular plate are based on the gauge measuring sensitivity of semiconductors, as well as the safety factor against yielding and buckling. The values are verified with theoretical calculations and computational stress analysis in Ansys Mechanical.

6.3.1 Stress and strain the annular flat plate

The following calculations are based on the theoretical equations presented in "*Roark's Formulas for Stress and Strain"* [30], in combination with *"Konstruksjonsmekanikk"* [31]. The procedure assumes homogenous isentropic material, and the acting forces are normal to the plane of the plate. The dimensions of the annular plate are designed to withstand the maximum load of 20 kN, while providing enough deflection to measure the lowest strain that will occur. The lowest loading condition is the static load of the turbine, which is equal to the weight of the components supported

by the deflecting plate. After consultation with the staff at Waterpower Laboratory, the static weight of turbine is estimated to 350 kg, which results in a minimum design load of approximately 3500 N.

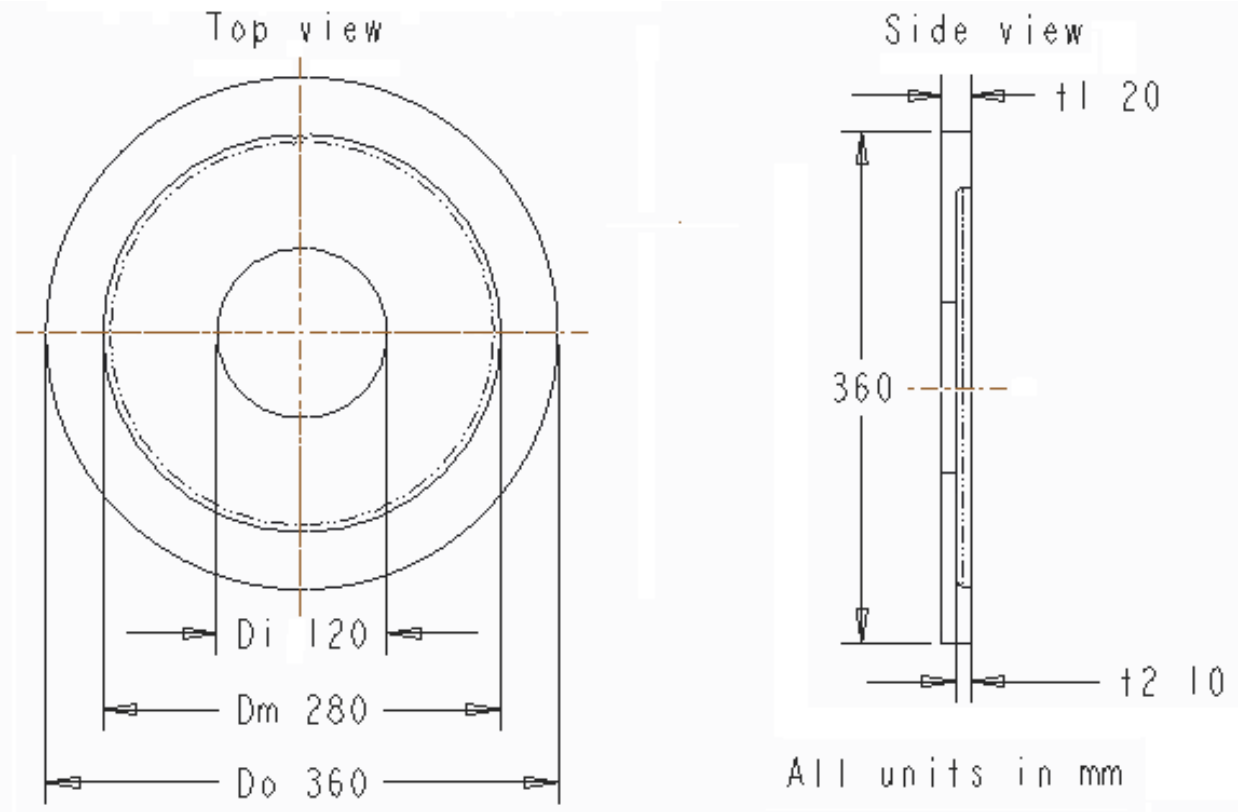

Figure 6.2: Schematic drawing of the annular plate.

In addition to the diameters shown in Figure 6.2, the effective diameter is utilized in the equations. This is the area of the plate at which the load is acting, in this case the contact area of the bearing block and the annular plate. The effective diameter is measured to $D_e = 207\,mm$, with a corresponding radius of $r_e = 103{,}5\,mm$. The thickness in this section, and thus used as critical area in the calculations, is given as t_2 in Figure 6.2.

The maximum stress and deflection of an annular flat plate exposed to a uniform load q is given by Equations (6.1) and (6.2):

$$y_b = -\frac{q{r_e}^2}{D}\left(\frac{C_1 L_{14}}{C_4} - L_{11}\right) \tag{6.1}$$

$$\sigma_{max} = \frac{6M_{max}}{t_e^2} \tag{6.2}$$

Where D, C_1 and C_4 are the plate constants, while L_{11} and L_{14} are loading constants dependent on the ratio of effective radius divided by the inner radius, r_e/r_i. The stress exerted on the annular plate is a function of maximum moment M_{max}, and effective plate thickness t_e. With stress unit available, the corresponding strain is calculated using Equation (6.3):

$$\varepsilon_{max} = \frac{\sigma_{max}}{E} \tag{6.3}$$

Type 304 stainless steel is used for the annular plate. The strain gauges are limited to a measuring range of 10 to 1000 microstrains. The calculated maximum and minimum strains are given in Table 6.4. Full calculation procedure is provided in Appendix B.1.

Table 6.4: Calculated results for the annular plate exposed to axial loads.

	F_{max}	F_{min}	**Unit**
Deflection [y]	0,15	0,027	mm
Stress [σ]	99,2	17,4	MPa
Strain [ε]	514	90	$\mu strain$
Safety Factor [SF]	2,1	$SF > 15$	–

The results of theoretical calculations will vary from the real values, due to assumptions and simplifications mentioned in the introduction to this section. Another source of error is the assumed Poisson's ratio of 0,3, which is rather closer to 0,29 for stainless steel 304 used in this design. The calculations are therefore verified with computational stress analysis prior to manufacturing the annular plate.

6.3.2 Stress analysis

The stress analysis are performed in Ansys Mechanical. The results are shown in Figure 6.3 and 6.4, and listed in Table 6.5.

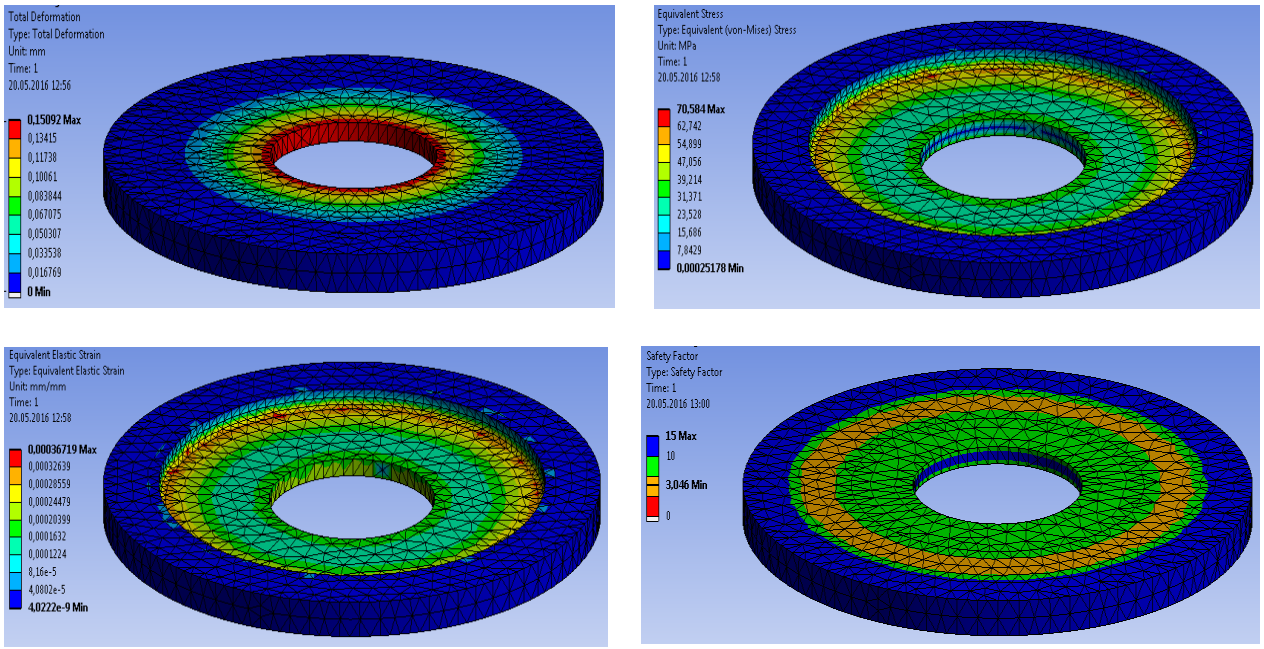

Figure 6.3a) to 6.3d): Analysis for F_{max}, Ansys Mechanical

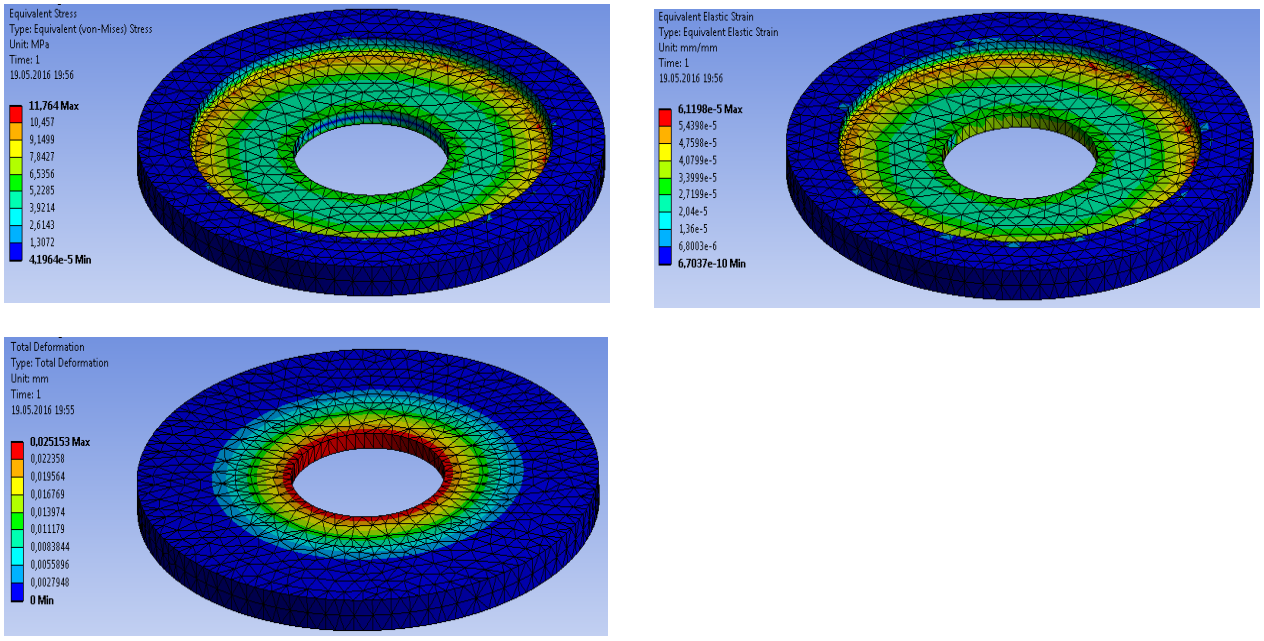

Figure 6.4a) to 6.4c) Analysis for $F_{min,}$ Ansys Mechanical.

Table 6.5: Results for the annular plate exposed to axial loads, Ansys analysis.

	F_{max}	F_{min}	**Unit**
Deflection [y]	0,15	0,025	mm
Stress [σ]	70,6	11,76	MPa
Strain [ε]	367	61,2	$\mu strain$
Safety Factor [SF]	3	$SF > 15$	$-$

The results show slightly lower stress and strain in comparison to the theoretical values. The plate dimensions are either way sufficient, in terms of both safety against yield and tensile, and sensing range of the strain gauges. The design also assures deflection below 500 micro-strain for maximum loading condition, which satisfies the fatigue life limit for infinite operation of the semiconductor gauges.

6.3.3 Installation procedure

Measurements including strain gauges require cautious handling of the equipment. The gauges are highly sensitive, and a step by step procedure is provided to ensure correct mounting. The necessary equipment for strain gauge mounting is provided by the gauge manufacturer, but can also be found in most laboratory facilities.

1. **Prepare the surface of the plate**

Clean the surface of the flat plate where the gauges are to be mounted. This includes removal of grease, dirt, rust etc. Depending on the condition of the plate, this step might require emery cloth, fine and course sand paper or a degreaser. When the shaft is cleaned for rust and dirt, rinse the surface with cleaning fluid, preferably an acid based conditioner to dissolve the remaining grime. Lastly, carefully clean the area with gauze pads.

2. **Prepare the gauges for mounting**

The gauges come in small encapsulations, protected from environmental influence. Take the sensors out and place them on the plate surface, with the bonding side down. Use of tweezers is

recommended when handling the gauges. Add a small piece of tape on top of the gauges, which will make it easier to align the elements in the correct orientation.

3. Position the gauges on the shaft

Top view of the flat plate is shown in Figure 6.5, with the axis indicating correct positioning of the gauges. Place two semiconductors facing towards the center of the plate, with equal distance *R* from the shaft axis. As mentioned in Chapter 6.3, the maximum deflection will occur at the transition zone, where the thickness reduces from 20 to 10 mm. The sensors are to be placed as close to this section as possible. Two other elements are mounted with similar orientation on the other side of the plate. Use an angle measuring tool to ensure correct positioning. Any misalignment will expose the gauges to either tension or compression, resulting in additional forces in the measurement readings.

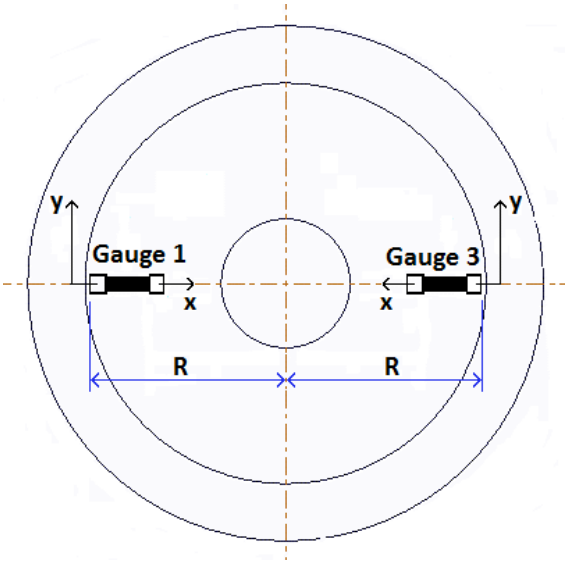

Figure 6.5 Orientation of the strain gauges

4. Glue the gauges to the shaft

When the orientation is in place, glue the sensors to the flat plate and apply pressure on top. Depending on the glue, this might take 3-5 minutes. Using a piece of tape as mentioned in step two will help to keep the gauges correctly oriented while gluing the bottom. As the glue sets, carefully remove the tape from the gauges.

The four gauges are to be connected in a full bridge configuration as illustrated in Figure 6.6. Unlike quarter or half bridge configurations, where the output is approximately linear, the full bridge will provide an output directly proportional to the applied force.

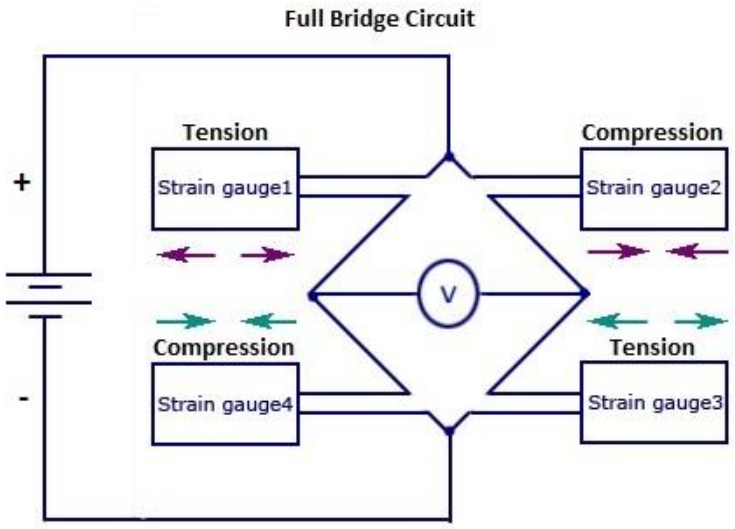

Figure 6.6: Full bridge configuration of the strain gauges.

Strain gauge 1 and 3 are located on top as shown in Figure 6.6, while 2 and 4 are on the opposite side, with similar location and orientation. When the plate is exposed to axial force, element 1 and 3 are in tension, while 2 and 4 are in compression. Gauge 2 and 4 will compensate for temperature variations in gauge 1 and 3 respectively. Due to the opposite sign of these gauges, the bridge output will be doubled for each pair.

6.3.4 Calibration Procedure

The suggested measurement setup is a secondary method according to IEC 60193 [2], and requires calibration by the primary method. Same calibration setup as for the Francis turbine rig at NTNU is to suggested for TTL. The design is detailed in Chapter 5.1. Uncertainty analysis are performed as described in Chapter 5.1.3, with the systematic part consisting of uncertainty in calibration weights, weight of the beam, friction in roller bearing and regression error, and the random part determined by the equipment and procedure.

6.4 Torque measurement

There are different ways of measuring torque on a turbine shaft, some of which already have been reviewed in previous chapters. Four effective methods of measuring the generator torque are presented in this section. Most of the solutions are strain gauge based, with data transmission by either direct contact or wirelessly. The measurement of frictional torque in bearings is covered in section 6.4.5.

6.4.1 Hydrostatic bearing

A hydrostatic bearing is used to support the generator. An arm is connected to the swinging frame of the generator, transferring the radial forces to a load cell. This is a primary method described in IEC 60193 as *"bearing of rotating parts not in balance"* [2]. The measurement is independent of the turbine bearing parts, and torque is determined for generator only. This solution exists for the Francis turbine test rig at NTNU.

6.4.2 Slip rings

The torque is measured with a strain gauge based sensor mounted to the shaft. The signal is sent to the stationary receiver through a set of conductive slip rings attached to the coupling. The rings are in constant contact with a series of brushes, transferring the signal from rotating to stationary parts of the system. Slip rings provide an economical solution, with only drawback being the wear of the elements in mechanical contact. This method is well suited for laboratory applications, but not recommended for continuous operation. This is also a primary method of *"bearing of rotating parts not in balance"* [2].

6.4.3 Torque meter

This strain gauge based torque measuring device is more expensive than slip rings, but provide high accuracy, load capacity and stiffness when in use. The solution is similar to slip rings, but instead of direct contact between the parts, the power is transmitted to the shaft transducer through

a rotary transformer. The power supplies the torque measuring device, and converts the signal into a digital output. Infrared light is used to transmit the digitized signal to the stationary receiver. The unit is also mounted on shaft coupling, and has integrated option for rotational speed measurement. The torque meter is space efficient, and with no bearings or slip rings giving mechanical contact, no maintenance is required. Similar solution of *"bearing of rotating parts not in balance"* [2] exists for the Pelton turbine test rig at NTNU.

6.4.4 Strain gauges with telemetry system

The high sensitivity of the silicon strain gauges makes it possible to measure the shaft torsion by direct application. With standard metal wire gauges, the general guideline is that torque must induce at least 100 micro-strain in order for the gauges to sense this motion. Semiconductors can measure same property down to 1-2 micro-strain. The low sensibility to noise of semiconductors is another advantage, as the noise often becomes a challenge at high speeds. The gauges are mounted on the shaft closest to the turbine. Utilizing the principle described in chapter 4.2, with sensors oriented with 45° angle to the shaft axis, the torque of the turbine is determined.

During operation of the turbine, the semiconductors are rotating with the speed of the shaft. Cabled connections cannot be used to transmit data to the acquisition equipment. This is solved by converting the voltage output to a digital signal, before wirelessly transmitting it to the stationary receiver. The method is described in detail in section 6.4.5.

6.4.5 Measurement of friction torque

One way of measuring the friction torque is by use of a load cell with a swinging arm. The method is described in Chapter 3.1.6, and involves a double cylindrical bearing house, one stationary and one in free rotation. The swinging arm is attached to the inner cylinder, and is only affected by the frictional forces of the bearings. The arrangement is exposed to high uncertainty due to the additional bearings between the two cylinders. Similar solution exists for the Pelton turbine test rig at NTNU.

Another method is to remove the turbine runner and drive the shaft with a motor. The deviance between the torque delivered by the motor and what is measured as the generator torque, amounts

for frictional torque in the bearings. Several factors will affect the accuracy of this method. One uncertainty is that motor input and output are rarely the same, due to mechanical losses in the transmission. Another uncertainty of this method is the assumption that the friction torque will be the same with the turbine in place.

It is suggested to measure the friction torque similarly to the generator torque measurement, using strain gauges in combination with wireless telemetry system. Strain gauges applied below the bearing block provide the turbine torque transmitted through the shaft. With the generator and turbine torques known, the deviance will account for friction loss in seals and bearings.

The wireless signal transmission setup consists of following equipment:

- Four semiconductor strain gauges
- Power battery
- Wireless rotary transmitter
- Remote control
- Stationary receiver

The signal transmitter is, along with the strain gauges and a battery, directly mounted on the shaft. The transmitter, powered by the battery, is used to condition and excite the strain gauges. The voltage output of the strain gauges is converted to a digital signal in form of frequency by the transmitter. This signal is in turn sent to the stationary receiver, where it is converted back to a voltage signal. In addition to providing an analog voltage signal, the receiver also amplifies the output in a range of 0-10 Volts. As there is no mechanical contact between the equipment, the need for maintenance is very low. The remote controller is useful in laboratory applications, for configuration of channel and gauge settings, as well as controlling the power supply. The setup is shown in Figure 6.7.

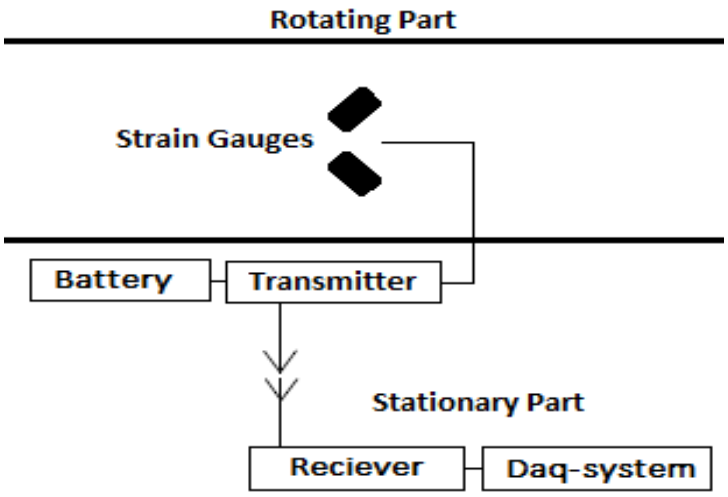

Figure 6.7: Shaft torque measurement setup with telemetry system.

With correct installation and equipment, the telemetry transmission method is highly beneficial. An obvious advantage is the economical aspect of it. This is more detailed in Section 6.5, "*Cost Estimation"*.

Four silicon strain gauges connected in a full bridge configuration are used to measure the torque. The gauges are oriented 45 degrees to the shaft axis, in pair of two on each side of the shaft, providing amplified output and temperature compensation. In order to comply with the transmission equipment, semiconductors of type D with 350 Ω resistance and 115 gage factor are chosen for this application.

Telemetry equipment for the exact purpose of strain gauge measurement is available in the market. A TorqueTrak kit is suggested for use of friction torque measurement at TTL. In addition to wireless transmission, the TorqueTrak equipment also include filter and signal processing tools for clean output. The unit is operating with 16 channels at 500 Hz frequency response. The equipment provided possibility for gain adjustment, a useful feature when low strain measurements are expected.

A 3D representation of the lower section of the turbine shaft is presented in Figure 6.8. The strain gauges are to be mounted close to the runner, before the shaft torque is affected by the friction in bearings. As the turbine requires a radial bearing as close to the turbine as possible to absorb the radial forces, the space between the runner and lower bearing is extremely limited. The strain gauges are small in size, between 2,5 to 6,5 millimetres, and can be mounted below the radial

bearing. The transmitter, on the other hand, must be located above the bearing, due to the limited space. It is suggested to run the cables connecting the strain gauges to the transmitter through the shaft, as shown in Figure 6.8. This is achieved by designing the shaft with a removable section for gauge installation. The section can be attached by either bolts or simply glued on. Once the cables are run through the shaft, there is no future need for removal of the shaft section.

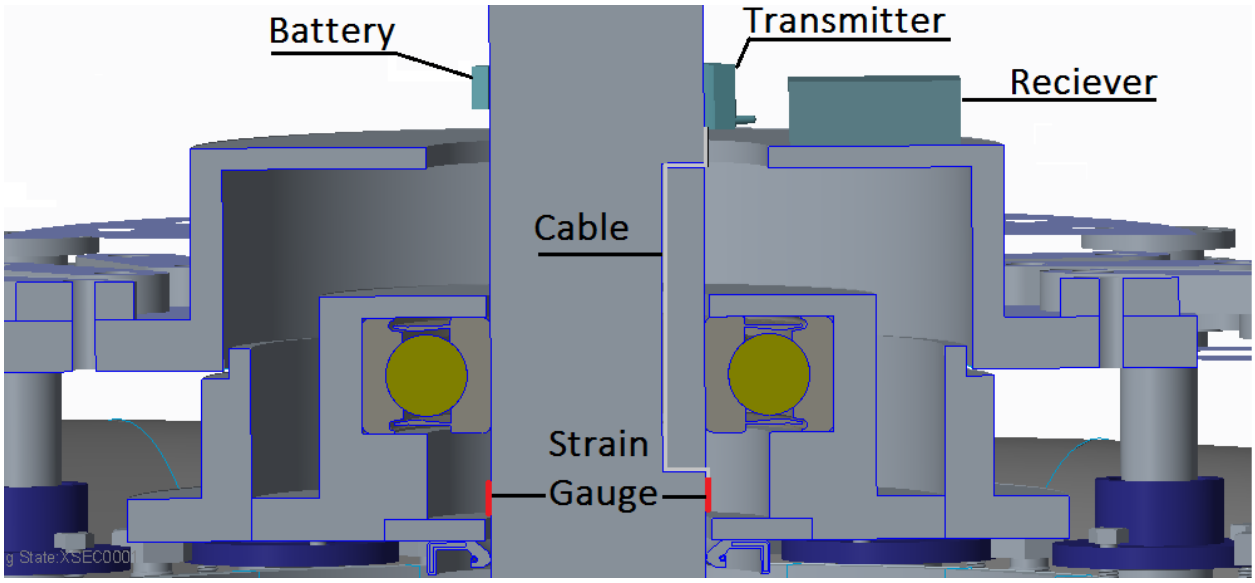

Figure 6.8: 3D model of the shaft torque measurement setup.

The signal transmitted wirelessly will cause a time delay on measurements. This delay is inevitable, and presents a challenge for friction torque measurement. Unless the both measurement setups are operating at exact same conditions, the generator and turbine torques will be measured at different periods. This issue is resolved by using the same receiver for the two setups, and adjusting the two transmitters to sample and transmit at equal rates.

The complete design of the Francis turbine test rig at the Turbine Testing Laboratory is presented in Figure 6.9.

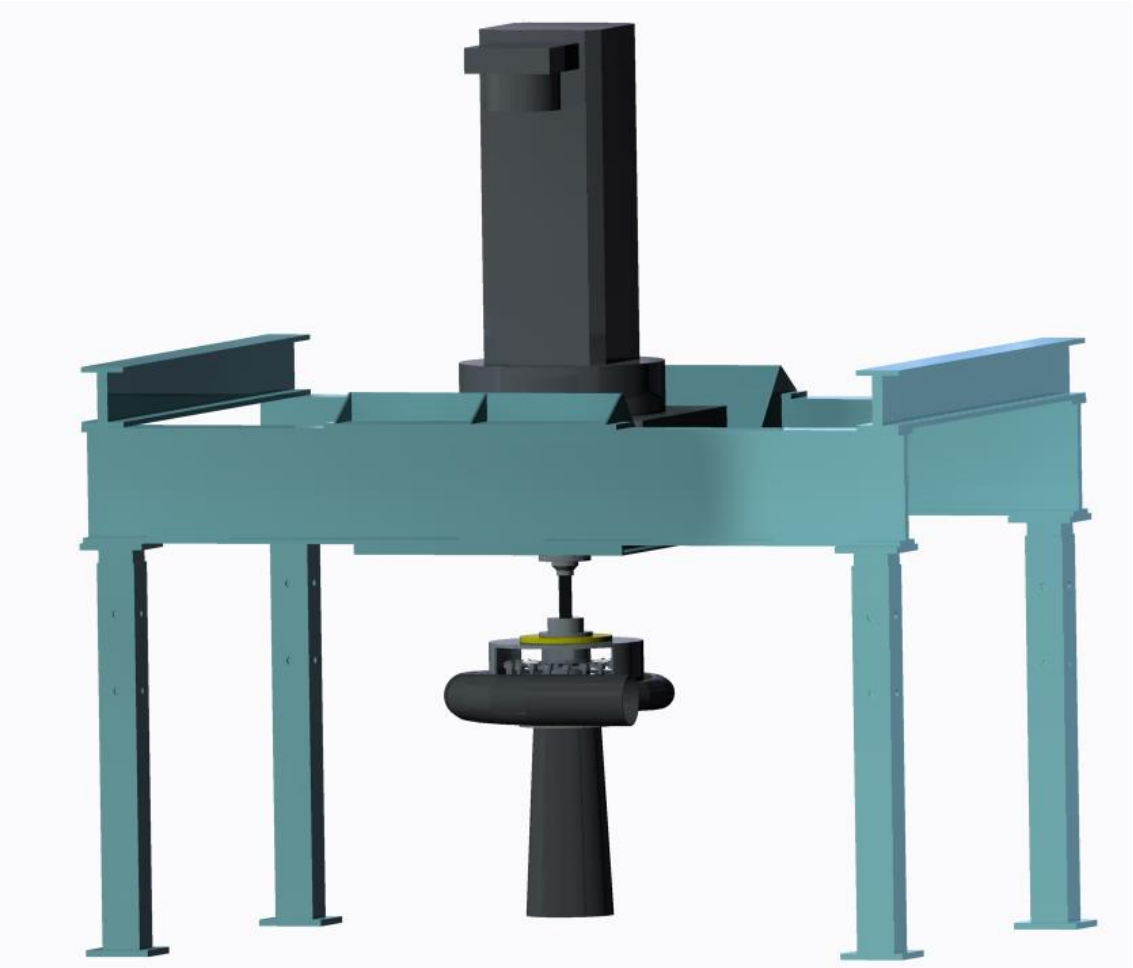

Figure 6.9: 3D model of the Francis turbine test rig at TTL.

6.4.6 Calibration

It is suggested to calibrate the measuring equipment with a known reference force. This is done with calibrated weights applied to the end of a cantilever beam. Similar arrangement is presented in Chapter 3.1.4. With length of the beam known, the applied torque is determined and can be compared to the strain gauge readings in order to determine the deviation and thus the uncertainty of the measurements. During the calibration, the shaft has to be restrained against movement in the generator section, while applying the known force of the opposite end. Due to the vertical alignment of the shaft, the calibration setup will also require a pulley converting the weight forces to torsional movement on the shaft.

6.5 Cost estimation

A total cost estimation of the component list is shown in Tables 6.6 - 6.8. This is a rough estimation performed by the author, based on the Norwegian prices of the equipment. Due to the large variety of applicable solutions, the costs of data acquisition equipment is not included.

Table 6.6: Cost estimation of equipment related to shaft and bearing arrangement.

Equipment	**Quantity**	**Cost [USD]**
Bearing block and seals	1	8000
Shaft	1	6500
Thrust bearing	1	1800
Radial bearing	1	700
Couplings	1	2600
Total		**19600**

Table 6.7: Cost estimation of equipment related to axial force measurement.

Equipment	**Quantity**	**Cost [USD]**
Annular flat plate	1	500
Semiconductor strain	4	200
gauges	1	250
Strain gauge accessory kit		
Total		**950**

Strain gauge accessory kit includes all the recommended equipment for placement and installation of the sensors. Proper installation is a requirement for reduced error in the measurements. The kit includes:

- Curing adhesive
- Sand paper
- Cleaning agent
- Protective coating
- Solder terminals
- Connecting wire

The costs of data acquisitions equipment are not included due to large variety of fitting solutions. In general, the instrumentation would consist of a signal conditioning amplifier, a detector and a recorder.

Table 6.8: Cost estimation of equipment related to torque measurement.

Equipment	**Quantity**	**Cost [USD]**
Semiconductor strain gauges	4	200
Strain gauge accessory kit	1	250
Telemetry equipment	1	4200
Total		**4650**

There is a large variety of wireless signal transmission equipment available in the marked. The price listed in Table 6.8 relates to a telemetry equipment kit, provided for the particular purpose of torque measurement with strain gauges. The kit includes mainly a transmitter, a power battery, a remote controller and a stationary receiver. In addition to this, accessories such as antenna element, cables, wall plug transformers and bridge simulator can be included. Cheaper solutions are available if desired, such as a commercial wireless microphone system. With small adjustments to the system, the gauge output could be converted to a microphone-complying signal for wireless transmission. The method has not been reviewed in detail in this thesis.

Chapter 7
Discussion

The focus has been to design setups for measurement of friction torque and axial force on the Francis turbine at both Waterpower Laboratory and Turbine Testing Laboratory. Simple design, accurate performance and low cost have been the dimensioning elements in solving the task. As no physical experiments were performed during this project, the estimation of measurement accuracy is limited to theoretical descriptions. The work presented in Chapters 5 and 6 is a fundamental starting point for the measurement setups, with further work on the subject presented in Chapter 9.

7.1 Axial force measurement and calibration setup at NTNU

The designed calibration setup was developed after discussion with professor Ole Gunnar Dahlhaug. The solution is accurate and reliable, and can be utilized for any type of thrust force measurement procedure. Critical parts of the setup have been evaluated in Chapter 5.1 to ensure safe design. The thickness of the individual components can be optimized further with detailed load analysis on each component. Reducing the required material thickness will result in lower manufacturing costs.

The idea of using a roller bearing to support the moving beam is to minimize the friction between the rotating and stationary parts. This is effective as long the bearing is ensured good performance, which requires correct lubrication and bearing design. All bearings are exposed to elastic deformation, affecting the performance and friction induction on the measurements. This has to be accounted for in long term operation.

7.2 Friction torque measurement setup at NTNU

Solving the challenge of a membrane induced friction torque was approached in many ways, with no immediate solution. The obvious answer has been to change the material of the membrane. A slightly more elasticity would provide a higher angle of rotation for the bearing house. Even though this would not completely remove the error, it would still reduce it extensively. The material of the current membrane is unknown. A good alternative would be Acrylonitrile-Butadiene (NBR), a material widely used to separate fluids in hydrostatic bearings. NBR has high resistance to oil and water and good mechanical properties in terms of elasticity

The suggested method for measurement of friction torque introduces new uncertainty factors, as mentioned in Chapter 5.2. Theoretically, the chosen screw based linear motion motor performs good enough to provide accurate measurements. For actual measurements, the estimated uncertainty will be higher due to random errors. If a higher accuracy is required, piezoelectric linear actuators at are available in the market, providing motion at nanoscopic level.

7.3 Axial force measurement setup KU

As Turbine Testing Laboratory at Kathmandu University requires cost efficient solution, use of hydrostatic bearing is not an option. The axial force is measured with semiconductor strain gauges, a choice based on recommendation from the staff at the Waterpower Laboratory. These highly sensitive gauges have been tested at the Waterpower Laboratory, and reliable performance characteristics have been observed.

The annular plate is designed to comply with measuring characteristics of strain gauges. Additionally, the dimensions are within the available space in the radial direction on the current design of the Francis rig at TTL. If any changes affecting the radial clearance are imposed to the design, an alternative solution is suggested in Figure 5. The arrangement consists of a cylinder with centered hole for shaft placement. The cylinder is supporting the bearing block, with axial forces acting vertically on the unit. As mentioned in Chapter 4.3, an important requirement when

measuring stress with strain gauges is that the sensors have to be placed at area of maximum occurrence. This is ensured by removing a two section of the wall in a rotating motion from top to bottom. Maximum stress will occur at area where the reduction is overlapping, circled red in Figure 7.1. Mounting semiconductors in this section will provide same result as the annular plate design suggested in Chapter 6.3. Machine drawing of the design is provided in Appendix C.3.

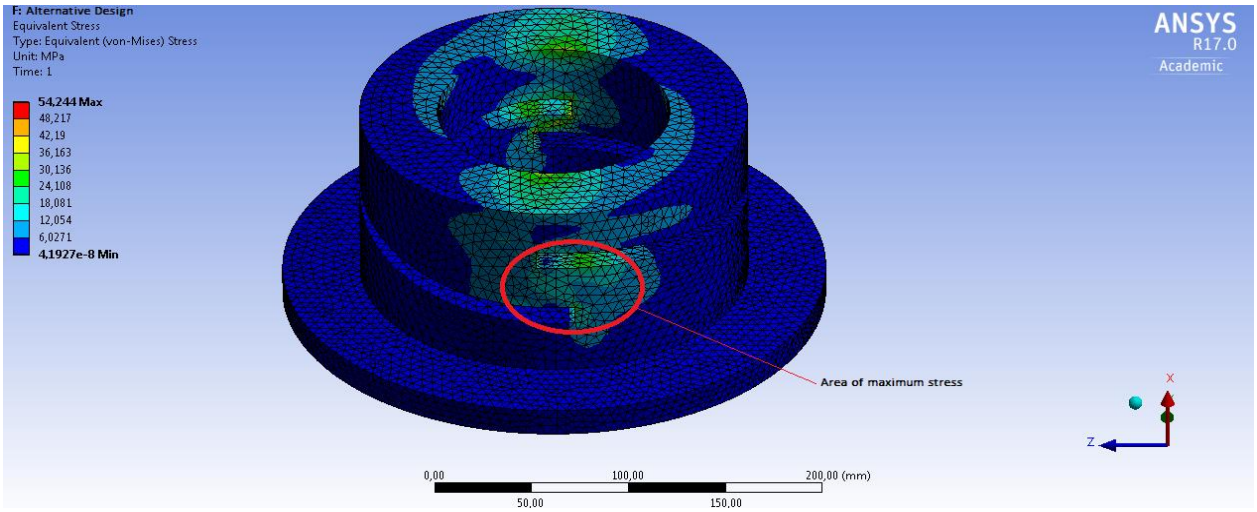

Figure 7.1 Friction torque measurement setup at KU

The suggested setup for measurement of frictional torque takes advantage of the high sensitivity of silicon strain gauges. With measurements down to 2 microstrains, the gauges are able to sense the smallest torsional forces of the shaft. As mentioned in Chapter 6.5, the signal transmission equipment suggested is not of the cheapest type. Wireless units are widely available, and more cost efficient solution can be considered if desirable.

Standard signal transmission range for TorqueTrak units is 0,5 m. If the receiver is located further than this, external transmitter and receiver antennas should be obtained. Transmission distance can be increased to 6 m or more with use of antennas, at the cost of higher time delay of the signal.

The cables of the strain gauges are run through the shaft. When designing the removable section, it is important to pay attention to the shaft properties, to avoid reduction in the design strength.

The desired torque exerted on the shaft by the turbine runner is obtained by mounting the strain gauges close to the runner. The purpose of measuring the generator and frictional torque separately is no longer present, and the design can consist of only one measurement setup. This will reduce the cost of equipment, as well as uncertainty resulting from two separate readings.

Chapter 8
Conclusion

Suggestions for the friction torque and axial force measurement setups have been developed for the Waterpower and Turbine Testing Laboratories. The rules and guidelines of IEC 60193 [2] have been utilized when forming the designs.

The new designs of the Waterpower Laboratory are based on the existing methods. The friction torque measurement and calibration setup has been modified for fit the requirements of the new thrust block. A linear stepper motor has been introduced, with the possibility of controlling the torque exerted on the load cell. 3D models have been made for both the existing and the new designs, as well as detailed machine drawings of the new setup.

The axial force calibration setup is designed to calibrate forces in both directions. Hand calculations and computational analysis are done to ensure the design sufficiency. The setup is dimensioned for a design load of $10\ kN$ in the axial direction. Uncertainty analysis are performed for the setup, and a systematic uncertainty of $0{,}0523\ \%$ is established. 3D models and machine drawings of the consisting parts are available.

Work related to the Turbine Testing Laboratory is an input to the development of a full scale hydropower laboratory in Nepal. Suggestions for measurement and calibration of friction torque and axial load are presented. Simple, cost efficient solutions that comply with the requirements of IEC 60193 [2] has been the main objective when developing the designs. As the test rig at TTL is not fully developed, the suggestions in this thesis are based on the operational data of the Francis turbine at the Waterpower Laboratory. The measurement setups are based on strain gauge technology, utilizing the high accuracy and sensitivity of silicon sensors.

A complete 3D model of the Francis test rig at TTL, including the suggested friction torque and axial force measuring arrangements, are provided in the Appendix H. The designs presented are an introduction to cost efficient methods for measurement of friction torque and axial force on the turbine, with further work on the subject presented in Chapter 9.

Chapter 9
Further Work

This chapter covers the recommendations for further development of the individual concepts.

Axial force measurement and calibration setup, Waterpower Laboratory, NTNU.

The calibration setup is simple in both design and operation. Due to the high magnitude of the calibration force, the resulting uncertainty is low relative to the measurements. The design has been briefly evaluated for stress and deflection, but further analysis is recommended. Thickness of the consisting parts should be optimized to reduce the material costs. The stress analysis is performed for standard structural steel. The hardness and chemical composition has to be decided based on price and availability of the material.

With the material and component thicknesses optimized, the parts should be manufactured and installed at the Waterpower Laboratory. Lastly, a full calibration process should be performed for the axial force measuring equipment.

Friction torque measurement and calibration setup, Waterpower Laboratory, NTNU.

As discussed in chapter 7.2, changing the material of the membrane will simplify, if not solve, the problem. The first step in further work should be to change the current material to something with higher elasticity and perform calibration of the friction torque to determine the influence of the membrane.

The main objective of the friction torque measurement setup presented in this thesis is to counteract the frictional forces of the membrane. This is achieved with linear actuator exerting torque on the load cell. In order to decide how much torque is needed, it is necessary to acquire knowledge on how much force the membrane is holding back with. It is suggested to find out how much the membrane stretches with the applied force, as well as determining the peak point of the elasticity. A way of estimating this would be to apply weight load on the calibration arm, with linearly increasing steps. For each weight added, the axial positioning of the arm will change slightly along

with the bearing cover. This change can be used to determine how much the resistance of the membrane increases with the applied load.

Most of the consisting parts can be reused from the existing setup. The remaining parts have to manufactured, and installed on the thrust block. A full calibration procedure of the friction torque measuring equipment should be performed for the both new and old systems, in order to compare the results and determine the deviance.

Axial force measurement and calibration setup, Turbine Testing Laboratory, KU.

The annular plate has been manufactured at the Waterpower Laboratory and is ready for experimental testing. It is suggested for further work to mount the strain gauges and perform axial force measurements. The dimensions are customized to the Francis turbine at TTL. This also includes the effective diameter, on which the bearing block is resting, and thus the area on which the force should be exerted on. New stress analysis should be performed if any changes are imposed to the bearing block design.

Friction torque measurement and calibration setup, Turbine Testing Laboratory, KU.

The work presented in Chapter 6.5 is an introduction to a simple and accurate method for torque measurement, customized to the Francis turbine test rig at TTL. The setup is not fully developed, and requires further detailing. It is suggested to invest time in developing a more cost efficient solution for signal transmission. Even though similar solutions are frequently used in shaft torque measurements, they usually comply for metal-foil based gauges. Though metal-foil and silicon elements both utilize resistance in material to measure strain, the performance characteristics of these are very different. This should be accounted for when considering telemetry options.

Regarding the cables connecting the semiconductors to the transmitter, the shaft design should be detailed further prior to manufacturing. This will require strength analysis of the shaft to assure no failure will occur due to the reduced material.

Bibliography

[1] Waterpower Laboratory, *"Procedure for the Francis Turbine Test Rig"*. *NTNU, 2016*

[2] International Electrotechnical Commission. *"IEC 60193 Hydraulic turbines, storage pumps and pump-turbines Model Acceptance tests"*, Second Edition, 1999.

[3] Kjølle, A., *"Mechanical Equipment"*. Waterpower laboratory, NTNU, 2001.

[4] Rasmussen, I. J., "*Design of a Francis model test rig at Kathmandu University"*. Waterpower laboratory, *NTNU, 2014*

[5] Brekke, H., "*Pumper & Turbiner"*. Waterpower laboratory, NTNU, 2003.

[6] Storli, P-T., S, *"Modelltest av Francis turbin I vannkraftlaboratoriet ved NTNU, Trondheim"*. NTNU 2006.

[7] Slocum, A., "*Fundamentals of Bearings"*. Massachusetts Institute of Technology, 2008

[8] Harnoy, A., *"Bearing Design in Machinery: Engineering Tribology and Lubrication"*. New Jersey Institute of Technology, 2003.

[9] Cline, R., "*Alignment of vertical shaft hydrounits, (2000 ed.)",* US Department of the Interior Bureau of Reclamation, Denver, Colorado.

[10] Swedish ball bearing company, SKF, 2016 http://www.skf.com/pk/products/bearings-units-housings

[11] Gûlich, J. F., "*Centrifugal pumps"*, Second edition, Springer-Verlag, 2008

[12] Hydroelectricity Investment & Development Company Limited. *"Nepal Hydropower Overview"*, 2014 – 2015

[13] Reinertsen, K., *"Testrigg for Peltonturbinmodeller ved Vannkraftlaboratoriet"*. Vannkraftlaboratoriet, NTNU, 2012.

[14] Brandåstrø, B., "*Presentation of the Waterpower Laboratory"*. Waterpower Laboratory, NTNU, 2005.

[15] Rajkarnikar, B., H., "*Design of a Francis turbine test rig"*, Waterpower Laboratory, NTNU, 2012

[16] Turbine Testing Laboratory, Kathmandu University http://www.ku.edu.np/ttl/

[17] Hamrock, B., J., & Anderson, W., J., *"Rolling-Element Bearings"*. NASA reference publication, June 1983.

[18] Heathcote, H., L., *"The ball bearing: In the making, under test and on service"*. Proceedings of the Institute of Automobile Engineers, 1921.

[19] Khonsari, M., M., & Booser R., E., *"Applied Tribology: Bearing Design and Lubrication"*, second edition. British Library Cataloguing in Publication Data, 2008.

[20] Tabor, D., *"The Mechanism of Rolling Friction. II. The Elastic Range"*. Royal Society, April 1955.

[21] Waterpower Laboratory, *"Procedure for Running the Francis turbine test rig". NTNU, 2016.*

[22] Hyun, C., H., *"Preload Effects of a Guide Bearing on the Metal Temperature and the Shaft Vibration".* Journal of Tribology, January 2001.

[23] National Instruments, *"Measuring with Strain Gages"*. National Instruments, 2016. http://www.ni.com/white-paper/3642/en/

[24] Regtien, P., P., L., *"Sensors for Mechatronics"*, 1st edition. Univercity of Twente, The Netherlands, 2012.

[25] Kulite Pressure Transducers, *" Semiconductor Strain Gage Manual"*, Kulite semiconductor products, 2016.

[26] Nâsselqvist, M., Gustavsson, R., Aidanpââ, J.-O., *"Bearing Load Measurment in a Hydropower Unit Using Strain Gauges Installed Inside Pivot Pin"*. Society for Experimental Mechanics, 2011.

[27] Gustavsson, R., K., Andanpââ, J.-O., *"The influence of magnetic pull on the stability of generator rotors"*. 10th International symposium on transport phenomena and dynamics of rotating machinery, Honolulu, Hawaii, 2004.

[28] Lundstrøm, L., P., Aidanpââ, J.-O., *"Whirling frequencies and amplitudes due to deviations of generator shape"*. International Journal of Non-Linear Mechanics, 2008.

[29] Lindeburg, M., R., *"Mechanical Engineering Reference Manual"*, 13th Edition. Professional Publications Inc., Belmont, USA, April 2015.

[30] Young, W., C., & Budynas, R., G., *"Roark's Formulas for Stress and Strain"*, Seventh Edition. McGraw-Hill Companies, Inc., 2002.

[31] Kolbein, B., *"Konstruksjonsmekanikk"*, Del 2. Fagbokforlaget, 2015.

[31] Consultation meetings with Professor Ole Gunnar Dahlhaug, supervisor for this thesis. Waterpower Laboratory, NTNU, 2016.

[32] Johansen, H., *"Styrkeberegning: skrueforbindelser"*. Kompendium, Høgskolen i Gjøvik, 2012.

[33] Norsk Standard, *"NS 1873-ISO 724 "*. Norsk verkstedsindustris Standardiseringssentral, 1983.

[34] Alternate Hydro Energy Center, "*Selection of Turbine and Governing System for Hydroelectric Project"*. Indian Institute of Technology, Roorkee, May 2011.

[35] Thomson Linear Motion http://www.thomsonlinear.com/

Appendix A

Systematic Uncertainty of the Axial Force Calibration Setup

The total systematic uncertainty of the axial force calibration setup $(f_{F_a})_s$ is given as the sum of:

- Uncertainty in calibration weights, f_{W_1}
- Regression error, f_{reg}
- Uncertainty due to the weight contribution of the setup, f_{W_2}
- Uncertainty caused by the friction in roller bearing, f_f

The total systematic uncertainty is given by Equation A.1.

$$(f_{F_a})_s = \pm\sqrt{(f_{W_1})^2 + (f_{reg})^2 + (f_{W_2})^2 + (f_f)^2}$$

A complete model test of the Francis turbine at the Waterpower Laboratory has been performed previously by Pål-Tore Storli [6]. The weights used by Storli in calibration of weighting tank are used when calibrating the axial force transducers as well. The variation in each weight was estimated by Storli to 75 grams. Two 500 kg weight blocks are used for calibration of 10 kN load, and the corresponding uncertainty is calculated:

$$f_{W_1} = \frac{(\sqrt{2} \cdot 75)}{(1000000/100)} = 0{,}01061\%$$

The uncertainty arising from the regression process is given by IEC 60193 [2]. It is stated in section 3.9.2.2.2 [2] that a conventional value of $\pm 0{,}05$ % can be assumed for this uncertainty.

The forces acting on the rotating beam in dead state are shown in Figure A.1.

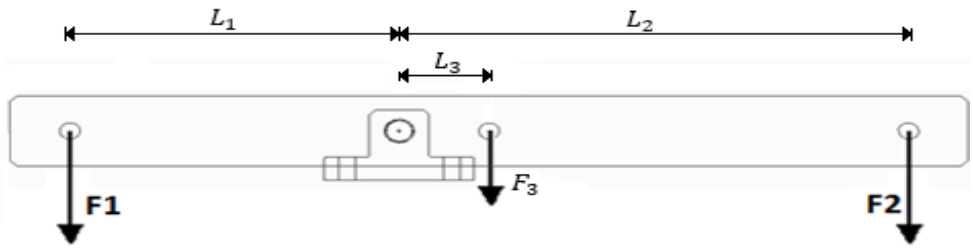

Figure A.1: Forces acting on the freely supported beam

Force F_3 is calculated by applying torque balance on the beam:

$$F_3 = \frac{F_1 L_1 - F_2 L_2}{L_3} = \frac{F(L_1 - L_2)}{L_3} \quad [N]$$

The mass of the empty weight holders is obtained from the properties of the 3D model generated in Creo 3.0 Parametric.

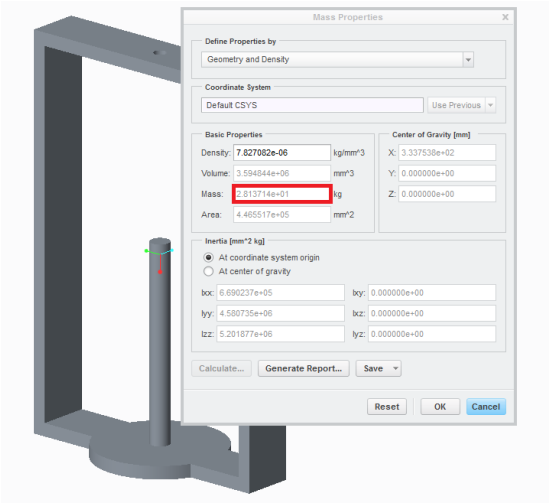

Figure A.2: Mass properties of the weight holder, Creo Parametric 3.0.

With each holder weighting 2,8 kg, the loads F_1 and F_2 are determined to $27{,}6\ N$. The length are found from machine drawing provided in Appendix D.1: $L_1 = 220\ mm$, $L_2 = 340\ mm$ and $L_3 = 60\ mm$.

$$F_3 = \frac{27{,}6 \cdot (220 - 340)}{60} = -55{,}2\ N$$

For a calibration load of 10 kN applied at distance L_1, the relative systematic uncertainty due to the weight contribution of the holders constitutes for $0{,}0025$ %. The uncertainty will vary in tact with the applied load.

The design load acting on a distance of $L_1 = 210\ mm$ from the support, exerts a torque of $21 * 10^5\ Nmm$ on the bearings. The friction forces counteracting this torque is another source of uncertainty. Anti-friction ball bearings are used specifically for the purpose of reducing this effect. The moment is estimated using the SKF model [10], detailed Appendix B.2. Two deep groove ball bearing with bore diameter $d = 25\ mm$ and sealed lubrication, would give a frictional moment of $235\ Nmm$. This constitutes for $0{,}011$ % uncertainty in the measurements.

Total relative systematic uncertainty is calculated:

$$(f_{F_a})_s = \pm\sqrt{0{,}01061^2 + 0{,}05^2 + 0{,}0025^2 + 0{,}011^2} = 0{,}0523\ \%$$

Appendix B Calculations

B.1 Stress and Deflection in the Annular Flat Plate

The calculations are performed according to *"Roark's Formulas for Stress and Strain"* [30] for annular

flat plate with poisons ratio $\nu = 0{,}3$. Material properties for 304 Stainless steel, along with the dimensional values of the annular plate are given in Table B.1.

Table B.1.1: Dimensional values for the annular plate exposed to axial loads.

Property	Notation	Value	Unit
Outer radius	r	180	mm
Middle radius	r_m	140	mm
Inner radius	r_i	60	mm
Effective radius	r_e	103,5	mm
Thickness	t	20	mm
Effective thickness	t_e	10	mm
Tensile yield strength	σ_y	210	MPa
Young's modulus	E	$193 * 10^3$	MPa
Maximum load	F_{max}	$10 * 10^3$	N
Minimum load	F_{min}	4000	N

The following equations are intended for the case of uniform load acting on an annular plate with fixed outer edge and free inner edge, as illustrated in figure A.1 [30]. The expressions are derived based on series of experimental investigations of the scenario.

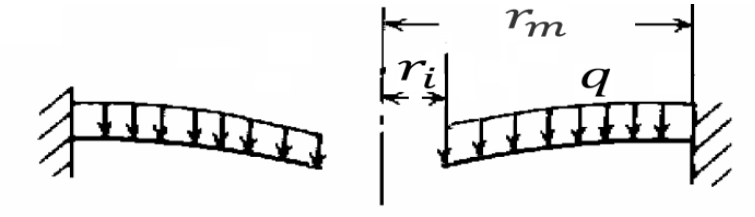

Figure B.1.1: Uniform load on an annular flat plate, [30].

Maximum deflection y_{max}, and stress σ_{max}, due to the uniform load on the plate is given by:

$$y_{max} = -\frac{q{r_m}^2}{D}\left(\frac{C_1 L_{14}}{C_4} - L_{11}\right)$$

$$\sigma_{max} = \frac{6M_{max}}{t_e^2}$$

q is defined as the force divided by effective area, A_e.

$$A_e = (r_e^2 - r_i^2)\pi = (103{,}5^2 - 60^2)\pi = 22344\ mm^2$$

$$q = \frac{F_x}{A_e} = \frac{20000}{22344} = 0{,}9\ N/mm^2$$

The plate constant D is a function of plate thickness and material properties:

$$D = \frac{E{t_e}^3}{12(1-\nu^2)}$$

$$D = \frac{(193 * 10^3)N/mm^2 * (10mm)^3}{12(1-0{,}3^2)} = 17673993\ Nmm$$

Maximum bending moment of the beam:

$$M_{max} = -qr_m^2\left(L_{17} - \frac{C_7}{C_4}L_{14}\right)$$

Furthermore, the plate constants C_1, C_4 and C_7, and the loading constants L_{11}, L_{14} and L_{17}, are dependent on the ration between middle radius, r_m, and inner radius r_i of the plate.

$$C_1 = \frac{1+\nu}{2}\frac{r_i}{r_m} + \ln\frac{r_m}{r_i} + \frac{1-\nu}{4}\left(\frac{r_m}{r_i} - \frac{r_i}{r_m}\right)$$

$$C_1 = \frac{1+0{,}3}{2}\frac{60}{140} + \ln\frac{140}{60} + \frac{1-0{,}3}{4}\left(\frac{140}{60} - \frac{60}{140}\right) = 0{,}57$$

$$C_4 = \frac{1}{2}\left((1+\nu)\frac{r_i}{r_m} + (1-\nu)\frac{r_m}{r_i}\right)$$

$$C_4 = \frac{1}{2}\left((1+0{,}3)\frac{60}{140} + (1-0{,}3)\frac{140}{60}\right) = 1{,}1$$

$$C_7 = \frac{1}{2}(1-\nu^2)\left(\frac{r_m}{r_i} - \frac{r_i}{r_m}\right)$$

$$C_7 = \frac{1}{2}(1-0{,}3^2)\left(\frac{140}{60} - \frac{60}{140}\right) = 0{,}867$$

$$L_{11} = \frac{1}{64}\left(1 + 4\left(\frac{r_i}{r_m}\right)^2 - 5\left(\frac{r_i}{r_m}\right)^4 - 4\left(\frac{r_i}{r_m}\right)^2 * \left(2 + \left(\frac{r_i}{r_m}\right)^2\right) ln\frac{r_m}{r_i}\right)$$

$$L_{11} = \frac{1}{64}\left(1 + 4\left(\frac{60}{140}\right)^2 - 5\left(\frac{60}{140}\right)^4 - 4\left(\frac{60}{140}\right)^2 * \left(2 + \left(\frac{60}{140}\right)^2\right) ln\frac{140}{60}\right) = 0{,}003$$

$$L_{14} = \frac{1}{16}\left(1 - \left(\frac{r_i}{r_m}\right)^4 - 4\left(\frac{r_i}{r_m}\right)^2 ln\frac{r_m}{r_i}\right)$$

$$L_{14} = \frac{1}{16}\left(1 - \left(\frac{60}{140}\right)^4 - 4\left(\frac{60}{140}\right)^2 ln\frac{140}{60}\right) = 0{,}0215$$

$$L_{17} = \frac{1}{4}\left(1 - \frac{1-\nu}{4}\left(1 - \left(\frac{r_i}{r_m}\right)^4\right) - \left(\frac{r_i}{r_m}\right)^2\left(1 + (1+\nu)ln\frac{r_m}{r_i}\right)\right)$$

$$L_{17} = \frac{1}{4}\left(1 - \frac{1-0{,}3}{4}\left(1 - \left(\frac{60}{140}\right)^4\right) - \left(\frac{60}{140}\right)^2\left(1 + (1+0{,}3)ln\frac{140}{60}\right)\right) = 0{,}111$$

The deflection will be highest at the free (inner) end of the beam. Inserted this provide the maximum deflection:

$$y_{max} = -\frac{q{r_m}^2}{D}\left(\frac{C_1 L_{14}}{C_4} - L_{11}\right) = -\frac{0{,}9 * 140^4}{17673993}\left(\frac{0{,}57 * 0{,}0215}{1{,}1} - 0{,}0032\right) = -0{,}15\ mm$$

Minus sign refers to deflection in negative y-direction.

The plate and load constants L_{14}, L_{17}, C_4 and C_7 inserted give the maximum deflection of the plate.

$$M_{max} = -qr_m^2\left(L_{17} - \frac{C_7}{C_4}L_{14}\right) = -0{,}45 * 140^2 * \left(0{,}111 - \frac{0{,}867}{1{,}1} * 0{,}0215\right) = -1654\ N$$

$$\sigma_{max} = \frac{6M_{max}}{t_e^2} = \frac{6 * (-1211)}{10^2} = -99{,}2\ MPa$$

The negative sign refers to compressive stress.

The resulting safety factor is determined by dividing the yield stress by the maximum allowable strass.

$$SF = \frac{\sigma_y}{\sigma_{max}} = \frac{210}{99{,}2} = 2{,}1$$

Maximum strain according to Hook's Law:

$$\varepsilon_{max} = \frac{\sigma_{max}}{E} = \frac{99{,}2}{193 * 10^3} = 514\ microstrain$$

Performing same procedure for F_{min}, the minimum strain that will be measured by the strain gauges is obtained:

$y_{max,min} = -0{,}027\ mm$ $\sigma_{min} = -17{,}4MPa$ $\varepsilon_{min} = 89\ microstrain$

B.2 The SKF Model for Estimation of Bearing Performance Characteristics

The calculations in this section are based on the theory of *Swedish ball bearing company*, SKF [10], and *Mechanical Engineering Reference Manual* [29].

There are several coefficients in the calculations that are dependent on bearing dimensions, material properties and lubricant. Table B.2.1 shows the bearing data provided by the vendor, SKF [10], factors and coefficients that are necessary for further calculations.

Table B.2.1: Bearing data, SKF [10].

	Turbine thrust bearing [3310 A-2Z]	**Turbine radial bearing [6310-2RS1]**
Coefficient of friction (μ)	0,0024	0,0015
Basic dynamic load rating (C)	90 kN	65 kN
Calculation factor (k_r)	0,07	0,03
Calculation factor (e)	0,8	–
Calculation factor (Y_1)	0,78	–
Calculation factor (Y_2)	1,24	–

Bearing life

In theory, bearings can be used in service as long 90% of the rolling elements are functional [29]. The parameter that estimates the time before 10% of the elements have failed, and thus estimates the design lifetime of the bearing, is the *basic life rating*, L_{10}. The parameter is measured in millions of revolutions, and is a function of the *basic dynamic load rating*, C, and the *equivalent dynamic radial load*, P.

$$L_{10} = \left(\frac{C}{P}\right)^3 \quad [millions\ of\ revolutions]$$

The SKF model includes two additional factors in this equation, a_1 and a_{SKF}, which takes into consideration the lubrication conditions and the contamination level. This provides a more accurate representation of the operating conditions.

$$L_{10m} = a_1 a_{SKF} \left(\frac{C}{P}\right)^3 \quad [millions\ of\ revolutions]$$

The equation is rewritten to an output in hours:

$$L_{10mh} = \left(\frac{10^6}{n_{rpm}\left(60\frac{min}{hr}\right)}\right) a_1 a_{SKF} \left(\frac{C}{P}\right)^3 \quad [hours]$$

Frictional moment

The total frictional moment in the bearing is given by Eq. 2.

$$M = \mu P \frac{d}{2}$$

Where

M – Total frictional moment

μ – friction coefficient

d – bearing bore diameter

$$P = F_r + Y_1 F_a \quad when \quad F_a/F_r \leq e \quad [Low\ axial\ loading]$$

$$P = 0{,}67F_r + Y_2 F_a \quad when \quad F_a/F_r > e \quad [High\ axial\ loading]$$

Where

e – limiting value for F_a/F_r

$Y_{1,2}$ – axial load calculation factors

F_a and F_r are the axial and radial components of the total forces respectively.

Starting torque

Assuming 60 % higher coefficient of viscosity at start-up [10], the starting torque is given by Eq. 4.

$$M = 1.6 \cdot \mu \cdot P \cdot \frac{d}{2} \quad [Nmm]$$

Power loss

Further, the loss in mechanical power due to the frictional forces of the bearings can be estimated using Eq. 5.

$$N_R = 1{,}05 \times 10^{-4} \cdot M \cdot n \; [W]$$

With total frictional moment, M, dependent on the rotational speed of the shaft, n. The coefficient 1,05 is the compensation for torque loss in the machinery.

Minimum radial load

$$F_{rm} = 0.02C$$

Appendix C Machine Drawing

C.1 Axial Force Measurement Setup, NTNU

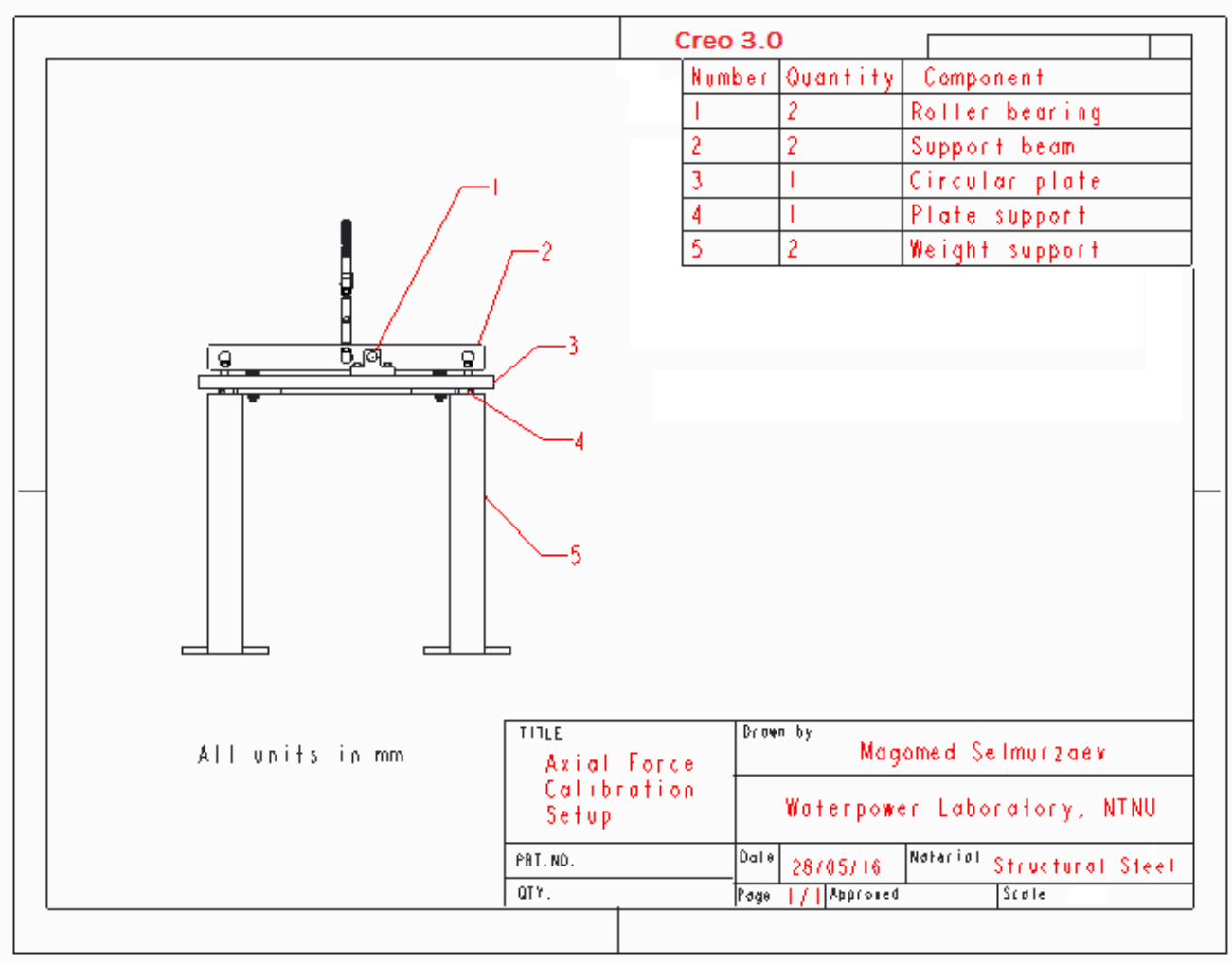

Creo 3.0

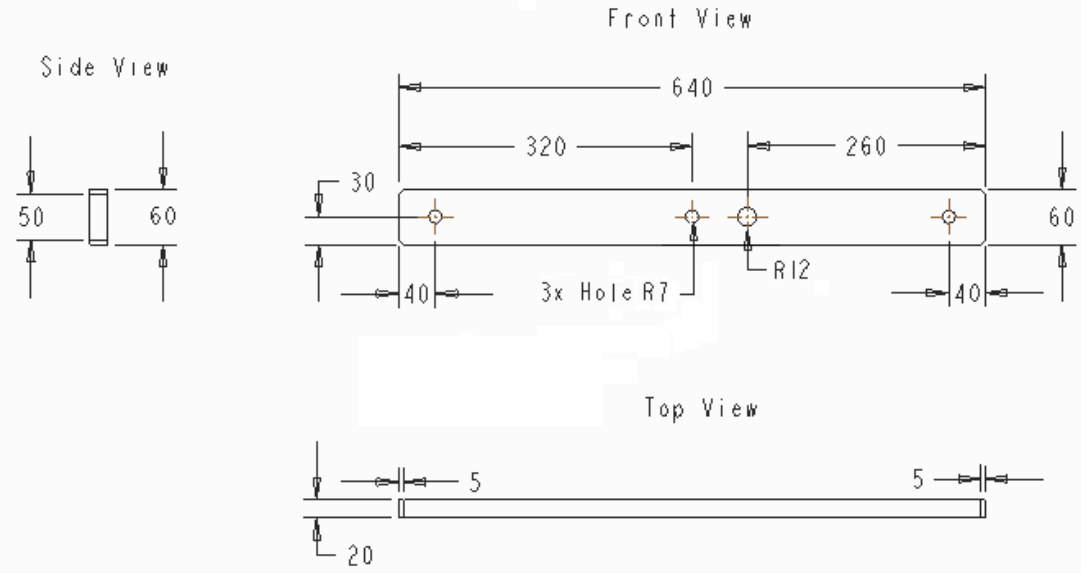

All Units in mm

TITLE: Support Beam	Drawn by: Magomed Selmurzaev	
	Waterpower Laboratory, NTNU	
PRT.NO. 2	Date 28/05/16	Material Structural Steel
QTY. 2	Page 1/1 Approved	Scale

Creo 3.0

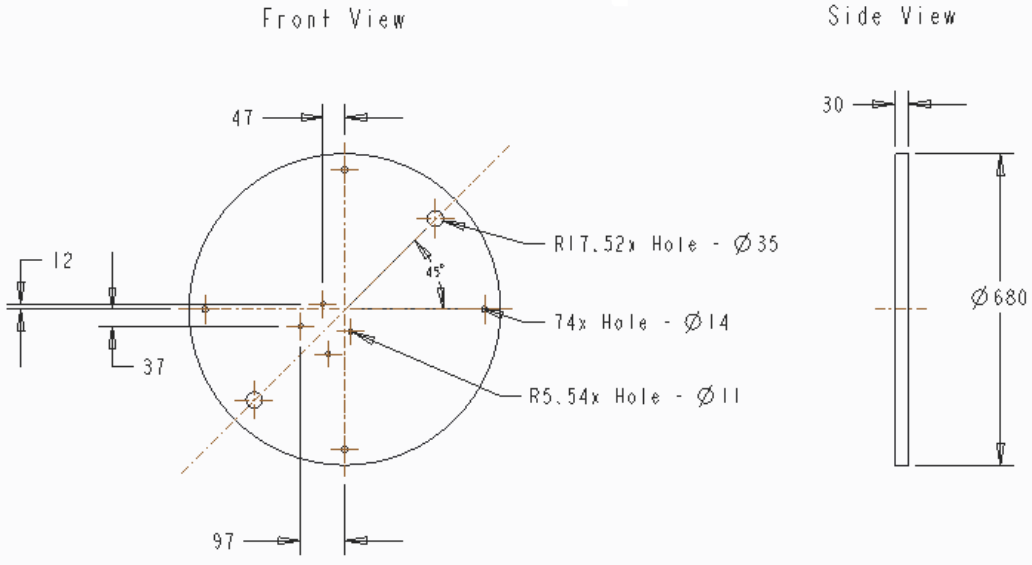

TITLE: Circular Plate	Drawn by: Magomed Se murzaev	
	Waterpower Laboratory, NTNU	
PRT.NO. 3	Date 28/05/16	Material Structural Steel
QTY. 1	Page /1 Approved	Scale

Creo 3.0

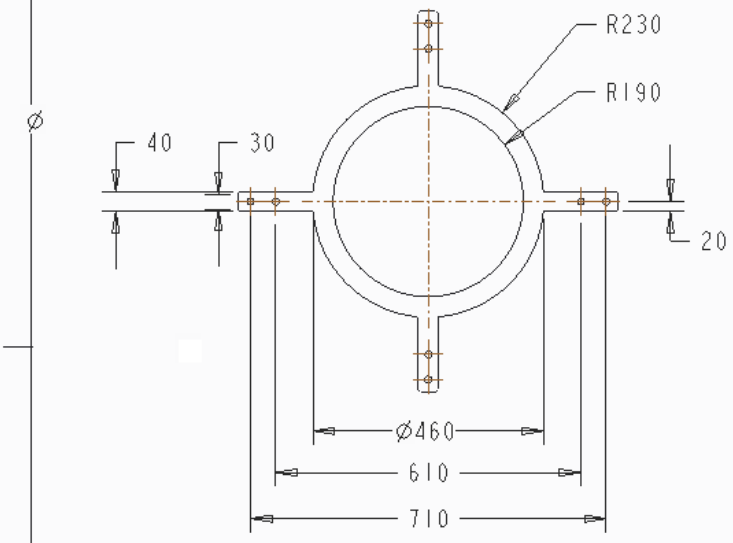

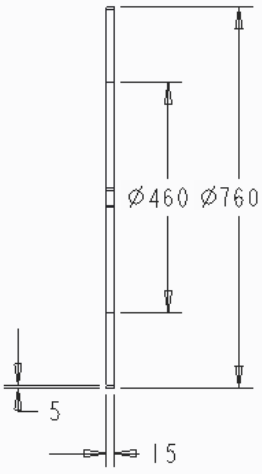

All units in mm

TITLE: Plate Support	Drawn by: Magomed Selmurzaev		
	Waterpower Laboratory, NTNU		
PRT.NO. 4	Date: 28/05/16	Material: Structural Steel	
QTY. 1	Page 1/1	Approved	Scale

Creo 3.0

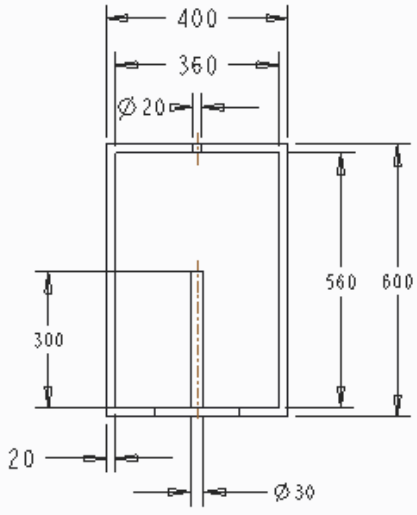

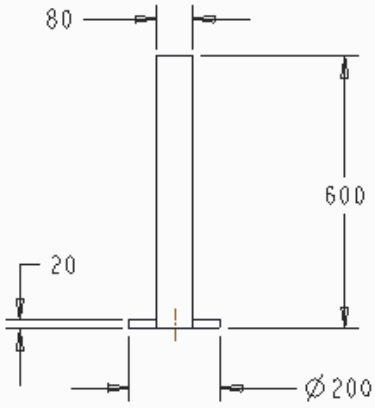

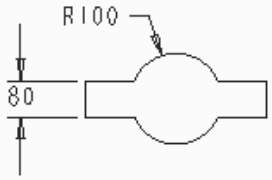

All units in mm

TITLE: Weight Support	Drawn by: Magomed Selmurzaev		
	Waterpower Laboratory, NTNU		
PRT.NO. 5	Date: 28/05/16	Material: Structural Steel	
QTY. 2	Page 1/1	Approved	Scale

C.2 Friction Torque Measurement Setup, NTNU

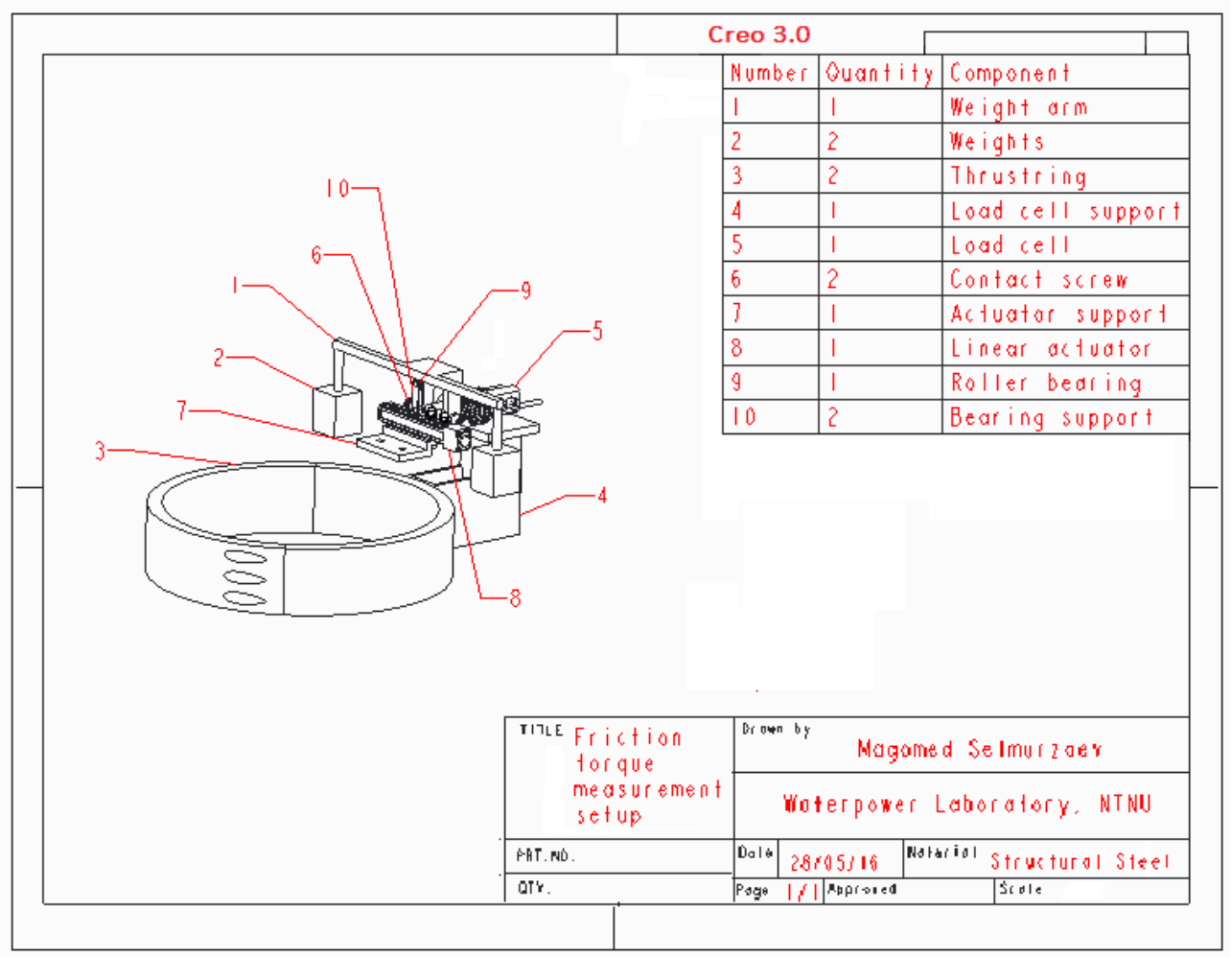

Creo 3.0

Left view

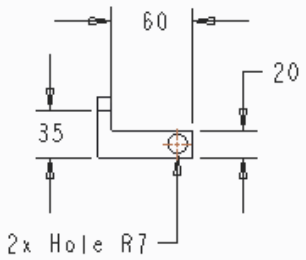

Top view

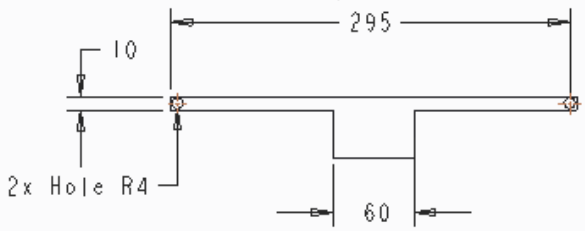

Front view

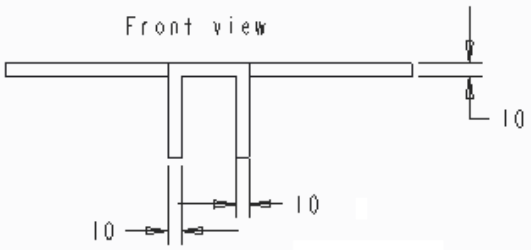

Isometric view

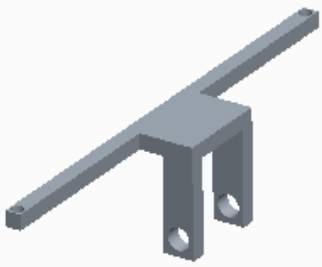

All units in mm

TITLE: Weight arm	Drawn by: Magomed Selmurzaev		
	Waterpower Laboratory, NTNU		
PRT.NO. 1	Date: 28/05/16	Material: Structural Steel	
QTY. 1	Page 1/1	Approved	Scale

Creo 3.0

Front view

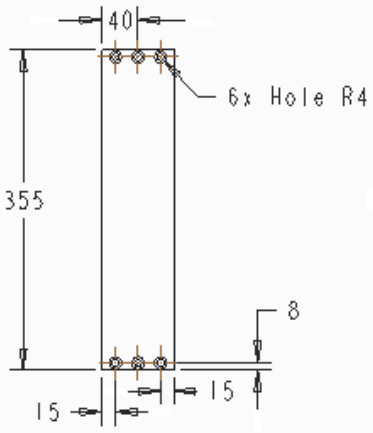

Top view

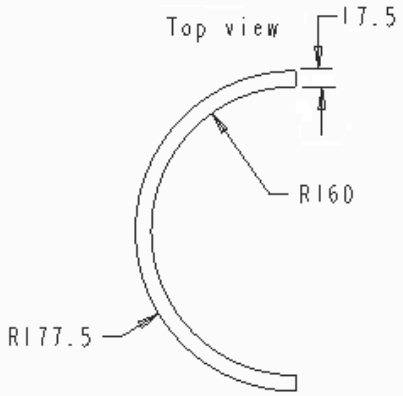

Side view

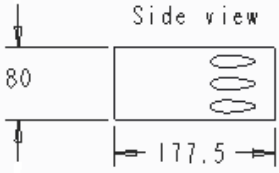

Isometric view

All units in mm

TITLE: Thrustring	Drawn by: Magomed Selmurzaev		
	Waterpower Laboratory, NTNU		
PRT.NO. 3	Date: 28/05/16	Material: Structural Steel	
QTY. 2	Page 1/1	Approved	Scale

Creo 3.0

Top view

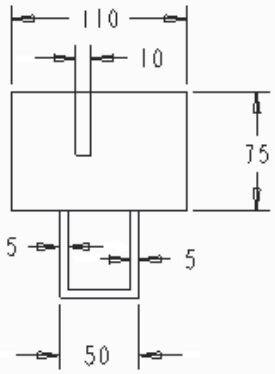

Side view

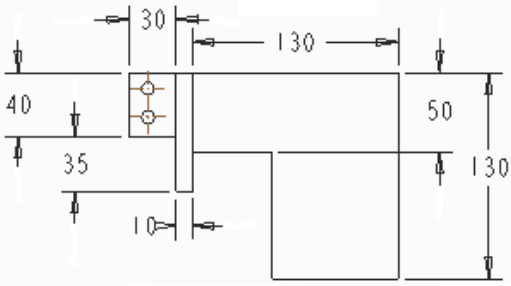

Back view

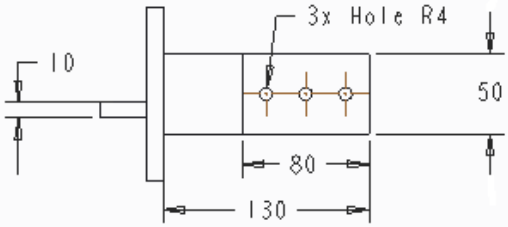

Isometric view

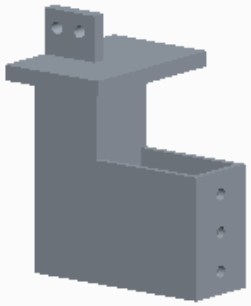

All units in mm

TITLE: Load Cell Support	Drawn by: Magomed Selmurzaev		
	Waterpower Laboratory, NTNU		
PRT.NO. 4	Date 28/05/16	Material Structural Steel	
QTY. 1	Page 1/1	Approved	Scale

Creo 3.0

Side view

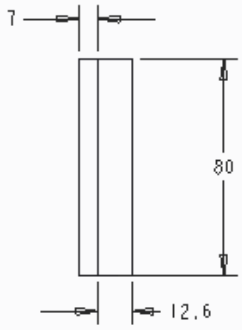

Top view

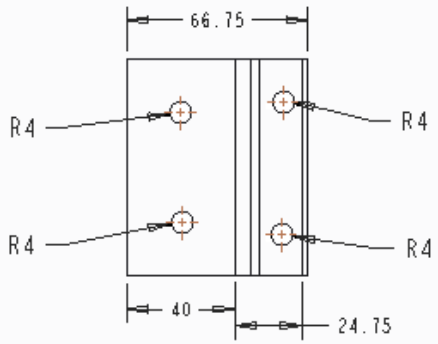

Front view

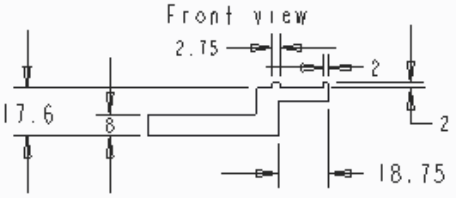

Isometric view

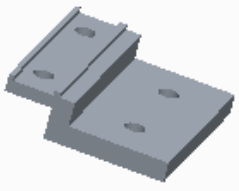

All units in mm

TITLE: Actuator support	Drawn by: Magomed Selmurzaev		
	Waterpower Laboratory, NTNU		
PRT.NO. 7	Date 28/05/16	Material Structural Steel	
QTY. 1	Page 1/1	Approved	Scale

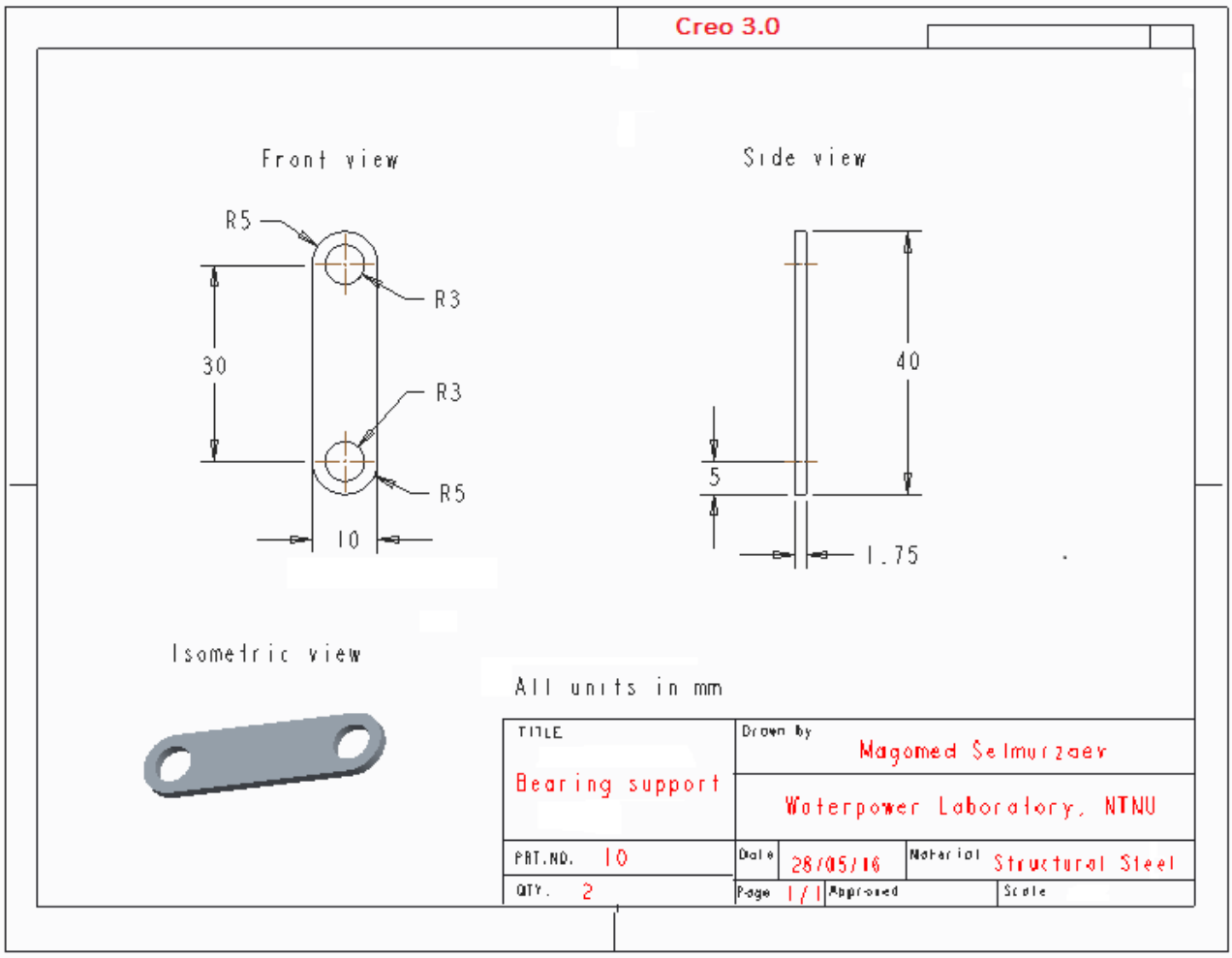
Creo 3.0
Front view
R5
R3
30
R3
R5
10
Side view
40
5
1.75
Isometric view
All units in mm
TITLE
Bearing support
Drawn by
Magomed Selmurzaev
Waterpower Laboratory, NTNU
PRT.NO. 10
Date 28/05/16
Material Structural Steel
QTY. 2
Page 1/1
Approved
Scale

C.3 Axial Force Measurement, TTL, KU

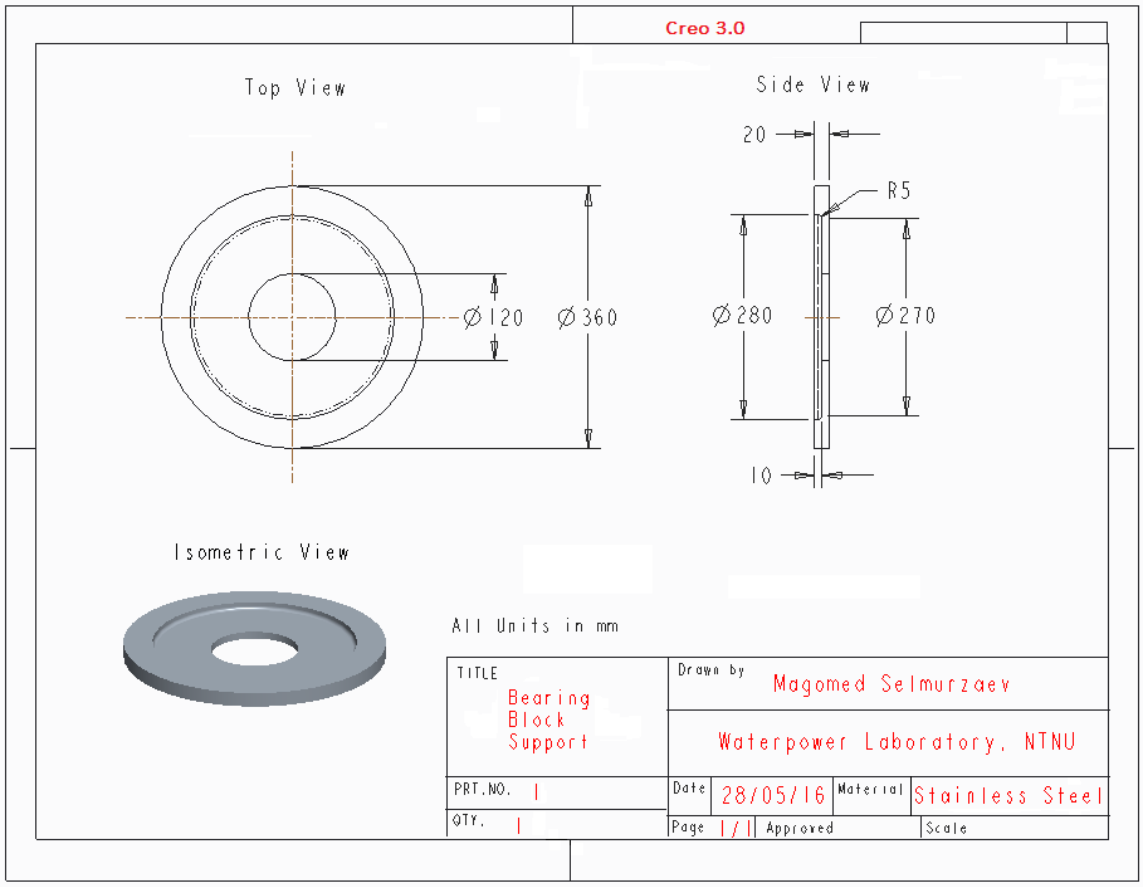

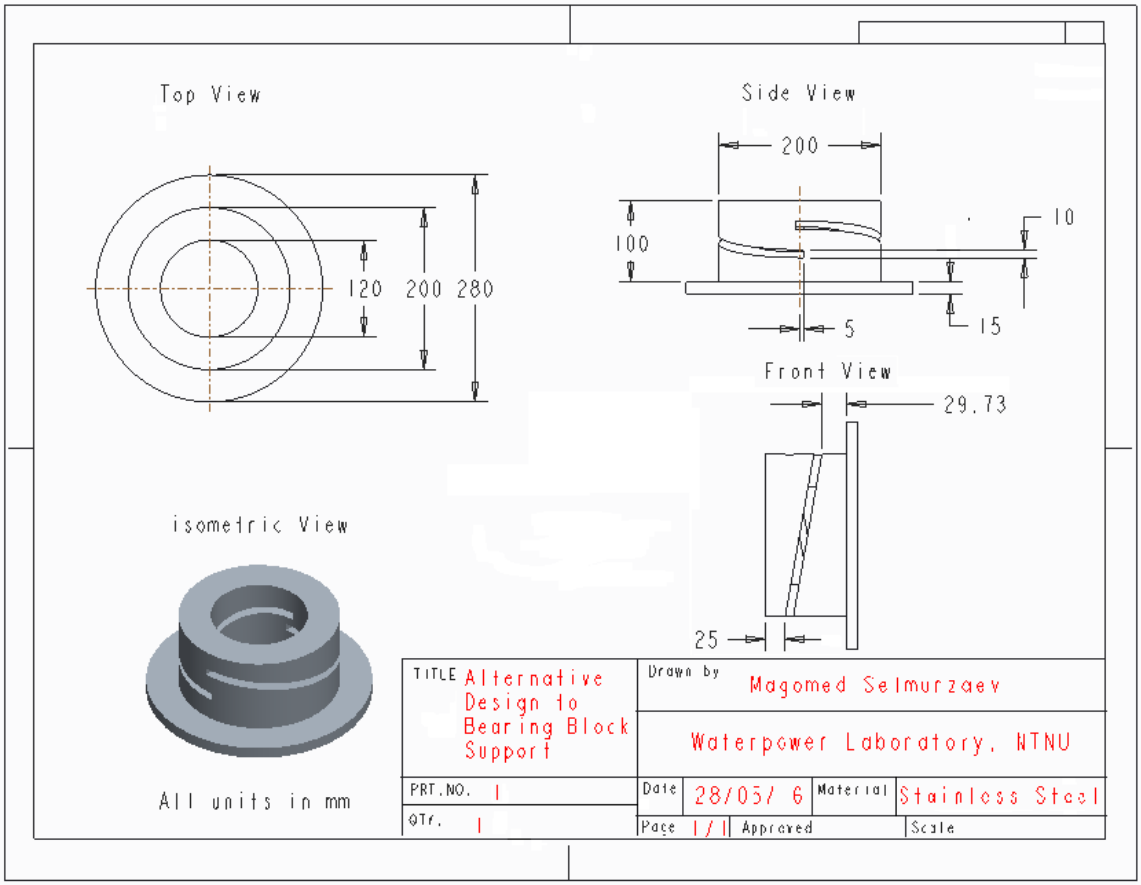

Appendix D Strain Gauge Data

D.1 Strain Gauge Characteristics and Selection Table

GAGE DOPING CODE	GAGE CHARACTERISTICS	PART NUMBER	FIGURE	EFFECTIVE LENGTH (GL)	GAGE WIDTH (GW)	ENCAPSULATION LENGTH ±10% (EL)	ENCAPSULATION WIDTH ±10% (EW)
C	GF + 100 TCR + 4 TCGF - 6 Linearity ± 0.2	ACP - 15 - 150	B1	.100	.020		
		ACP - 30 - 150	B1	.100	.010		
		ACP - 120 - 300	B1	.250	.009		
		UCP - 120 - 090	B2	.060	.020		
		S/ACP - 120 - 300	E1	.250	.009	.500	.210
		S/UCP - 120 - 090	E2	.060	.020	.280	.140
D	GF + 115 TCR + 3 TCGF - 8 Linearity ± 0.2	ADP - 250 - 220	B1	.186	.09		
		ADP - 350 - 300	B1	.250	.010		
		UDP - 350 - 175	B2	.140	.016		
		S/ADP - 350 - 300	E1	.250	.010	.500	.210
		S/UDP - 350 - 175	E2	.140	.020	.350	.140
E	GF + 130 TCR + 6 TCGF - 10 Linearity ± 0.2	UEP - 350 - 090	B2	.060	.020		
		AEP - 350 - 220	B1	.170	.009		
		AEP - 500 - 300	B1	.250	.010		
		UEP - 350 - 060	B2	.030	.020		
		S/AEP - 500 - 300	E1	.250	.010	.500	.210
		S/UEP - 350 - 090	E2	.060	.020	.280	.140
F	GF + 140 TCR + 10 TCGF - 11 Linearity ± 0.2	AFP - 500 - 090	B1	.060	.010		
		AFP - 350 - 090	B1	.060	.010		
		UFP - 750 - 090	B2	.060	.020		
		S/AFP - 500 - 090	E1	.060	.010	.280	.140
		S/UFP - 750 - 090	E2	.060	.020	.280	.140
G	GF + 155 TCR + 18 TCGF - 13 Linearity ± 0.2	AGP - 350 - 090	B1	.060	.010		
		AGP - 500 - 090	B1	.060	.010		
		AGP - 1000 - 300	B1	.250	.010		
		UGP - 1000 - 090	B2	.065	.020		
		UGP - 1000 - 060	B2	.030	.020		
		S/AGP - 1000 - 300	E1	.250	.010	.500	.210
		S/UGP - 1000 - 090	E2	.060	.020	.280	.140
H	GF + 175 TCR + 45 TCGF - 23 Linearity ± 0.2	AHP - 10000 - 220	B1	.170	.009		
		AHP - 10000 - 300	B1	.250	.009		
		UHP - 5000 - 060	B2	.030	.020		
		S/AHP - 10000 - 220	E1	.170	.009	.250	.150
		S/AHP - 10000 - 300	E1	.250	.009	.500	.210
		S/UHP - 5000 - 060	E2	.030	.020	.250	.140

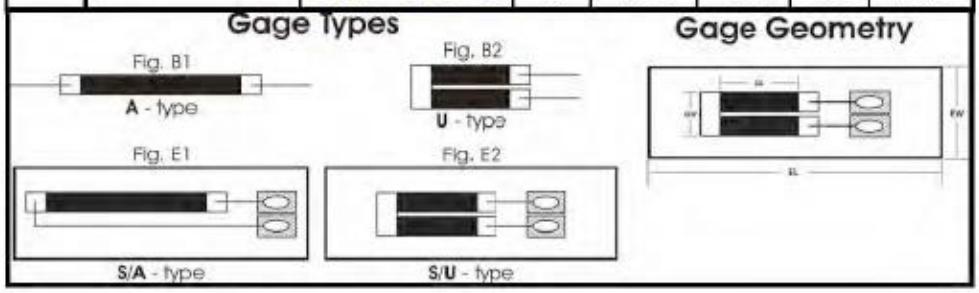

D.2 Comparison of Metal Foil and Silicon Strain Gauges

CHARACTERISTIC	METAL-FOIL	SILICON
Size for 1000 Ω	~0.04 in^2	~0.0004 in^2
Gage Factor	1 to 4	30 to 200
Resistance	120 Ohms to 5K Ohms	120 Ohms to 10K Ohms
TCR	1%/100F Typical	+10 to +20%/100 F Typical
TCGF	-3%/100F	-1 to -16%/100 F Typical
Fatigue Life	10^4 to 10^7 Cycles	infinite at <500 µstrain
Operating Strain	500 to 10,000 µstrain	500 to 1,000 µstrain
Transverse Strain Sensitivity	3% Typical	1% Typical
Power Density	1 to 15 Watts/in^2	25 TO 150 Watts/in^2
Resolution	.1 µstrain Typical	.005 µstrain Dynamic
Noise "Floor" Level	2 x 10^{-3} $(\mu strain)^2/Hz$	1 x 10^{-6} $(\mu strain)^2/Hz$
Gaged Null Stability	Good*	Good*
Long-Term Drift	Good*	Good*
Operating Temperature	Cryogenic to +350 F	Cryogenic to +750 F***
Resulting Sensor Compliance	Y microinches	Y/100 microinches
Sensor Thermal Zero Shift	<±1%FSO/100F	±1%FSO/100F**
Sensor Thermal Sensitivity Shift	±1%/100F	±1%/100F Typical**
Sensitivity to Thermal Transients	Low	Low**
Other Mechanical Inputs Sensitivity	Low*	Low*
Sensor Acceleration Sensitivity	Low	Extremely Low (100 Times less)
Sensor Output at 500 µstrain	10 mV FSO Typical	500 mV FSO Typical
Sensor Frequency Response	[0 to n] Hertz	[0 to 100n] Hertz

* Mounting Dependent

** With Proper Thermal Compensation

*** Higher Temperature SOI gages Available with Special Mounting

Appendix E Motorized Lead Screw Datasheet

Specifications – ML14

Size 14A motor (single stack type) with rotating screw

Features and Benefits

- Higher torque density than the competition.
- NEMA 14 motor (size 35 mm).
- Rotating screw versions only.
- Choose between a variety of inch and metric lead screws.
- Recommended max. thrust force 50 lbs (222 N).
- Recommended max. lead screw length of 8 in (203 mm) for optimal performance. Longer length lead screws available, see diagrams on page 24.

Motor Options

Motor code	Holding torque		Voltage / phase* [V]	Current / phase [A]	Resistance [Ω]	Inductance [mH]	Power draw [W]	Step angle [°]	Motor length, maximum (Lm)		Rotor inertia [oz/in² (kg/cm²)]	Motor weight [lbs (kg)]
	[oz-in]	[N-m]							[in]	[mm]		
14A088	25.8	0.182	3.42	0.88	3.89	5.51	3.01	1.8	1.34	34.0	0.10 (0.018)	0.41 (0.19)
14A135	23.0	0.162	1.71	1.35	1.27	1.79	2.31	1.8	1.34	34.0	0.10 (0.018)	0.41 (0.19)

* Applied voltage can be any value above this number as long as the driver output current is controlled at the rated RMS current.

Inch Lead Screw Options

Screw code	Diameter [in]	Lead [in]	Travel / step [in]
25-0031	0.250	0.0313	0.00016
25-0066		0.0625	0.00031
25-0125		0.1250	0.00063
25-0250		0.2500	0.00125
25-0500		0.5000	0.00250
25-0750		0.7500	0.00375

Metric Lead Screw Options

Screw code	Diameter [mm]	Lead [mm]	Travel / step [mm]
M06-01	6	1	0.00500
M06-06		6	0.03000
M06-12		12	0.06000

Note: Other diameters and leads available – please contact Thomson for more information about custom lead screw availability.

Dimension	Value
Humidity, Max	85 %
Inductance	5.22 mH
(MLS) Rotor Inertia	0.06 oz-in^2
[L3]	1.26 in
Backlash, Max	0.01 in
Concentricity of Mounting Pilot to Shaft (TIR)	0.003 in
Current/Phase	0.51 A
Diameter, Major	0.188 in
Dielectric Strength	500 VAC for 1 minute
Holding Torque	9.3 oz-in
Insulation Resistance	100 Mohm @ 500 VDC
Magnet Wire Insulation	Class B 266 °F
Motor Code	11A051
Motor Name	NEMA 11
Motor Size	28 mm
Motor Weight	0.24 lb
Perpendicularity of Shaft to Mounting Face (TIR)	0.003 in
Power Draw	1.96 W - delete
Radial Play, End	0.002 in @ 2 lb
Radial Play, Max	0.001 in @ 1 lb
Recommended Max. Thrust Force	20 lbf
Resistance	7.54 Ω
Rotation Type	Rotating Screw
Screw Length, Max Recommended	4 in
Screw Runout	0.007 in/ft
Screw Straightness	0.005 in/ft
Stack Type	Single Stack
Standard Lead Accuracy ±	0.01 in/ft
Standard Screw Coating	None
Step Angle	1.8 °
Temperature, Case - Max	140 °F
Temperature, Storage	-4 to 122 °F
travel per shaft rev	0.05 in
Travel/Step	0.00025 in
Voltage	3.85 Vdc

Dimensions	Projection
Inch [mm]	

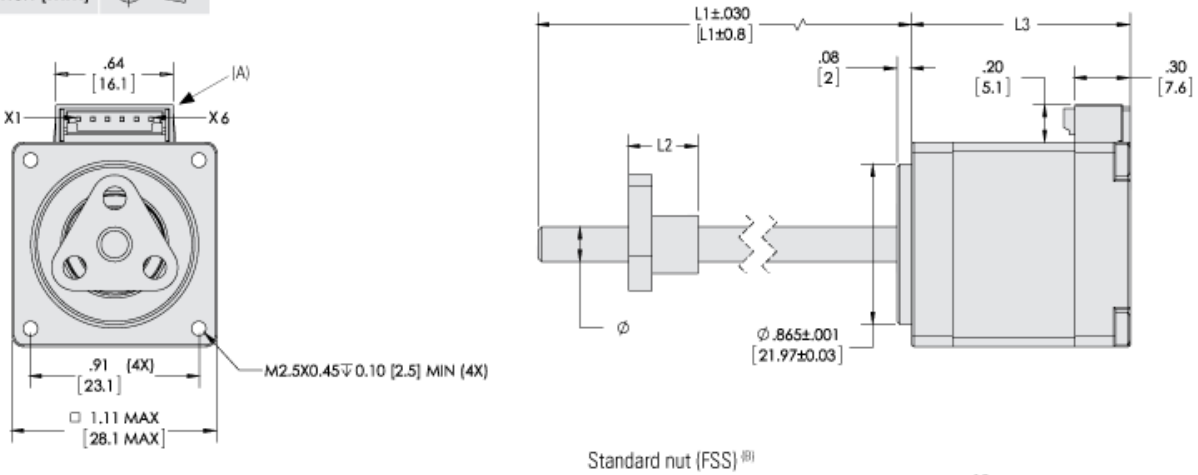

Maximum Stroke (Smax)
Smax = Ls - Ln - 0.08 in (2 mm)

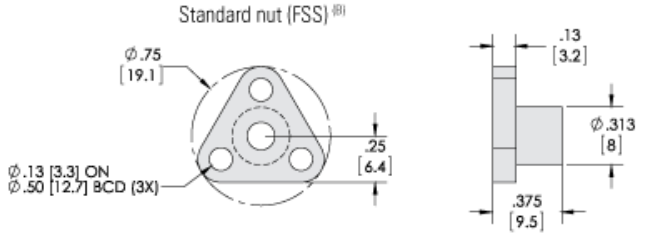

(A) 6-pin connector as standard (X1 = pin 1, X6 = pin 6). Custom connection solutions possible. Contact Thomson for more information.
(B) For dimensions and data on anti-backlash nut, please contact Thomson for more information.

Motor Connection

Molex Connector *	
Pin	Phase
1	A-
2	not used
3	A+
4	B-
5	not used
6	B+

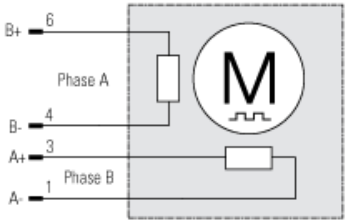

* Molex connector p/n 53253-0670. Mates with Molex connector p/n 51065-0600.

Motor Connector Kit with Flying Leads - Optional

- Compatible with the above motor connector.
- Lead length 12.5 in (318 mm).
- 26 AWG lead wires.
- Part number MC11-001.
- Contact Thomson for more information.

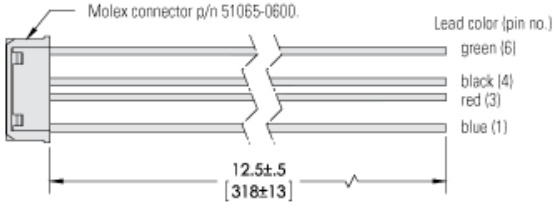

Appendix F

Theoretical Calculation of Hydraulic Axial Forces on the Francis Turbine.

```
% Theoretical calculation of hydraulic axial forces on the Francis
 Turbine

%state of operation:
n = 1500 %rpm
Q = 1 %m^3/s

% Draft tube outlet Area
A3 = (3.14*0.524^2)/4

% Physical properties
ru = 1000 %kg/m^3
g = 9.82 %m/s^2
patm = 101.3*10^3 %[Pa]

% Turbine Dimensions,[m]
D0 = 0.706
r0 = D0/2
D2 = 0.353
r2 = D2/2
D11 = 0.630
r11 = D11/2
D12 = 0.630
r12 = D12/2
D11L = 0.412
r11L = D11L/2
D12L = 0.412
r12L = D12L/2
Dp = 0.363
rp = Dp/2
D2L = 0.363
r2L = D2L/2
Dr = 0.192
rr = Dr/2
B1 = 0.06
```

```
%Inlet velocity [m/s]
cm1 = Q/(3.14*D11*B1)
%Outlet velocity [m/s]
cm2 = (4*Q)/(3.14*D2^2)
%Assumptions are constant, uniform flow at inlet and outlet

%Net Head [m]
Hn = 50

%Assuming 50% reduction of pressure at the inlet to the rotor [m]
h1 = Hn/2

% k is a constant chosen between 0.5 and 0.55
k = 0.5

%rotational speed [1/rad]

w = (n*3.14)/30

%This give: h11 = h12 = Hi [m]
h11 = h1-ru*g*(B1/2)*0.0001019977334
h12 = h1+ru*g*(B1/2)*0.0001019977334

%Using Bernoulli equation to estimate h2:
%Heights [m]
z1 = 1.793
z2 = 1.61
z3 = 1.152
z4 = 2.152
z5 = 2.5

%From continuity, draft tube outlet velocity:
v3 = Q*A3
v4 = 0 % - assuming
%
h4 = patm/(ru*g)
h3 = h4-((v4^2)/(2*g))+z4-((v3^2)/(2*g))-z3
h2 = h3+v3^2/(2*g)+z3-cm2^2/(2*g)-z2
%h2 = h4+z4-cm2^2/(2*g)-z2

%Other pressure relations:
h11L = h11-((k^2*w^2)/(2*g))*(r11^2-r11L^2)
h12L = h12-((k^2*w^2)/(2*g))*(r12^2-r12L^2)
hp = (patm/(ru*g))+((k^2*w^2)/(2*g))*(rp^2-rr^2)
hs = h2+((k^2*w^2)/(2*g))*(r12L^2-r2L^2)
```

```
hmid_ovre = (ru*g*(h11L+hp))/2
hmid_nedre = (ru*g*(h12L+hs))/2


%Reaction forces at the inlet and outlet of the runner [N]
F1 = 0.5*ru*g*(h11+h12)*(3.14/4)*(D12^2-D11^2)
F2 = ru*Q*cm1 %teta = 0
F3 = ru*g*h2*(3.14*D2L^2)/4
F4 = ru*Q*cm2

%Forces due to pressure difference between runner and top cover [N]
F5 = ru*g*3.14*hp*(rp^2-rr^2)-ru*g*3.14*((k^2*w^2)/(4*g))*(rp^2-
rr^2)^2
F6 = ((ru*g*3.14*h11)/4)*(D11^2-D11L^2)-((ru*g*k^2*w^2)/64)*(D11^2-
D11L^2)^2
F7 = ((ru*g*3.14*h12)/4)*(D12^2-D12L^2)-((ru*g*k^2*w^2)/64)*(D12^2-
D12L^2)^2

%Forces due to pressure differences inside the labyrinth [N]
F8 = ((ru*g*(h11L+hp))/2)*((3.14*(D11L^2-Dp^2))/4)
F9 = ((ru*g*(h12L+hs))/2)*((3.14*(D12L^2-D2L^2))/4)

%Total hydraulic axial forces [N]
Fhyd = F1+F2-F3-F4+F5+F6-F7+F8-F9


%Axial forces due to turbine/shaft weight [N]
Fmech = 400*g

Ftot = Fhyd+Fmech

%Effective Area [m^2]
innerD=0.183
outerD=0.225
Aeff=((outerD^2-innerD^2)*3.14)/4

%pressure [Pa]
P=Ftot/Aeff

%10% uncertainity of the calculations:

Ftot_2=Fmech+(Fhyd*1.1)

%Calibration weights for maximum axial load [kg]
W=Ftot_2/g
```

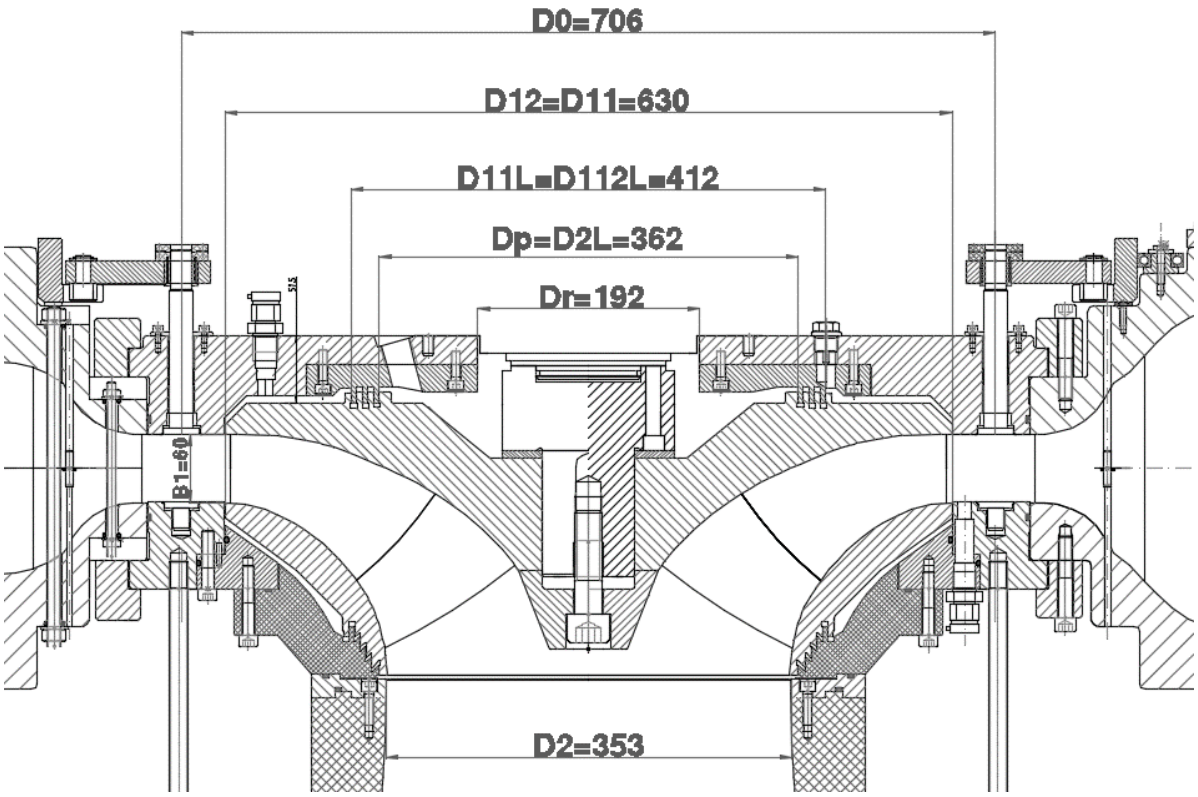

Bernoulli's equation:

$$\frac{p_1}{2\rho} + \frac{v_1^2}{2g} + z_1 = \frac{p_2}{2\rho} + \frac{v_2^2}{2g} + z_2$$

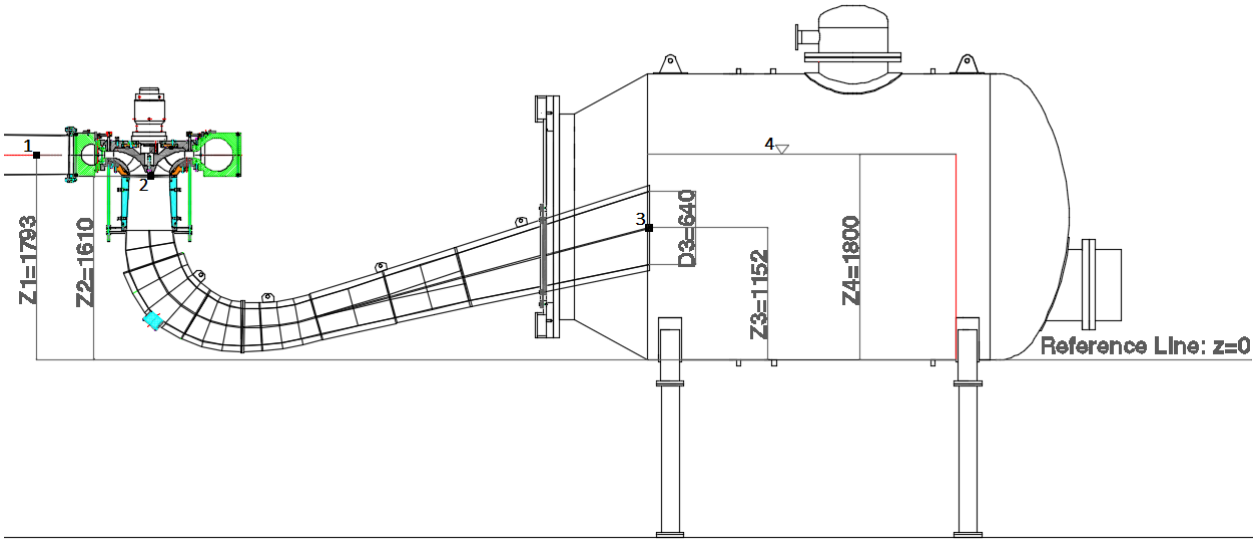

Figure F.1a) and F.1b): Dimensions of the Francis turbine test rig at the Waterpower Laboratory, NTNU. All unit are in millimeters.

Appendix G.1

Calibration of friction torque measurement in the Francis Turbine Test Rig

The Waterpower Laboratory NTNU

Doc No:	Rev:	Date:	
FC-4331-2	0	2006-06-27	
Prepared by:	**Approved by:**	**Classification:**	**Page:**
Jørgen Ramdal	Ole G. Dahlhaug	Open	1 of 5

1 General

This procedure describes calibration of the generator friction torque in the Francis Turbine Test Rig.

1.1 Definitions and abbreviations

T	Torque	[Nm]
m	Mass of weights	[kg]
l	Length of torque arm	[m]
m.v.	Measured value	[V]
a	Slope in calibration equation	[Nm/V]
b	Intersection constant in calibration equation	[Nm]
g	Gravity	[m/s^2]
hct	Holding clamp thickness	[m]
d	Shaft diameter	[m]
L	Total length measured with micrometer	[m]

Constant of gravity (g) is 9.8215 m/s^2.

2 The system

2.1 Description

The system consists of a hydraulic bearing, and a weighing cell of type Hottinger Z6FC3 with external amplifier. Two mechanical bearings connected to the generator shaft are absorbing all radial and axial movement in the turbine. These two bearings are inserted into a hydraulic bearing/thrust block that makes it possible to measure axial thrust and radial friction. The load cell, connected to the hydraulic bearing unit and a mechanical stop, is absorbing all friction in the two bearings connected to the generator axle. The weight range for the weighing cell is 0-10 kg and an external amplifier in connection with the weighing cell gives an output signal from 0-10 V that is sent to the data acquisition unit for post processing.

The torque for calibration is generated by using weights supplied to a scale pan on the arm. The scale pan is attached to the generator torque measuring rig via a roller bearing. The generators torque arm length from the centre of the generator shaft, is found using a micrometer.

2.2 Equipment used in calibration

- Load cell
  - Hottinger Z6FC3 (Reg. no. 4331-2)
- Measuring amplifier
  - Hottinger ME30 (Reg. no.
- Hydraulic thrust block
- Data acquisition unit
  - National Instruments data acquisition unit
  - LabView for computation and presentation of data.
  - External 24 V power supply
- Hanging fixture
- Calibrated weights
- Micrometer

3 Calibration

3.1 Preparations

1. In order to cancel out oil temperature differences in the hydrostatic bearing the oil pump should be started at least one hour before the rest of the calibration is performed.

2. Connect the data acquisition unit, and make sure the signals are present. Ensure the computer is on and that the signal is present.

3. Find the torque arm length using a micrometer.

3.2 Calibration

1. Start the generator and let it run on 100 rpm. This is done to cancel out effects that occur because friction behaves differently when a system is still.

2. Record the voltage without any weights added. Attach the scale pan to the torque arm. Record the voltage.

3. Place the weights one by one onto the scale pan. The scale pan and the weights in use all have a known weight and are calibrated by Justervesenet.(Norwegian metrology service)

4. For every 2 kg weight applied the voltage reading from the weight cell is recorded. The voltage reading is presented on the computer screen. Make sure the weights have no pendulum motion or no rotation when the recording is made.

5. When the final amount of weights has been placed onto the scale pan, record the reading of the voltage value. Then add a little force by slightly pressing down on the weights for a few seconds. After releasing, record the reading again.

6. Remove the weights one by one. Note the voltage signal at the same points as when the weights were put on.

7. Change the direction of rotation on the generator, but keep the same rotational speed. Perform the prior steps once again. It is assumed that averaging the voltage values for both rotational directions will give the correct offset. This is checked during computations.

4 Computations

The friction torque (T) as a known mass (m) is added is calculated by:

$$T = m \cdot g \cdot l \qquad \text{[Nm]} \qquad (1)$$

Gravity (g) is already known.

The arm length (l) is found by using a micrometer to measure the length (L) from the furthermost side of the shaft to the end of the load cell holding clamp. Then half the shaft diameter (d), and half the holding clamp thickness (hct) is subtracted from the total length.

$$l = L - (\frac{d}{2}) - \frac{hct}{2} \qquad \text{[m]} \qquad (2)$$

The load cell gives an output signal in Volts varying linearly with the torque/weights applied. Voltage values are averaged for each weight point, and the calibration equation is determined using linear interpolation.

$$T = a \cdot [m.v.] + b \qquad \text{[Nm]} \qquad (3)$$

For both rotational directions the slope (a) should be approximately the same. The offset (b) is correct if the difference between the voltage signals in both rotational directions is the same in all reading points.

5 Figures

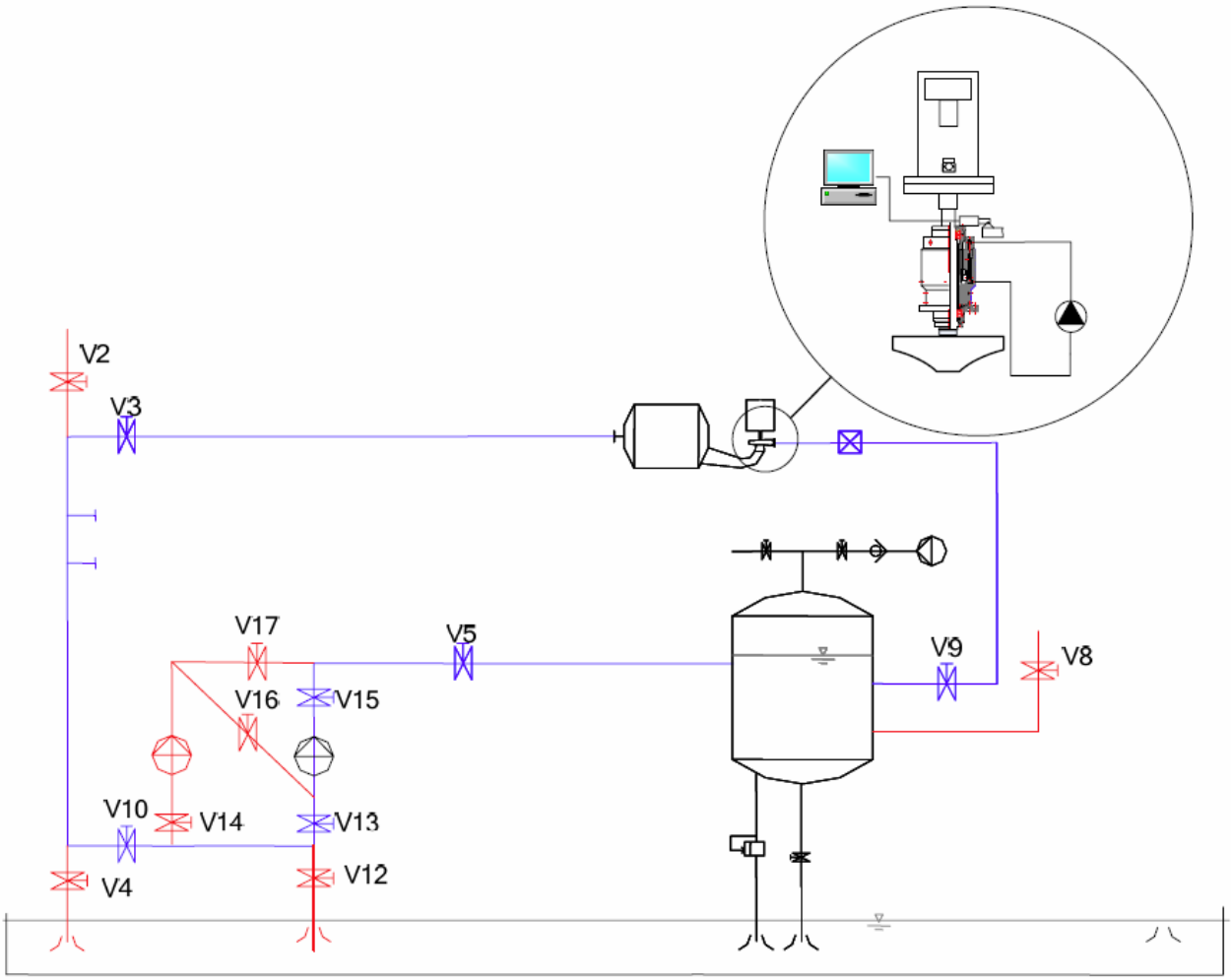

Figure 1: Arrangement

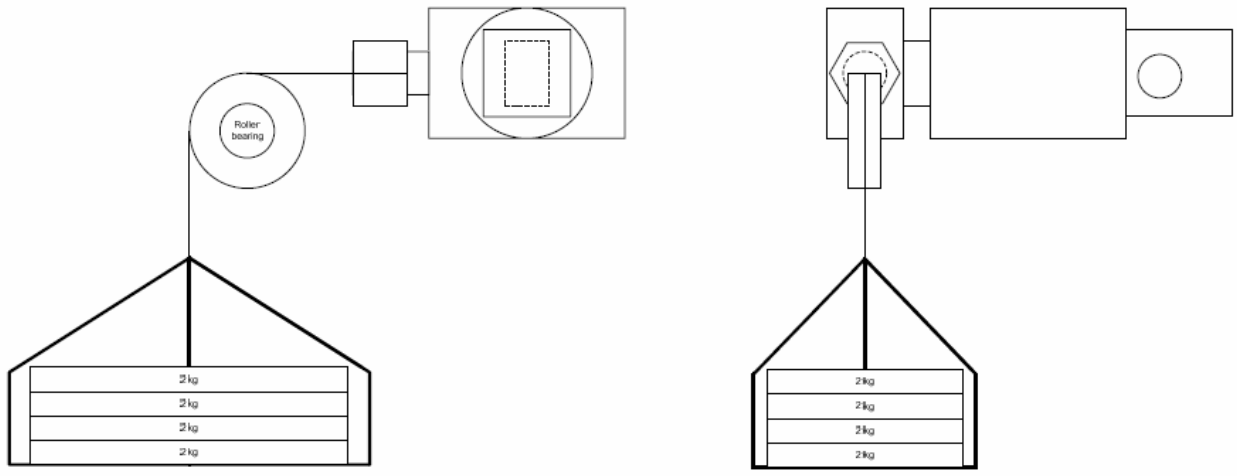

Figure 2: Calibration setup

Appendix G.2

Calibration of axial force measuring system on the Francis Turbine Test Rig

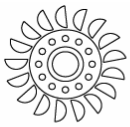

The Waterpower Laboratory NTNU

Doc No:	Rev:	Date:	
FC-4536-8	0	2006-01-31	
Prepared by:	**Approved by:**	**Classification:**	**Page:**
Jørgen Ramdal	Ole G. Dahlhaug	Open	1 of 5

1 General

This procedure describes the calibration of the axial force measuring system on the Francis Turbine Test Rig.

1.1 Definitions and abbreviations

W	-	Weight	[kg]
m.v.	-	Measured value	
a	-	Slope in calibration equation	
b	-	Intersection constant in calibration equation	
g	-	Gravity	[m/s^2]
F	-	Force	[N]
p	-	Pressure	[kPa]
A	-	Area	[m^2]

Gravity (g) is 9,8215 m/s^2.

2 The system

2.1 Description

The measuring system consists of a hydraulic thrust bearing (Figure 1) and a differential pressure transducer (Figure 2)

Oil pressure is fed to the differential pressure transducer from the two sections of the axial thrust bearing, and the differential pressure is directly dependent on the hydraulic axial thrust.

The output signal from the pressure transducer is 4 – 20 mA. The signal is being transformed into 2-10 VDC using a drop resistor before the data acquisition system.

The pressure range for the transducer is 0 to 3000 kPa which gives a weight range from 0 to app. 1230 kg.

2.2 Equipment used in calibration

- Differential pressure transducer
  - Fuji Electric FKCW38V4AKCYYAE. (Reg. no. 4536-8)
- Drop resistance
  - Type Econsistor 8E16 500 ohm
- Hydraulic axial thrust bearing
- Calibrated weights
- Oil hydraulic pump unit for feeding oil to bearing

3 Calibration

3.1 Preparations

1. Turn on oil hydraulic pump unit.

2. Make sure the display for visualization of the measured volt signal is present on the da acquisition system

3.2 Calibration

1. Record the volt signal with no weights on.

2. Connect the equipment necessary to suspend weights to the end of the generator shaft.

3. Load on the weights one by one and record the total weight (W) and corresponding measured volt signal (m.v) for each weight suspended to the generator shaft. The volt signal should be stable before the reading is taken. A minimum of 5 points are needed to find a satisfying calibration equation and the whole range (0-1230 kg) has to be covered.

4. Load off the weights one by one and record the volt signals for each weight again. For each point a minimum of 4 points should be read.

5. Repeat 1., 2. 3. and 4 obtaining minimum two sets of data

4 Computations

The relation between the force and the pressure measured by the differential pressure transducer is

$$F = W \cdot g = \frac{p}{A} \qquad [\mathrm{N}] \tag{1}$$

Since A is constant in the hydraulic axial thrust bearing, the force is determined directly by using the voltage signal from the pressure transducer.

The calibration equation is a linear equation

$$F = (a \cdot (m.v) + b) \cdot g \qquad [\mathrm{N}] \tag{2}$$

and the relationship is determined using linear interpolation.

5 Figures

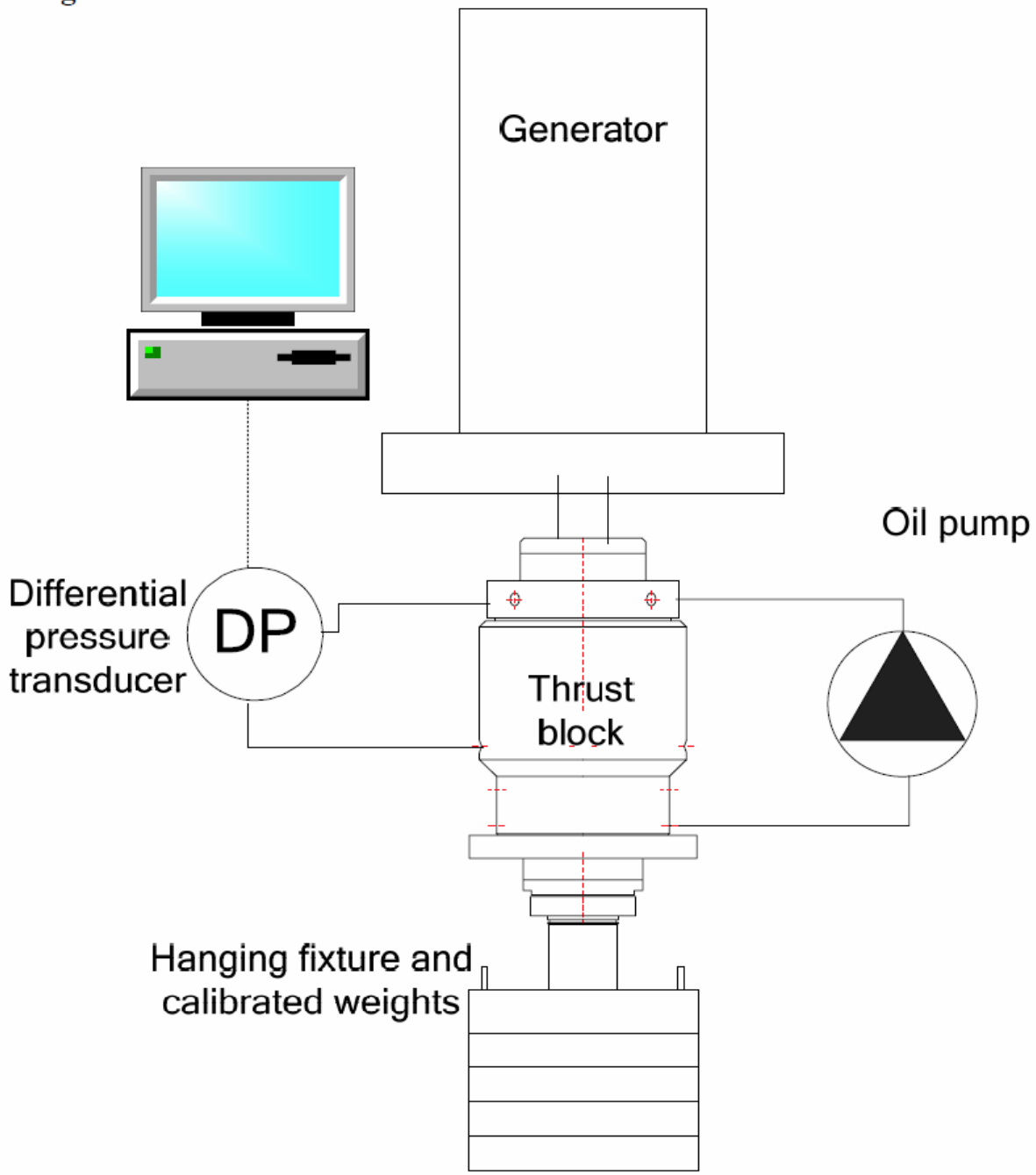

Figure 1: Arrangement

6 References

– Calibration document for calibrated weights and hanging fixture from Justervesenet (Norwegian Metrology Service) (LS-Sertifikat på lodder og vekter ved VKL)
– Documentation for gravity at the Waterpower Laboratory from NGU (LS-Sertifikat på målt "g" ved VKL)
– Specification for Fuji Electric FKCW38V4A differential pressure transducer. (doc IA-4536-1/2/4/5/8)

Appendix H

3D models of the Francis Turbine Test Rigs at Waterpower Laboratory and Turbine Testing Laboratory.

NTNU
Innovation and Creativity